

12-2014

Carbon Black Mediated Conductive Polymer Composite

Mohamed Hussein Faris Ali

Follow this and additional works at: https://scholarworks.uaeu.ac.ae/all_theses

Part of the [Mechanical Engineering Commons](#)

Recommended Citation

Faris Ali, Mohamed Hussein, "Carbon Black Mediated Conductive Polymer Composite" (2014). *Theses*. 176.
https://scholarworks.uaeu.ac.ae/all_theses/176

This Thesis is brought to you for free and open access by the Electronic Theses and Dissertations at Scholarworks@UAEU. It has been accepted for inclusion in Theses by an authorized administrator of Scholarworks@UAEU. For more information, please contact fadl.musa@uaeu.ac.ae.

UAEU



جامعة الإمارات العربية المتحدة
United Arab Emirates University

United Arab Emirates University

College of Engineering

Department of Mechanical Engineering

CARBON BLACK MEDIATED CONDUCTIVE POLYMER
COMPOSITE

Mohamed Hussein Faris Ali

This thesis is submitted in partial fulfillment of the requirements for the degree of
Master of Science in Mechanical Engineering

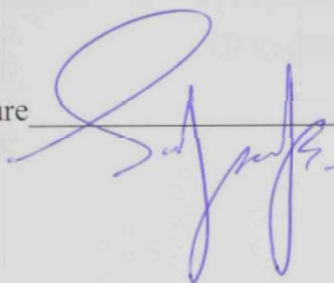
Under the Supervision of Professor Yousef Haik

December 2014

Declaration of Original Work

I, Mohamed Hussein Faris Ali, the undersigned, a graduate student at the United Arab Emirates University (UAEU) and the author of the thesis titled "Carbon Black Mediated Conductive Polymer Composite", hereby solemnly declare that this thesis is an original work that has been done and prepared by me under the supervision of Prof. Yousef Haik, in the College of Engineering at UAEU. This work has not been previously formed as the basis for the award of any academic degree, diploma or similar title at this or any other university. The materials borrowed from other sources and included in my thesis have been properly acknowledged.

Student's Signature



Date

4/2/2015

Copyright © 2014 by Mohamed Hussein Faris Ali
All Rights Reserved

APPROVAL OF THE MASTER THESIS

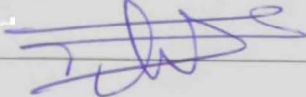
This Master Thesis is approved by the following Examining Committee Members:

- 1) Advisor (Committee Chair): Dr. Yousef Haik

Title: Professor

Department: Mechanical Engineering

College of: Engineering

Signature  Date 18/12/2014

- 2) Member: Dr. Ahmed Alawar

Title: Assistant Professor

Department: Mechanical Engineering

College: Engineering

Signature  Date 18/01/15

- 3) Member: N/A

Title:

Department:

College:

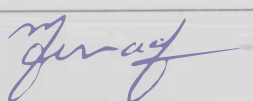
Signature _____ Date _____

- 4) Member (External Examiner): Andriaan Stephanous Luyt

Title: Professor

Department: Chemistry

College: Material Sciences/ University of the Free State- South Africa

Signature Prof-Abdel-Hamid Ismail Mourad Date _____


This Master Thesis is accepted by:

Dean of the College of Engineering: Prof. Mohsen Sherif

Signature Mohsen Sherif Date Feb. 4th, 2015

Dean of the College of Graduate Studies: Prof. Nagi Wakim

Signature Nagi Wakim Date 5/2/2015

Abstract

The central goal of this thesis is to produce electrically conductive nanocomposites made out of carbon black obtained from waste tires as filler into a polymeric matrix. Waste tires are discarded in substantial numbers on a daily basis, posing a significant environmental concern. By weight, about 25-35% of a tire is carbon black. Pyrolysis is a convenient and environmentally friendly process to produce carbon black from tires. Due to carbon black's low density, high electrical conductivity and economical feasibility, this thesis investigates the electrical conductivity of nanocomposites that utilizes carbon black particles as fillers. As a result of its modified and controllable properties, composites with fillers present a radical alternative to conventional polymers and their blends. The small size of the fillers leads to exceptionally large interfacial area in the composites. The interface controls the degree of the interaction between the filler and the polymer thus controlling the properties.

The effect of annealing temperature (550°C-1250°C) on the electrical properties of carbon black obtained from tires was investigated. Generally, the DC electrical conductivity improved when the annealing temperature increased. The modulation of the electrical conductivity as a function of annealing temperatures was explored using Raman spectroscopy, Energy dispersive X-ray, Scanning electron microscopy, X-Ray diffraction and thermo-gravimetric analysis. Annealed carbon black was used as filler in a polymeric matrix. The annealed waste carbon black was blended into epoxy at different wt. % to investigate the electrical conductivity. Furthermore, annealed carbon black was used as filler in a Carbon Fiber Reinforced

Polymer (CFRP) and then the effect of different percentage of waste carbon black was studied. After that, through plane electrical conductivity, surface electrical conductivity, through plane thermal conductivity and flexural strength were examined.

The results showed that the electrical conductivity for the annealed carbon black at 1250°C was improved to a value 40 σ/cm . Furthermore, impregnating a high amount of annealed carbon black (40 wt. %) in a polymeric matrix resulted in a low electrical conductivity of 0.0034 σ/cm .

Blending annealed carbon black into carbon fiber reinforced polymer (CFRP) resulted in alternating the electrical conductivity of the composite material. The surface conductivity of carbon fiber polymer was 2.5 σ (per square). However, the surface conductivity of impregnating 2 wt. % of annealed waste carbon black into CFRP was 13 σ (per square). The results also showed that addition of 5 wt. % of waste carbon black noticeably decreased the area specific resistance of CFRP from 199 to 98 $\text{m}\Omega\cdot\text{cm}^2$. The through-plane thermal conductivity of CFRP increased as carbon black wt. % increased. The through plane-thermal conductivity increased by 78% when the waste carbon black loading reached 16 wt. %. However, loading the composite with waste carbon black resulted in decreasing the flexural strength.

It is recommended to blend 5 wt. % of waste carbon black annealed at 1250°C into CFRP to provide enhancement in both the through-plane and surface electrical conductivity. The surface conductivity was enhanced by 80% when blending 5 wt. % of waste carbon black. The through plane resistivity reduced 51% by adding 5 wt. %

of waste carbon black. However, the flexural strength was negatively affected with a reduction of 8% only by blending 5 wt. % of waste carbon black.

Keywords: Conductive polymer composite, Waste carbon black, through plane electrical conductivity, surface electrical conductivity, and carbon fiber reinforced composite.

المواد البلمرية المركبة الموصلة بواسطة الكربون الأسود

تهدف هذه الرسالة إلى إنتاج (تحضير) مادة بلمرية مركبة موصلة كهربائياً وذلك باستخدام الكربون الأسود الموصل المتخرج من الإطارات المستهلكة. وقد تم الحصول على هذه المواد المركبة الموصلة بغرس حثوات موصلة داخل بنية المادة البلمرية. وقد هدف هذا العمل لاستخدام الكربون العالي التوصيل (والمسمى بالكربون الأسود) والمستخدم في عملية الحشو من الإطارات المستهلكة. ويتم الحصول على الكربون الأسود عن طريق عملية الإنحلال الحراري، ثم يتم عمل تخمير لهذا الكربون الأسود عند درجات حرارة مختلفة تتراوح بين 550 إلى 1250 درجة سيليزية وذلك لفحص التشكل والموصلية الكهربائية عند درجات الحرارة المختلفة. وقد لوحظ تحسن الموصلية الكهربائية المباشرة بزيادة درجة حرارة التخمير. وقد تم التأكد من هذا الإستنتاج من خلال استخدام تحليل رامان الطيفي، وتقنية حيود الأشعة السينية، والميكروسكوب الإلكتروني الماسح، وكذا تقنية الإنحلال الوزني الحراري تحت تأثير درجات حرارة مختلفة لعملية التخمير. وقد لوحظ تحسن خواص الكربون الأسود الذي حصلنا عليه من الإطارات المستهلكة وذلك بزيادة درجة الحرارة التي يتم إجراء عملية التخمير عندها.

ويمكننا استخدام الكربون الأسود المعالج حرارياً كحشو في العديد من التطبيقات العملية التي تحتاج إلى تعزيز في خواص التوصيلية للمواد المركبة. وقد تم استخدام أفضل مؤشرات المعالجة الحرارية للكربون الأسود وذلك كحشو عند تحضير وتوصيف المواد المركبة المصنعة من مادة الإيبوكسي المقواة بألياف الكربون.

وقد تم أيضاً دراسة تأثير امتداد نسب مئوية مختلفة من مادة الكربون الأسود وذلك على الموصلية الكهربائية الحجمية، والموصلية الكهربائية السطحية وإجراء اختبار متانة الانحناء إلى جانب إجراء اختبار الموصلية الحرارية.

وقد تركز الاهتمام على احتمالية زيادة الموصلية الكهربائية بزيادة النسبة المئوية لوزن الكربون الأسود المستخدم كحشو في طبقات المواد المركبة. ويتم تصنيع المواد المركبة من دمج نفايات الكربون الأسود مع مادة الإيبوكسي. ويتم التصنيع بعمل طبقات من الألياف يدويا ويتبع ذلك ضغطها باستخدام تقنية الكبس الحراري.

وقد وضحت النتائج أنه تزداد خاصية التوصيل الكهربائية للكربون الأسود كلما زادت درجة حرارة التخمير. حيث تحسنت قيمة التوصيل الكهربائية إلى (40 S/cm). وهذا يعادل أكثر من 37 ضعفاً من القيمة التوصيل الكهربائية لدرجة تخمير 550 سيليزية. وقد وضحت النتائج أنه مع زيادة النسبة المئوية الوزنية لنفايات الكربون الأسود بالمواد المركبة التي تم تحضيرها، تزداد الموصلية الكهربائية السطحية بوضوح حتى 2% من النسبة المئوية الكلية. وعلاوة على ذلك تم تسجيل زيادة الموصلية الكهربائية الحجمية بزيادة النسبة المئوية الوزنية من نفايات الكربون الأسود وذلك حتى نسبة محدودة منه. ومن ناحية الخواص الميكانيكية فقد لوحظ نقص متانة الإنحناء في المواد المركبة المحشوة بالكربون الأسود مع زيادة النسبة المئوية الوزنية منه. أما من حيث

الموصلية الحرارية، فقد لوحظ زيادتها في المواد المركبة المحشوة بالكربون الأسود مع زيادة النسبة المئوية الوزنية منه.

تقترح هذه الدراسة لاستخدام الكربون الأسود المعالج حرارياً و المستخرج من نفايات الاطارات بنسبة 5% من الوزن الكلي بنية المادة المركبة المحشوة بألياف الكربون. حيث تزداد خاصية التوصيل الكهربائية السطحية بنسبة 80%. كما تنقص المقاومة الكهربائية الحجمية بنسبة 51% على الرغم من نقصان متانة الانحناء بنسبة 8%.

Acknowledgments

I would like to thank Professor Yousef Haik for his support and guidance through this research and my graduate education. Both my experimental work and studies have been a rewarding and enjoyable experience. I also would like to thank Dr. Ahmed Al-Awar, for serving on my thesis committee. I would like to express gratitude to Dr. Ahmad Ayesh and Dr. Mohamed Hamdan for assisting me all over my research. Furthermore, I would like to thank Eng. Asmaa, Eng. Muthanna, Eng. Abulsattar and Mr. Taher for the assistance with the present work.

Finally, my special thanks go to my parents, and sisters who helped along the way. I am sure they suspected it was endless.

Dedication

To my beloved mother

Table of Contents

Declaration of Original Work	ii
Approval of the Master Thesis.....	iv
Abstract	vi
Acknowledgments.....	xi
Dedication	xii
Table of Contents.....	xiii
List of Tables	xvii
List of Figures	xviii
 CHAPTER ONE: INTRODUCTION.....	 1
1.1 Overview.....	1
1.2 Background	4
1.2.1 Intrinsic conductive polymers.....	4
1.2.2 Conductive polymer composites.....	6
1.2.3 Electrical conductive carbon fiber reinforced composite	9
1.2.4 Improvement on electrical conductivity of carbon-based polymer	10
1.3 Thesis scope.....	11
 CHAPTER TWO: CARBON BASED CONDUCTIVE MATERIAL.....	 13
2.1 Carbon based conductive filler	13
2.1.1 Graphite.....	14
2.1.2 Carbon Nanotubes.....	15
2.1.3 Carbon fiber	17

2.1.4 Carbon black	19
2.1.5 Carbon black from waste tire	20
2.1.6 The effect of the amount of carbon-based filler on the electrical conductivity	22
2.1.7 Percolation threshold concentration	23
2.2 ThermoSetting composite manufacturing techniques	24

CHAPTER THREE: CHARACTERIZATIONS AND RESULT OF WASTE

CARBON BLACK	28
3.1 Preparation of waste carbon black	28
3.2 Electrical conductivity of waste carbon black	28
3.2.1 Electrical conductivity of carbon black measuring technique	29
3.2.2 Electrical conductivity of carbon black result	31
3.3 Raman Spectrum	35
3.3.1 Raman Spectroscopy Overview	35
3.3.2 Raman spectrum result	36
3.4 Thermo-gravimetric analysis (TGA)	37
3.4.1 Thermo-gravimetric Analysis (TGA) working principle	38
3.4.2 Thermo-gravimetric analysis (TGA) result	40
3.5 X-ray diffraction technique (XRD)	42
3.5.1 X-ray diffraction principle	42
3.5.2 X-ray diffraction analysis	43
3.6 Scanning electron microscope and EDX	50

CHAPTER FOUR: CHARACTERIZATIONS RESULT OF CARBON BLACK

WITH EPOXY RESIN	55
4.1 Preparation of composite made of epoxy loaded with low wt. % of waste CB	55
4.2 Thermal properties	57
4.2.1 Thermo-gravimetric analysis (TGA)	57
4.2.2 Differential scanning calorimetry (DSC).....	59
4.3 Fourier transform infrared spectrum ((FTIR)	64
4.4 Nano-indentation of epoxy and waste carbon black	66
4.5 Electrical conductivity	69
4.5.1 Electrical conductivity using network analyzer	69
4.5.2 Electrical conductivity of highly loaded epoxy with waste CB.....	72

CHAPTER FIVE: CARBON BLACK MEDIATED CARBON FIBER

REINFORCED EPOXY CONDUCTIVE POLYMER COMPOSITE	78
5.1 Preparation of polymer matrix loaded with waste carbon black.....	78
5.2 Fabrication of fiber reinforced polymer.....	79
5.3 Through plane conductivity of solid material	83
5.3.1 Through plane conductivity of solid material	83
5.3.2 D.C result of through-plane electrical conductivity of composite sample.	85
5.4 In-plane electrical conductivity of solid material	87
5.4.1 Surface electrical conductivity of solid material measuring technique	88
5.4.2 D.C surface electrical conductivity of composite sample result.....	90
5.5 Through plane thermal conductivity	94
5.5.1 Through plane thermal conductivity measuring technique.....	96

5.5.2 Through plane thermal conductivity result	100
5.6 Mechanical properties	104
5.6.1 Flexural strength	105
5.6.2 Flexural Strength Result	106
CHAPTER SIX: SUMMARY AND CONCLUSION.....	113
Bibliography	116
Appendix A: TGA graphs for waste carbon black.....	124
Appendix B: TGA graphs for waste carbon black blended in epoxy	127
Appendix C: FTIR Spectrums for waste carbon black blended in epoxy.....	129
Appendix D: Permittivity and Reflection coefficient obtained from vector network analyzer	131
Appendix E: Load vs. deflection curves from three points bending test.	135

List of Tables

Table 3-1: ZnO XRD peaks comparison between the reference and the peaks obtained	45
Table 3-2: ZnS XRD peaks comparison between the reference and the peaks obtained	46
Table 3-3: Energy dispersive X-ray for different post heat treatment temperature....	51
Table 4-1: Technical data of ARALDITE® AY105 IN epoxy resin.....	56
Table 4-2: Different weight % of waste CB loaded in epoxy resin	56
Table 4-3: Epoxide group FTIR peaks.....	64
Table 4-4: The result of nano-indentation of epoxy loaded with different wt.% of waste CB	69
Table 4-5: Conductivity measurement for epoxy loaded with high % of waste CB ..	76
Table 5-1: Technical data of 6K, 5HS weave carbon fiber.....	79
Table 5-3: Hot press machine pressing parameters	80
Table 5-4: Determination of waste CB weight% after curing	81
Table 5-5: The result of surface conductivity	93
Table 5-6: Temperature distribution along the working bar.....	101
Table 5-7: Determination of T_A and T_B	101
Table 5-8: Result of thermal conductivity for different Wt. % of waste CB.....	102
Table 5-9: Flexural strength result obtained from three points bending test	107
Table 5-10: Modulus of elasticity from three points bending test.....	109

List of Figures

Figure 1-1: Thesis work map	4
Figure 2-1: The crystal structure of graphite	15
Figure 2-2: Models for (a) armchair (b) zigzag (c) chiral single-wall carbon nanotubes	16
Figure 2-3: Microstructural change from mesophase to graphite under heat treatment	20
Figure 2-4: Conflicting Scenarios in Achieving Good Electrical Conductivity and Mechanical Properties.....	23
Figure 2-5: Classification of polymers used as a binder in producing composite material	24
Figure 2-6: Epoxide Structure.....	25
Figure 3-1: Fixture diagram for measuring the electrical conductivity of waste carbon black	30
Figure 3-2: Measuring the electrical resistance of empty cell	32
Figure 3-3: Measuring the electrical resistance of waste CB powder annealed at 500°C	33
Figure 3-4: Electrical conductivity of post heat treated CB powder vs. the temperature of furnace	34
Figure 3-5: Raman spectra for waste CB under different heat treatment temperatures	37
Figure 3-6: TGA graph of carbon based material	39

Figure 3-7: Oxidation temperature obtained from TGA for different annealing temperatures	40
Figure 3-8: Amount of residual mass (wt. %) obtained from TGA for different annealing temperatures	42
Figure 3-9: Diffractograms of post heat treatment CB powder at different heat treatment	44
Figure 3-10: XRD peaks related to ZnO for waste CB annealed at 500°C	46
Figure 3-11: XRD peaks related to ZnS for waste CB annealed at 500°C	47
Figure 3-12: XRD peaks related to ZnS for waste CB annealed at 750°C	47
Figure 3-13: XRD peaks related to ZnS for waste CB annealed at 1000°C	48
Figure 3-14: XRD diffractogram of waste CB annealed at 1250°C	49
Figure 3-15: The common peak at $2\theta=25.2^\circ$ for all the annealing condition.....	50
Figure 3-16: SEM images for HT500	53
Figure 3-17: SEM images for HT750	53
Figure 3-18: SEM images for HT1000	54
Figure 3-19: SEM images for HT1250	54
Figure 4-1: TGA thermo-gram epoxy mixed with different wt. % of waste CB.....	57
Figure 4-2: Thermal decomposition as a function of waste CB Wt. %	58
Figure 4-3: Residual Wt. % vs. Waste CB Wt. %	59
Figure 4-4: DSC graphs for epoxy mixed with different wt. % of waste CB.....	60
Figure 4-5: Determination of Tg for neat epoxy.....	61
Figure 4-6: Determination of Tg for epoxy mixed with 3 wt. % of CB	62
Figure 4-7: Determination of Tg for epoxy mixed with 6 wt. % of CB	62

Figure 4-8: Determination of Tg for epoxy mixed with 9 wt. % of CB	63
Figure 4-9: Glass transition temperature as a function of waste CB Wt. %	63
Figure 4-10: FTIR spectra for epoxy mixed with different wt. % of waste CB	65
Figure 4-11: Loading-unloading curve for neat epoxy	67
Figure 4-12: Loading-unloading curve for epoxy mixed with 3 wt.% of waste CB ..	67
Figure 4-13: Loading-unloading curve for epoxy mixed with 6 wt. % of waste CB .	68
Figure 4-14: Loading-unloading curve for epoxy mixed with 9 wt. % of waste CB .	68
Figure 4-15: Conductivity as a function of electromagnetic frequency for epoxy with different waste CB wt.%	71
Figure 4-16: Placing epoxy/CB sample between electrodes.....	72
Figure 4-17: Cross section area of the prepared epoxy/CB samples	74
Figure 4-18: I-V plot for epoxy with 30 wt. % of waste CB	75
Figure 4-19: I-V plot for epoxy with 40 wt. % of waste CB	75
Figure 4-20: Result of electrical conductivity of epoxy/CB.....	76
Figure 5-1: Hot press machine	80
Figure 5-2: Waste CB wt. % vs. sample thickness	82
Figure 5-3: Wt. % of the matrix included waste CB vs. sample thickness.....	83
Figure 5-4: Through plane electrical conductivity measuring setup	84
Figure 5-5: Through plane electrical conductivity result.....	86
Figure 5-6: Area specific resistance (ASR) of carbon fiber composite at different waste carbon black loadings	87
Figure 5-7: Surface electrical conductivity (four points' probes.) setup using conductive paste	89

Figure 5-8: Surface electrical conductivity (surface conductivity) using copper strips as electrodes under compression load.....	89
Figure 5-9: Four point connections using silver conductive paste for in-plane conductivity test.....	91
Figure 5-10: Four point connections using copper electrodes for surface conductivity test.....	92
Figure 5-11: Surface electrical conductivity σ (per square) vs. waste CB wt. %.....	94
Figure 5-12: Schematic illustration of through-plane and in-plane directions.....	96
Figure 5-13: Thermal conductivity apparatus.....	97
Figure 5-14: Setup and location of thermocouples.....	99
Figure 5-15: Temperature distribution along apparatus bar for all the prepared carbon fiber reinforced samples.....	102
Figure 5-16: Thermal conductivity of the laminate vs. wt. % of waste CB.....	103
Figure 5-17: Flexural strength obtained from three points bending test.....	108
Figure 5-18: Modulus of elasticity obtained from three points bending test.....	109
Figure 5-19: Fracture for sample with 0% of waste CB.....	110
Figure 5-20: Fracture for sample with 2% of waste CB.....	111
Figure 5-21: Fracture for sample with 8% of waste CB.....	111
Figure 5-22: Fracture for sample with 16% of waste CB.....	112

CHAPTER ONE

INTRODUCTION

Electrically conductive polymers are sought for a number of industrial applications. This chapter outlines the difference between the intrinsically conductive polymers and electrically conductive composites. The aim of this thesis is to produce an electrically conductive polymer composite that utilizes a byproduct of tires recycling as a filler. The electrical conductivity of the composite is modulated by the percentage of the filler in a polymeric matrix.

1.1 Overview

A good number of research results have recently surfaced in the literature to signify the different approaches in producing highly electrical and thermal conductive polymer composite material to replace metallic components. Researchers are focusing on conductive polymers for applications such as; bipolar plate used in Proton Exchange Membrane Fuel Cell (PEMFC), antistatic material, conductive films and electromagnetic shielding material. Many factors contribute to the performance of conductive composites, such as the electrical conductivity of fillers, diameter and structure of fillers, state of dispersion, process type, and most importantly the concentration of fillers. Carbon black is used as conductive filler to produce electrical conductive polymer composite.

Conductive composites are achieved by impregnating fillers into the matrix. In order to enhance the electrical conductivity of composite material, high filler loadings are necessary to generate network of conductive channels. The bulk majority

of literature reports have been focusing on carbon based polymer composites. The growing interest in carbon fillers is related to the fact that they have low density and can be produced in different particle size and morphology. Different carbon base materials are commercially available such as carbon nanotubes (CNT), expanded graphite and carbon black (CB) in which they are electrically conductive filler. However, the production of highly electrical and thermal conductive carbon based composite has been achieved but is not yet economically feasible due to the following reasons:

- The quality of dispersion is an important factor that affects the generation of conductive channel in the composite and the dispersion of conductive filler is not uniform if conventional industrial plastic manufacturing techniques are used.
- Extra rich polymer layer is generated on the top surface of composite material which results in blocking the electrical conductive network generated by the filler.
- High loading of conductive filler results in decreasing the mechanical properties of the composite.

The main focus of this research is to develop electrically conductive material made out of polymer composite. The objective is to develop a material that is easy to manufacture by utilizing carbon-based material from waste tires as a conductive filler.

The research work is divided into three parts as is shown in Figure 1-1. The first part includes the preparation and the characterization of CB obtained from waste

tires by a pyrolysis process. Firstly, in order to enhance its electrical conductivity, the CB was annealed under different temperatures from 550°C to 1250°C. Then, morphology and the electrical conductivity were investigated. Later, the DC electrical conductivity was improved by increasing the annealing temperature. The resulting electrical conductivity was correlated to Raman spectroscopy, Energy dispersive X-ray, scanning electron microscopy, X-ray diffraction and thermogravimetric analysis.

Secondly, carbon black with the highest electrical conductivity was mixed with epoxy resin to investigate the feasibility of using CB in polymer binder and generate a valuable solid composite material. Different percentages of waste CB were mixed with epoxy resin. After that the mixture was casted into molds to investigate the electrical conductivity as a function of waste CB Wt. %.

In the third part, the highest annealing condition of waste CB was used as a filler in the preparation and characterization of composite material that was made of carbon fiber reinforced with epoxy resin (CFRP). The effect of different percentages of waste CB is also investigated. In-plane electrical conductivity, through plane electrical conductivity, flexural strength and thermal properties were investigated. The attention was focused on the possibility of increasing the electrical conductivity as a function of the waste carbon black weight percentage in the composite laminate. The composite was manufactured by incorporating the waste CB into the epoxy resin. The composite is fabricated by hand lay-up followed by hot pressing.

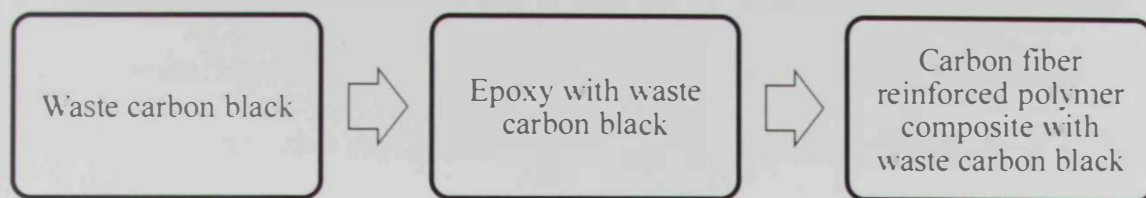


Figure 1-1: Thesis work map

1.2 Background

Generally, the conductive polymeric materials are classified into two parts, intrinsically conducting polymers (ICPs) and conductive polymeric composites (CPCs). The intrinsically conducting polymers are organic polymer semiconductors. Unfortunately, the cost of its production is relatively high and its applicability is limited as a result of poor productivity (Gurunathan et al., 1999).

On the other hand, conductive polymeric composites possess large-scale variation in electrical conductivity. However, its mechanical performance is limited (Taherian et al., 2013).

1.2.1 Intrinsic conductive polymers

Intrinsic conductive polymers are typically conjugated hydrocarbon and aromatic heterocyclic polymers. Some examples of intrinsic conductive polymers that have been investigated include: polyacetylene (PA), poly(p-phenylene) (PPP), poly(p-phenylene vinylene) (PPV), poly(p-phenylene sulfide) (PPS), polyaniline (PANI), polypyrrole (PPy) and polythiophene (PT) (Gurunathan et al., 1999). These polymers suffer from their inability to resist harsh industrial operational conditions, like acidic environment, high temperature and high humidity. In addition to being infusible and insoluble, the processability of most conductive polymers is very poor. Also,

manipulating conductive polymers into desired shapes is quite difficult. The dopants used in manufacturing the polymers make them highly reactive and chemically unstable. They are also costly and yet prone to thermal degradation. Structurally, conductive intrinsic polymers are generally rigid and brittle. These features are also detrimental to the mechanical properties of the polymer. Research has been conducted to determine the best combination for conductive polymers.

A low conductivity was reported for doped PANI/poly (methyl methacrylate) (PMMA) blend that was developed and tested by (Minto et al., 1996). The reported conductivity at 20wt% of PANI was less than 10 S/cm, which is extremely low.

Also, Banerjee and Mandal (1995) developed and tested a polyaniline (PANI) nanoparticle that was filled with poly (vinyl alcohol) (PVA) composites. The percolation threshold concentration used in the development was just 9 wt% of PANI, while a low electrical conductivity of 1 S/cm was obtained. Other polymers that can be used as matrix include: poly-vinyl-chloride (PVC), polystyrene (PS), poly-methyl-methacrylate (PMMA), and poly-vinyl-acetate (PVAc). Cho (2004) prepared nano-sized polyaniline (PANI) particles dispersed in aqueous solution. The polymeric stabilizers used in the development were poly-vinyl-alcohol (PVA) and poly-styrene-sulfonic acid (PSSA). A very low conductivity that is less than 0.1 S/cm was reported. An improved polyethylene/polyaniline (PE/PANI) was developed by Annala and Löfgren (2006). The mechanical properties of the blend was greatly boosted by plasticized PANI/camphorsulfonic acid (CSA) complexes and -OH functionalized polyethylene (PE). However, the reported electrical conductivity was less than 1 S/cm.

1.2.2 Conductive polymer composites

Conductive polymer composites offer more reliable electrical conductivity and better mechanical properties than intrinsic conductive polymeric materials. This is significant especially where good mechanical properties are important to replace the metallic parts. These polymers are obtained by incorporating the conductive filler into the structural design of the polymer matrix. The fillers are usually in the form of powder, flakes, fibers, or layered forms and are mostly carbon-based material. The incorporation process is obtained through melting or solution mixing. The dispersed materials are then molded to different parts by using readily available processing methods, such as injection molding, compression molding or extrusion, etc.

During the molding process, it is possible to manipulate the mechanical and electrical properties of the final products by integrating different types, grades and quantities of conductive fillers. The main materials used as conductive fillers include graphite, nanotube, carbon fiber, carbon black, etc. The advantages of conductive composites over intrinsic conductive polymers have encouraged research, which has consequently led to the production of different conductive composites.

This class of polymer composite has been widely investigated by a number of researchers. Specific studies aimed at understanding the applicability of carbon-based composite with both thermoplastic and thermosetting resins, have been extensively carried out.

Carbon-based polymer composites were studied in both polymer types, thermosetting and thermoplastic resins. The thermoplastic resins that are generally used include liquid crystalline polymers, polypropylene (PP), polyether sulphone

(PES), polyethylene (PE), poly-arylene-disulfide, poly-vinylidene-fluoride (PVDF), PET /PVDF blend, poly-phenyl-sulphone (PPS), nylon 6 (PA6) and polyethylene terephthalate (PET), while thermosetting resins include epoxy resin, vinyl-ester, cyanate ester and polyester. Commonly, the electrical conductivity of these polymers can be increased by utilizing conductive fillers such as expanded graphite, natural graphite, synthetic graphite, carbon black, carbon nanotubes and nanofibers (Antunes et al., 2011).

Different manufacturing techniques are adopted in the production of conductive composites. Composites with thermoplastic resin are restricted to the technique of extrusion and injection molding. However, composites with thermosetting resin use different techniques such as wet layup, resin transfer mold, vacuum infusion, autoclave and light resin transfer mold. The quality of filler dispersion is highly dependent on the proper manufacturing process.

In the following section; some examples of conductive polymer composites include both thermoplastic and thermosetting polymers that have been developed are discussed.

Dweiri and Sahari (2007) determined the electrical conductivity of PP/graphite/CB composite, which are manufactured by compression molding process. The value obtained at a graphite loading that is below 80 wt.%, is found to be 7S/cm. In other research, Yin (2007) discovered that an electrical conductivity of 100S/cm can be obtained by very high loading of 85 wt. % graphite powder.

The electrical conductivity value of carbon-based polymer composite that is filled with carbon black, carbon fiber, unexpanded graphite or their combination

ranges between 10^{-3} and 300 S/cm. There is an urgent need for future research to investigate alternative conductive fillers or filler combinations. One of the best choices is expanded graphite as suggested by Du (2008).

Liao (2008) reported the bulk conductivity of PP/graphite composite mixed with multiwall carbon nanotubes, that is manufactured by melt compounding and compression molding processes. The value obtained at a graphite loading that is below 80 wt. %, was found to be above 100S/cm.

Leu (2012) used the selective laser sintering method to develop conductive composite plates that are made up of different graphite materials. When compared to conventional methods like compression molding and injection molding, the selective laser sintering is found to be less expensive and more convenient for developing conductive plates. The different graphite materials that were used and compared are Natural Graphite (NG), Synthetic Graphite (SG), Carbon Fiber (CF) and Carbon Black (CB). The conductive plates were fabricated using the selective laser sintering process with the material composition of 45vol% natural graphite, 10vol% carbon fiber, 10vol% synthetic graphite and 35vol% binder. The results showed an increased electrical conductivity with natural graphite and increased flexural strength with carbon fiber.

On the other hand a negative result was obtained when the nano-sized carbon blacks - which cover the surface of natural graphite particles - were used. In this case, the values of both the electrical conductivity and flexural strength dropped (Alayavalli and Bourell, 2010).

Leu (2012) also recorded a reduction in electrical conductivity with synthetic graphite and an insignificant negative effect on flexural strength. While the methods employed in manufacturing the conductive plates had no significant effect on the electrical and mechanical properties. Thus, the results obtained by Leu (2012) are still similar to what is obtainable with graphite composite fabricated using injection molding and compression molding methods. For instance, in an experiment to determine the effect of graphite nanofibers on poly (methyl methacrylate) nanocomposites for conductive plates, Park (2009) discovered improvement in the electrical, thermal, and mechanical properties of the poly (methyl methacrylate) (PMMA) polymer. The results show that the desirable properties of graphite can be improved through the use of graphite nanofibers. The electrical and mechanical properties are all improved by these components.

1.2.3 Electrical conductive carbon fiber reinforced composite

Carbon fiber reinforced composites are widely used for lightweight structure because of the high strength to weight ratio and good corrosion resistance. Moreover, carbon fiber is highly electrically conductive although the polymer matrix is not conductive.

Many studies demonstrated that it is feasible to produce highly electrically conductive material made from polymer composite to replace the metallic part. Those studies can be used, for example in fuel cells stacks application, to avoid corrosion phenomena while maintaining good electrical conductivity. Moreover, the carbon fiber reinforced composite used in aerospace structures must be electrically conductive to avoid build up charge generated due to air friction and lightning strikes (Pozegic et al., 2014).

The uniqueness of this electrically conductive composites depends on the amount of graphite weight percentage in which they are produced through different techniques with different electrical and mechanical properties. Many types of electrically conductive composite are commercialized but they are not economical.

1.2.4 Improvement on electrical conductivity of carbon-based polymer

Many studies have demonstrated that increasing the electrical, mechanical and thermal properties of the composite can be achieved by reinforcing the polymer with carbon based fillers such as carbon black and carbon nanotubes. However, the top and bottom surfaces of the conductive carbon-based composite suffer from the growing extra rich layer of polymer, which prevents the electrical conductive carbon network generated from the carbon-based filler this consequently leads to a drop in electrical conductivity.

Usually, the techniques of improving the electrical surface conductivity are classified into two categories:

1. Rectification of conductive composite surface

Rectification of the surface of a composite polymer strongly depends on the composite fabrication technique. An extra rich layer of polymer is generated on the part that is produced by injection molding for thermoplastic polymer. Moreover, thermosetting polymers also generate an extra rich layer of polymer for the part produced by wet layup. As a result, an extra operation is needed in order to remove this extra rich polymer layer. Kim et al. (2012) and Kim et al., (2013) demonstrated that treating the surface of composite can be done by different techniques, either by

flaming or coating the surface with graphite through which it can increase the surface conductivity or using a 120-grit silicon carbide in removing the extra rich polymer layer. Although these techniques solve the problem they will however increase the cost of composite preparation. On the other hand, producing conductive polymer composite from compression molding did not suffer from this extra rich layer of polymer that blocks the electrical network channel and hence surface rectification was not needed (Du, 2008).

2. The use of a conductive-tie layer (CTL).

It has been reported by Besmann (2000), (Kumar et al., 2003), (Pozio et al., 2008) (Antunes et al., 2011), and (Kim et al., 2012) that the interfacial contact resistance between the conductive composite material contributes more than the bulk resistance of the material especially at low compression pressure. The contact resistance depends on different factors; the roughness of the surface, compression pressure and the flatness of the part. To reduce the contact resistance, a highly conductive tie is placed on the surface to mitigate the previously mentioned factors.

1.3 Thesis scope

The purpose of this work is to produce electrically conductive composite material made out of carbon based polymer by utilizing the carbon black recovered from waste tires. Mainly, the recovered waste carbon undergoes a post heat treatment to enhance the electrical conductivity. Hence, the effect of post heat treatment condition on the waste carbon black was studied. Then, a carbon fiber/epoxy composite reinforced with CB obtained from waste tire is prepared using different

weight percentages. After that, the influence of the weight percentage of the waste CB on the electrical properties, flexural strength, and thermal conductivity was investigated.

The electrically conductive composites can be used widely in the application of conductive materials such as fuel cell electrodes, antistatic material, sensors, batteries and electromagnetic interference shielding material. The motivation of this thesis is to produce a solid conductive composite that can be produced in any desired geometry with thickness approximately 2mm. Therefore, the utilizing of waste carbon black will be investigated.

CHAPTER TWO

CARBON BASED CONDUCTIVE MATERIAL

As this study focuses on utilizing carbon black from waste tires, different types of carbon based conductive fillers such as graphite, carbon black and carbon nanotubes are presented in this chapter. In addition, the production techniques of carbon black are presented.

2.1 Carbon based conductive filler

Diverse kinds of carbon based conductive fillers are commercially available such as expanded graphite, carbon nanotubes and carbon black. Carbon is known for being the lightest element within the group IV and the sixth element in the periodic table. Moreover, carbon has four electrons in its valence shell. The configuration of the electrons is $1s^2 2s^2 2p^2$, this energy shell can share up to four different atoms. sp^2 is the ground state phase of carbon called bonded graphite. At higher temperature and pressure, sp^3 is the stable form of bonded cubic diamond (Bandaru, 2007).

Carbon can be found naturally in three allotropic forms, amorphous carbon, graphite and diamond. Recently, researchers have focused on the graphite and its derivatives which have a potential use in semiconductor and electronics applications (Bandaru, 2007).

Although metallic particles have higher electrical conductivity than carbon base conductive fillers, they have higher density and suffer from corrosion especially in applications that require exposure to high acidic environments such as fuel cells.

Diffusion of acidic solution into conductive parts results in corrosion of metallic fillers in which the electrical conductivity and mechanical properties drop.

2.1.1 Graphite

Figure 2-1 shows that atomic structure of graphite consists of graphene layers arranged in hexagonal linked carbon atoms. The intermolecular forces between the parallel graphene layers are Van Der Waals forces. The interatomic distance within the layer (a) is 1.42 Å where the interlayer distance (d) between planes is 3.35 Å. The covalent bonding is generated between three carbon atoms and the fourth valence (π electron) resonates between the valence bond structures. A strong chemical bonding force exists within the graphene plane. However, the bonding force between the graphene planes is the Van Der Waals force in which this force is only around three percent of the bonding force within the layer. The graphene layers are stacked in ABAB sequence (Inaba, 2009).

The overlap of π orbitals on adjacent atoms in a given plane provides the electron bond network responsible for the high mobility of graphite. Van Der Waals is a weak force and it is a result of dipole moments, which does not contribute significantly to the high mobility (Bandaru, 2007).

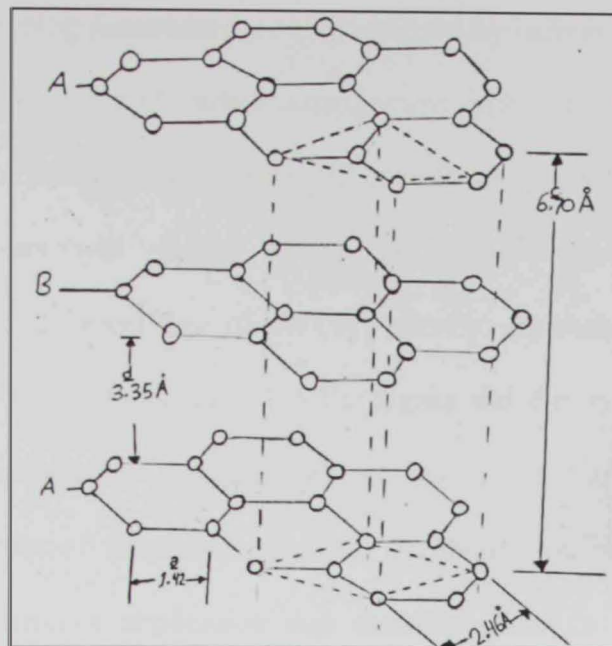


Figure 2-1: The crystal structure of graphite (Inaba, 2009)

2.1.2 Carbon Nanotubes

Carbon nanotubes (CNT) consist of graphene sheets rolled in cylindrical shape with hemispheres of fullerenes at both ends. Since the discovery of fullerenes by Kroto et al in 1985 (Callister et al., 2008) and carbon nanotube in 1991 (Popov et al., 2006), many researchers have focused on small carbon clusters. The name is derived from the long and hollow structure of the graphene sheet. The most stable form of CNT is C_{60} . Different structures of the produced CNT due to different growth conditions are shown in Figure 2-2. The sheets of graphene layers are rolled with specific angles and radius that determine the nanotube properties. Nanotubes are classified as single walled nanotubes (SWNTs) and multiwall nanotubes (MWNTs) (Bandaru, 2007).

SWNTs have a diameter close to 1 nanometer with length to diameter ratio reaching to millions. SWNTs are shaped into seamless cylinders by wrapping a single layer of

graphene. The wrapping parameters are characterized by indices (n, m) which donate the number of unit vector of carbon arrangement within the flat single sheet of graphene layer. The indices arrangement will change the properties of SWNTs as the wrapping parameters will change. Figure 2-2 shows that different wrapping parameters generate different type of SWCNT namely, armchair, zigzag, and chiral. For example, if $m=0$ this means that SWNT is zigzag and if $n=m$ then this means that the nanotube is armchair. As a result, SWNTs have different arrangements that will change the properties of nanotubes based on the indices (n, m) . SWNT is one of candidates in electronics application and electrical wires as they are excellent conductors (Bandaru, 2007).

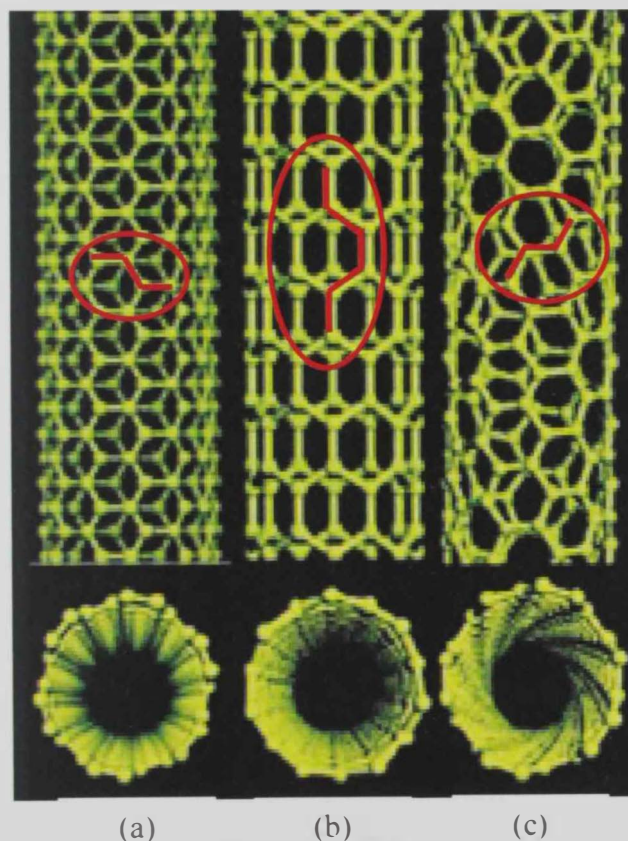


Figure 2-2: Models for (a) armchair (b) zigzag (c) chiral single-wall carbon nanotubes

(Bandaru, 2007)

The second classification of carbon nanotubes is the multiwalled nanotubes (MWNT). MWNT consists of multiple graphene layers (concentric tubes) wrapped into a cylindrical shape. Two different models can describe MWNTs; one of them is where the sheets of graphene are arranged into concentric cylinders, while, in the other description, one single sheet of graphene is rolled around itself. The interlayer distance in MWNTs is close to the interlayer distance between graphene layers in graphite and is approximately 3.4Å (Bandaru, 2007).

2.1.3 Carbon fiber

Carbon fiber is widely used in manufacturing of structures and sport equipment. For instance, Airbus Co. produces passenger airplanes with 20% of the structure made of carbon fiber reinforced polymer (CFRP) (Mangalgi, 2008). The new structure is 25% stronger and 20% lighter than aluminum structure. This is expected to reduce fuel consumption and also to decrease the environmental impact even though it's still expensive to produce as compared to aluminum airframe (Hoa,1980; Hahn,2009).

Carbon fiber is a type of graphite related material. The fiber is made into fine thread, and woven fiber of different directional, chopped short cloths and braids. This type of fiber measures 5-10 micrometers in diameter and is mainly composed of carbon atoms. It is known as graphite fiber and its chemical structure consists of carbon atoms which are bonded together in crystal along the axis of fiber. In this type of fiber the longitudinal strength is higher than the transverse strength. In addition, it is made of thousands of carbon filaments. The atomic structure of carbon fiber is similar to graphite which is made of graphene sheets arranged in a hexagonal pattern

connected with an intermolecular force, the Van Der Waals forces similar to those in graphite (Inaba, 2009).

Depending on the precursor to make the fiber, carbon fiber may be turbostratic, graphitic, or have a hybrid structure with both graphitic and turbostratic parts present (Mallick, 2008). In turbostratic carbon fiber, the sheets of carbon atoms are haphazardly folded and crumpled together. Usually, carbon fibers derived from polyacrylonitrile (PAN) are turbostratic whereas carbon fibers derived from mesophase pitch after heat treatment at temperatures exceeding 2200 °C are graphitic. Turbostratic carbon fibers tend to have high tensile strength whereas heat-treated mesophase-pitch-derived carbon fibers have high Young's modulus (i.e., high stiffness or resistance to extension under load) and high thermal conductivity (Hoa, 2009; Mallick, 2008).

Below the advantages and disadvantages of carbon fiber are briefly listed.

1. Advantages of carbon fiber:

- Highly electrical conductivity
- High strength to volume ratio
- High chemical resistance
- Low thermal expansion
- Vibration damping (Mallick, 2008)

2. Disadvantages of carbon fiber:

- High cost
- Low impact resistance (Mallick, 2008)

2.1.4 Carbon black

Carbon black (CB) is a form of disordered carbon that is widely used in industry as dispersed fillers to modify the mechanical, electrical and optical properties of materials. It is an amorphous carbon and that is referred to the nongraphitic. CB is composed of pure carbon in aciniform (cluster like grapes). Each entity of aciniform consists of spheroidal particles fused together in a cluster branched with irregular shape called aggregates.

X-ray investigation demonstrated that the carbon structure of CB contains some random distorted graphene layers within the layer planes which are called turbostratic. CB can be heat treated to become graphite at temperatures between 1700 to 3000°C as it shown in Figure 2-3. The process of heat treatment classifies the carbon into two categories, graphitizing and nongraphitizing. The differences are in the apparent stack height (higher in graphitizing), average number of layers per stack (less for nongraphitizing) and the long range order of graphene layers stacking for graphitizing. Moreover, the interlayer spacing and crystallite size also are affected by the heat treatment. The interlayer spacing decreases as heat treatment temperature increases (Arai, 1993).

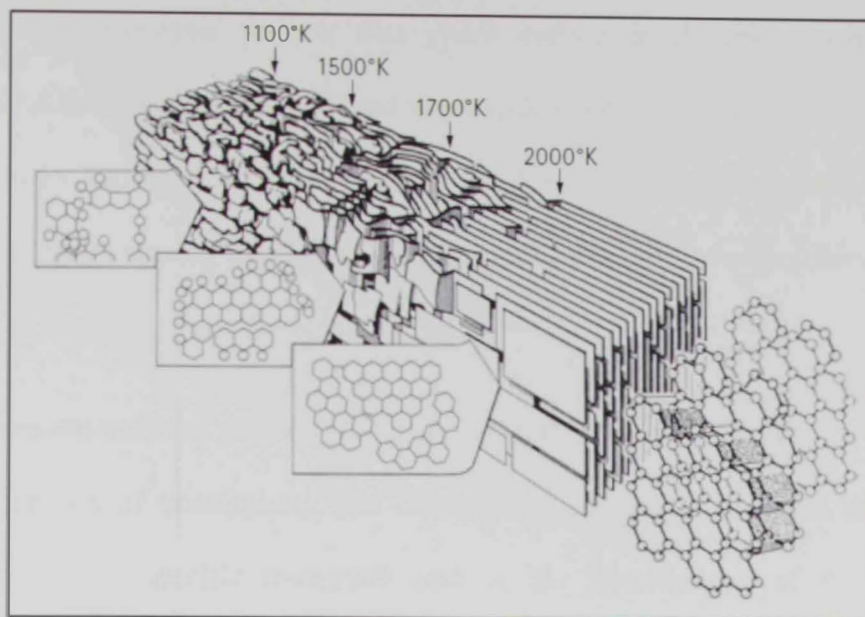


Figure 2-3: Microstructural change from mesophase to graphite under heat treatment

An enhanced type of graphite called expanded graphite (EG) is more effective than carbon black especially in producing electrically conductive polymer composites. EG can be produced by using intercalation agents like sulphur or nitrogen compounds to introduce atoms or small molecules of carbon between the carbon layers (Du, 2008).

2.1.5 Carbon black from waste tire

A number of industrial processes have been utilized to produce carbon blacks. For example, thermal decomposition of natural gas produces thermal blacks, partial combustion of oil produces furnace blacks, and exothermic decomposition of acetylene produces acetylene blacks. The chemical and physical properties for the carbon blacks vary with the synthesis route. A number of studies, namely (Celzard, 2002; Undria et al., 2013; Pantea et al. 2003; Darmstadta et al., 2000; DanielMartínez et al., 2013; Betancur et al., 2009; Mis-Fernandez et al., 2008) have shown the possibility of synthesis of carbon black from waste tires. The tires are

subjected to a pyrolysis process that yields carbon black among other carbon products. 1.4 million tires are produced worldwide every year. Despite an increase of tires durability and increase of recycling, the volume of scrap tires is still increasing because of the increasing number of vehicles and traffic worldwide (European Tyre and Rubber Manufacturers' Association, 2010).

Tires are made of rubber (60–65 wt.%), carbon black (CB) (25–35 wt.%) and the rest consists of accelerators and fillers (like sulphur, zinc oxide and others) depending on the specific trademark and on the specific use of the tire. The accelerators are usually added toward the end of the mixing cycle when the temperature of the mill or internal mixer falls (DanielMartínez et al., 2013).

Pyrolysis is a convenient environmentally-friendly process to convert the scrap tires into valuable products. Different studies were carried out to optimize the process of pyrolysis by modifying the process condition parameters (such as pyrolysis temperature and heating rate) to obtain more wt. % yield of char and liquids, but without significant improvement in the CB grade (Betancur et al., 2009). The economics of this process depends on the quality and value of extracted products (European Tyre and Rubber Manufacturers' Association, 2010; DanielMartínez et al., 2013; Pantea et al., 2003).

The commercial CB is an amorphous carbon of quasi-graphitic structure. The XRD studies on CB indicated small graphite-like layers in which the carbon atoms had the same atomic positions and short range order as in graphite. CB obtained from pyrolysis differs from the commercial CB since it contains amounts of inorganic

components such as ZnO and S. The carbonaceous is formed by polymerizing the hydrocarbon generated from the decomposing elastomer during the pyrolysis process (Darmstadta et al., 2000). Thus, the CB obtained from the pyrolysis process contains some amount of carbonaceous material deposited on the surface of CB.

(Pantea et al., 2003) studied the effect of heat treatment of CB obtained from pyrolysis and found out that this can improve the polyaromatic character of the CB surface by desorbing some amount of carbonaceous deposition. Thus, heat treatment of the CB from pyrolysis can improve the chemical properties and hence increase the economic value of scrap tires.

2.1.6 The effect of the amount of carbon-based filler on the electrical conductivity

The amount of conductive filler immersed in composite material is characterized by the percolation threshold. The conductivity of material depends on and increases as a function of the amount of filler. At a certain amount of filler, the conductivity value starts to be almost constant and only slightly increases as the filler weight increases. This phenomenon is called the percolation threshold. Many studies recommended preparing conductive composite material within the percolation threshold region because large filler contents dramatically reduce the mechanical properties of the conductive material. Hence, the amount of filler must be optimized and well dispersed in the polymer matrix to achieve high electrical conductivity without significant reduction in the mechanical properties. As the filler concentration increases, global networks of conductive particles are generated to form electron conductive paths. These two requirements are illustrated in Figure 2-4, which shows

that good electrical conductivity and high mechanical properties are conflicting with each other. Therefore, the amount of conductive filler must be within the percolation threshold concentration (Du, 2008).

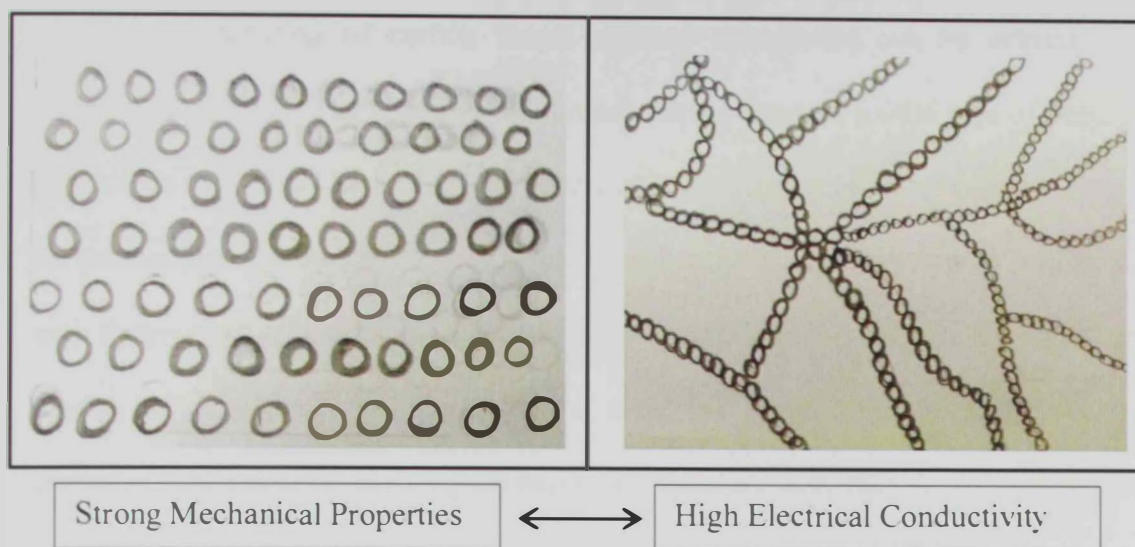


Figure 2-4: Conflicting Scenarios in Achieving Good Electrical Conductivity and Mechanical Properties

2.1.7 Percolation threshold concentration

The percolation theory describes the behavior of the connected clusters in a random pattern. The percolation threshold represents a quantification of the percolation theory. It describes the creation of a long range order of conductivities in a system. Below this threshold, the connected components do not exist. In a carbon-based polymer, the electrons percolate in the connecting path of conductive carbon particles. At the percolation threshold, the electrical conductivity increases by many orders of magnitude. Therefore, the material undergoes a transition from insulator to conductor. It is also noted that the polymer can be loaded with a limited amount of carbon based filler in which the polymer can bind to the particles. In this case the

material is at the CPVC condition. It is also noted that the material becomes more brittle and porous at levels that approach or pass the CPVC (Du, 2008).

2.2 Thermosetting composite manufacturing techniques

Manufacturing of carbon based polymer composites can be achieved by different techniques. The technique of manufacturing depends on the type of polymer (binder) as shown in Figure 2-5. Different manufacturing techniques were adopted in the production of conductive composites. The manufacturing processes of composites with thermoplastic binders are different from those of composites with thermosetting binders. Composites with thermoplastic resin are limited to the techniques of extrusion and injection molding. Whereas composites with thermosetting resin are produced by various techniques such as wet layup, resin transfer mold, vacuum infusion, autoclave and light resin transfer mold. On the other hand, the quality of filler dispersion is highly dependent on the proper manufacturing process.

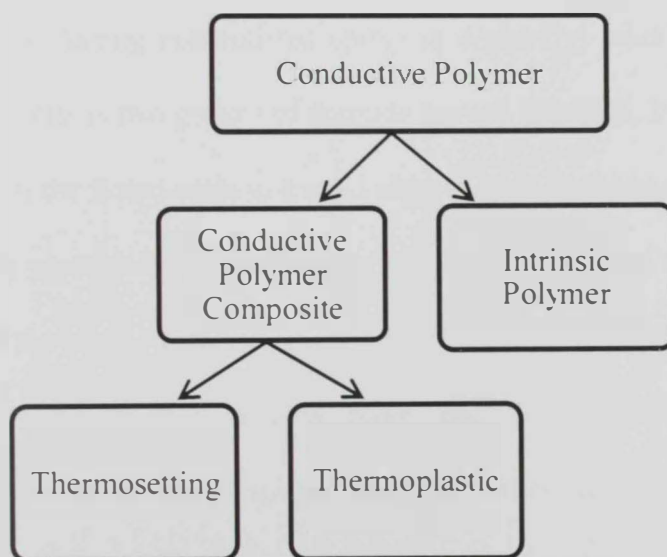


Figure 2-5: Classification of polymers used as a binder in producing composite material

In this study, a thermosetting composite was adopted. Thermosetting resins include epoxy resin, vinyl-ester, cyanate ester and polyester. Epoxy is the most common thermoset resin that is widely used in industry such as composite matrix, structural adhesives and coatings because of the low cost, corrosion resistance, low shrinkage after curing and excellent mechanical properties compared to other thermosetting resins (Rane et al., 2014). It is a low molecular weight organic liquid containing a number of epoxide groups shown in Figure 2-6, which are three member rings of one oxygen and two carbon atoms (Mallick, 2008).

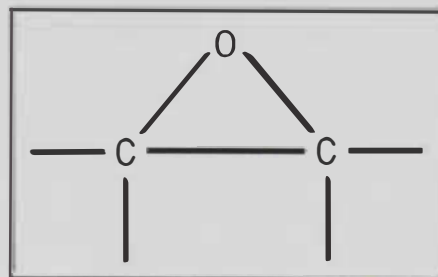


Figure 2-6: Epoxide Structure (Mallick, 2008)

The common starting material for epoxy is diglycidyl ether of bisphenol A (DGEBA), which contains two groups of epoxide groups (Mallick, 2008). The curing reaction to transform the liquid resin to a solid state is done by adding a small amount of a reactive curing agent (called catalyst) just before impregnating the fiber into the liquid mix. One of the simple catalysts is diethylene triamine (DETA). The hydrogen atoms in amine NH_2 group of DETA molecule react with the epoxide groups of DGEBA molecules to form cross linkages with each other and a three dimensional network structure is formed. Finally, the result is a solid epoxy polymer. (Mallick, 2008). The strained three-membered epoxide groups are quite reactive towards various catalysts and cross linking agents. The glycidyl groups in an aromatic epoxy

resin are flexible segments that reduce the resin viscosity and enhance the processability. The linkages in glycidyl groups are the source of thermal degradation of cured epoxy.

Moreover, the amount and type of catalyst strongly affects the properties of the final solid polymer. It also affects the speed of curing and the chemistry of polymerization. The polymerization takes place by three steps: initiation, propagation and termination. Organic bases (Lewis bases) are suitable for curing of epoxy such as tertiary amines. The ratio of catalyst to resin is also an important factor in the speed of curing and final material performance (Mallick, 2008).

Selection of composite materials in the design stage provides design flexibility given that the geometry can be easily copied into complex shaped molds. Further, production of composite panels with specific mechanical properties is achievable since the composite is made of a sandwich of layers, foam cores and fillers. Consequently, the composite material can be designed to meet specific requirements or specifications (Mallick, 2008).

Many manufacturing processes for composite panels are widely used. Selection of any of them depends on different requirements including the following:

1. Number of panels needed to be produced
2. Configuration of the panel
3. Type of fiber and resin
4. Geometrical and dimensional tolerances
5. Volume fraction between the fiber and resin
6. Surface finish (Mallick, 2008).

A hand lay-up process technique was adopted. The hand lay-up is the simplest and cheapest process for low production.

1. The advantages of using hand-layup:

- 1.1 Any type of fibers and resins can be used in this technique
- 1.2 Low cost of tooling
- 1.3 Adaptation of mold modification to produce different configurations

2. Disadvantages of using hand-layup:

- 2.1 Poor quality in geometry and thickness of the panel due to lack of compaction control and the entrapment of air during lamination process
- 2.2 Only one surface can be controlled so it cannot provide uniform thickness along the panel
- 2.3 Very difficult to control the ratio between fiber and resin
- 2.4 High probability of generation of some voids and air traps that influence the structure properties and the quality. Therefore, the quality of the panel depends on the skills of the labor (Mallick, 2008).

However, the disadvantages of hand-layup will be eliminated by using a second operation which is hot pressing. Hot pressing is used to eliminate any voids and air traps within the laminates and provide high quality flat surfaces on both sides of the produced samples. Furthermore, hot pressing will squeeze the laminated composite and remove the extra amount of resin. Thus, the volume fraction of fiber to resin will be controlled.

CHAPTER THREE

CHARACTERIZATIONS AND RESULT OF WASTE CARBON BLACK

This chapter illustrates the adopted techniques to investigate the effect of annealing waste carbon black on electrical conductivity at different annealing temperatures. The effect on electrical conductivity is also correlated with other tests such as Raman spectroscopy, X-ray diffraction and thermo-gravimetric analysis. The result of each technique is reported.

3.1 Preparation of waste carbon black

CB was produced using a pyrolysis process of waste tires using similar procedure as reported in (Undria et al., 2013; DanielMartínez et al., 2013; Betancur et al., 2009; Mis-Fernandez et al., 2008; Pantea et al., 2003). Briefly, 20 tires, 7 kg each were placed in a pyrolysis reactor. Oil, CB and tire steels were extracted. After that, the CB obtained from the pyrolysis process was annealed under different temperatures. This was performed by filling a steel container with roughly 20 grams of CB. Then, the container was placed in the furnace that has a maximum operation temperature of 1400°C (RHF1600, Carbolite, UK) under ambient pressure. The heating rate and annealing duration were fixed for all the samples at 50 °C per minutes and 1 hour respectively. The prepared samples were labeled according to the temperature of heat treatment which are HT500, HT750, HT1000 and HT1250.

3.2 Electrical conductivity of waste carbon black

In this section, the technique and the result of electrical conductivity of waste carbon black powder under different annealing are reported.

3.2.1 Electrical conductivity of carbon black measuring technique

A fixture was customized to measure the DC electrical conductivity of the waste CB as described in Figure 3-1. A sample holder disk made of electrical insulated material (Teflon) was prepared. Moreover, a bore with 10 mm in diameter was drilled into the center of the Teflon disk to create the sample cavity. Then, two copper electrodes with 30 mm length and 9.95 mm diameter were made. One of the prepared copper electrodes was fitted in one side to hold the CB powder sample. 30 mg of waste CB powder was poured into the disk cavity. The weight of the filled CB powder was constant for all the samples and under each measurement in order to maintain a uniform distribution of the pressure and hence increase the reliability of the system. After filling the sample, the second copper electrode was fitted on the other side of the sample holder cavity. The powder was pressed between two copper electrodes of 10mm diameter each, the pressing was performed in a hydraulic press at 2 MPa to obtain the same packing factor for all the samples. Following applying the pressure on the copper electrodes, the total height was measured by a Vernier caliper. The height of the two electrodes was subtracted from the total height of the filled cylinder to determine the height (l) of the compressed powder. The DC power source was switched on to start taking the reading of the voltage drop across the sample and the passing current.

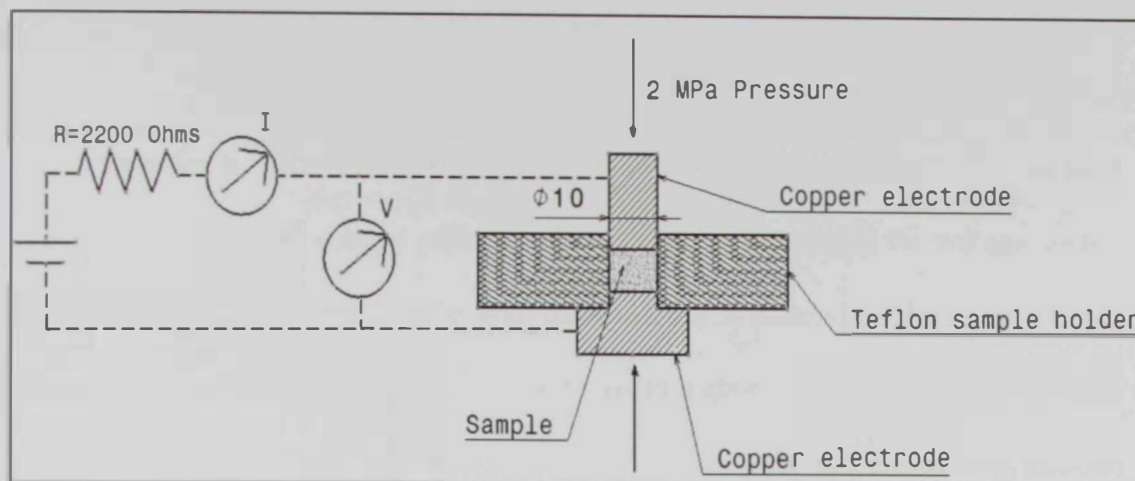


Figure 3-1: Fixture diagram for measuring the electrical conductivity of waste carbon black

The source of DC power was PowerFlex CPX200 (from Thurlby Thander Instruments TTi, United Kingdom). The voltage drop across the CB powder and current through the circuit were measured using DDMM240 (from Multimetrix, France) and 34405A (Agilent technologies, USA), respectively.

The conductivity of the measured samples is given by:

$$\sigma = \frac{l}{R \cdot A} \quad (1)$$

where:

R is the electrical resistance in Ω .

A is the cross sectional area of the copper electrode

l is the height of the compressed CB powder in the cavity.

The electrical resistance of the measured samples was determined by Ohm's law:

$$R = \frac{V}{I} \quad (2)$$

In order to determine the electrical conductivity using equation (1), at least five different electrical voltage sources were applied by alternating the voltage source to the entire circuit. A resistance with 2200 Ω (as illustrated in Figure 3-1) was connected in series with the power source to avoid a short circuit in case the material is highly conductive. The resistance also helps to reduce the current passing through the circuit to avoid the heating factor that might affect the resistance value of the compressed CB. The results showed that the maximum value of the current did not exceed 1 amp. The voltage drop across the sample and the current passing were plotted according to equation (2) to obtain the electrical resistance of the tested sample.

Before filling the insulated disk with powder, the resistance of the empty disk under compression of the two electrodes was measured. The reading of the empty insulated disk resistance was then subtracted from the reading of the filled disk to obtain the reading of the compressed CB resistance.

Before filling another sample, the surfaces of both copper electrodes which are exposed to the powder were polished to remove any contaminations or impurities that may affect the reading of electrical resistance.

3.2.2 Electrical conductivity of carbon black result

This section illustrates an example describing the summary of the previous mentioned process (section 3.2.1) for calculating the electrical conductivity of waste

CB powder. Furthermore, the electrical conductivity of waste CB at different annealing temperatures is reported.

The test was performed by measuring the resistance of the powder cell before filling the waste CB and after filling the waste CB respectively. The test was repeated three times by filling new sample in the powder cell.

For example, the resistance of the empty sample holder was extracted from the plot of V vs. I as shown in Figure 3-2. The figure shows the plot of V vs. I for all the three runs. It was noticed that the current reading was stable (without fluctuation) for the entire reading of voltage drop across the sample. The slope of each sample gave a value with R-squared value=0.999 which reveals good ohmic contact between the CB powder and the electrodes.

For sample no. 1, the resistance is 0.118 Ω .

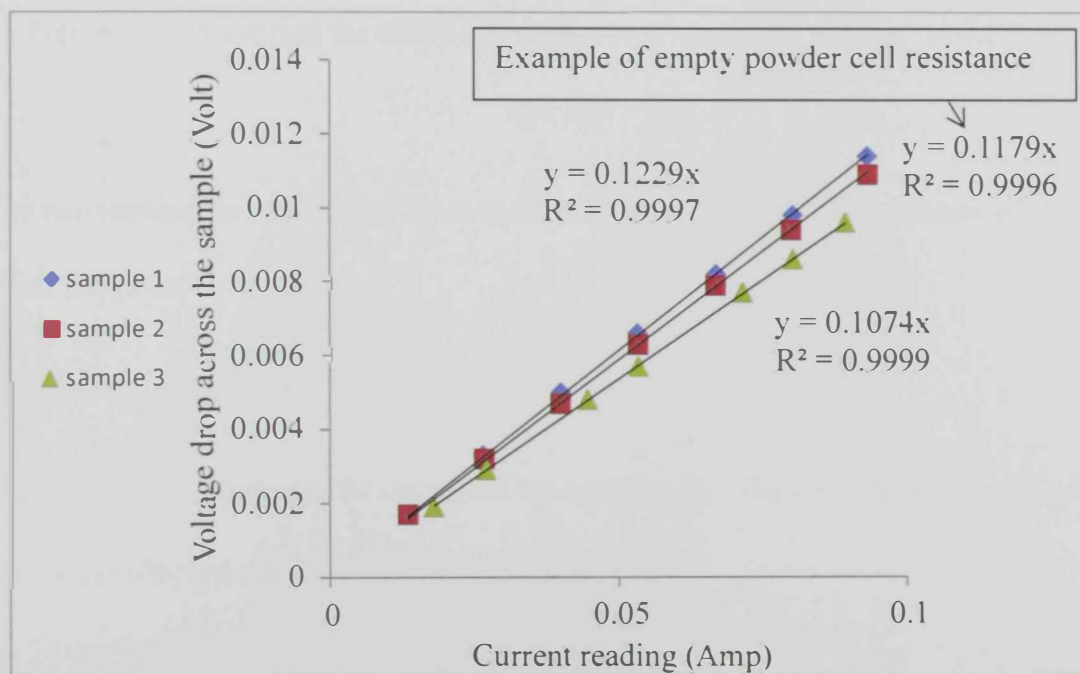


Figure 3-2: Measuring the electrical resistance of empty cell

After filling the powder cell with the powder, the resistance of the filled powder cell was extracted from V vs. I as demonstrated in Figure 3-3 and the resistance is 0.232 Ω .

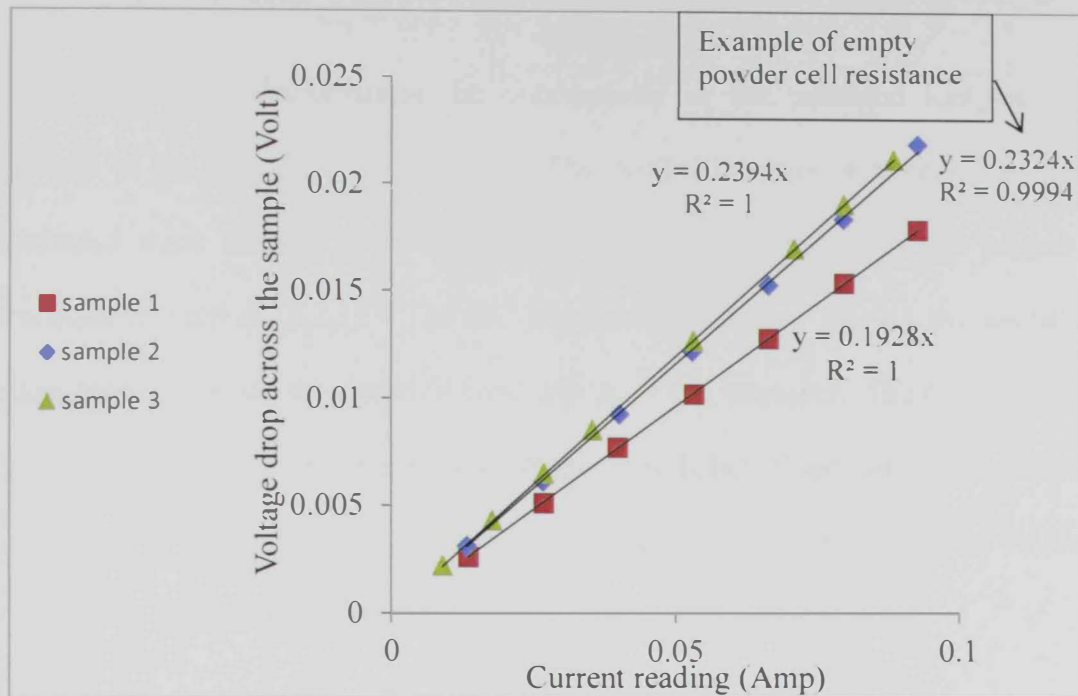


Figure 3-3: Measuring the electrical resistance of waste CB powder annealed at 500°C

The two readings are subtracted from each other to obtain the pure resistance of the waste CB powder.

$$R_{\text{waste CB}} = 0.232 - 0.118 = 0.114 \Omega$$

Then, the conductivity can be calculated by equation (1). The cross sectional area of the copper electrode = $\frac{\pi}{4} (0.995)^2 = 0.778 \text{ cm}^2$

The height $l = 0.217 \text{ cm}$

$$\sigma = \frac{0.217}{0.114 * 0.778} = 2.447 \frac{\text{S}}{\text{cm}}$$

The above calculation was performed for all the prepared samples under different annealing temperatures.

Figure 3-4 demonstrates the conductivity of the annealed samples as a function of the annealing temperature. The conductivity measurement tests were conducted three times for each annealing condition by repeating the procedure described in section (3.2.1). The DC conductivity showed that as the annealing temperature increases, the electrical conductivity of CB increases. The increase in the conductivity as a function of annealing temperature is best fitted with an exponential fit function in which the electrical conductivity reaches to an average value 40 σ/cm at annealing temperature 1250°C.

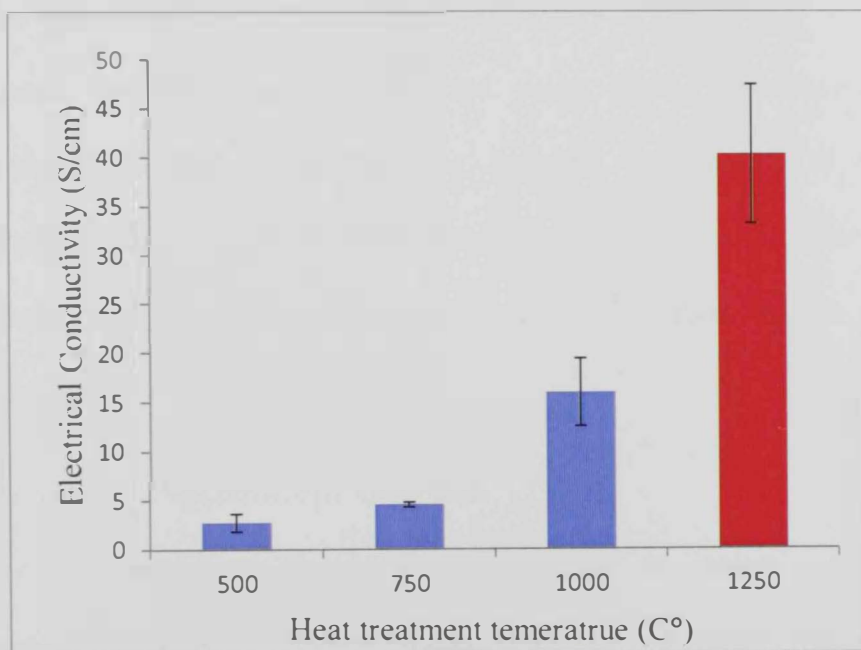


Figure 3-4: Electrical conductivity of post heat treated CB powder vs. the temperature of furnace

As described previously in (section 2.1.4), CB contains some random distorted graphene layers within the layer planes which are called turbostratic. CB can be heat treated to become graphite at temperature between 1700 to 3000°C. It is known that the electrical conductivity of the graphite can reach up to 1000 S/cm. As the heat treatment temperature increases, the CB will start graphitizing and enhance the ordering of the graphene plane, moreover, it will increase the long range orders of the structuring.

It is anticipated that the electrical conductivity will increase with temperatures beyond what is reported in this study, however due to the furnace limitation the reported values are indicative of the increase. The result of increasing electrical conductivity of waste CB as the heat treatment temperature increases is also correlated with the Raman spectrum result and X-ray diffraction.

3.3 Raman Spectrum

Raman spectrum has been obtained using Raman spectrometer model: XploRA (from HORIBA Scientific). The electrical conductivity of the carbon material can be related to their structural modification which can be investigated by Raman spectroscopy. Raman scattering provides information on the amount of ordering and degree of bonding.

3.3.1 Raman Spectroscopy Overview

Raman spectroscopy is a technique based on inelastic scattering of monochromatic light from a laser source. Inelastic scattering means that the frequency of photons generated by the monochromatic light changes upon interaction with a sample. The frequency of these photons is shifted up or down in comparison

with the source frequency which is called a Raman shift. Raman shifts provide information about vibrational and rotational modes of the system. Raman scattering also provides information on the amount of ordering and degree of bonding. Raman shifts provide also the finger print of the tested material. The models structures of carbon material have properties based on the constructed carbon bonds such as single bond (C-C), double bond (C=C) and triple bond (C≡C). These bonds have different vibrational frequencies depending on the bond length and bond order. Example: at Raman band 1575cm^{-1} , it was observed that in the single crystals of graphite a doubly degenerate deformation vibration of the hexagonal rings of graphite (Nakamizo, 1973).

3.3.2 Raman spectrum result

In the first-order Raman spectra, the D band ranges from 1330 to 1360 cm^{-1} is assigned to defect and amorphous carbon. It is normally strong in disordered graphitic material. The G peak is around 1575 cm^{-1} is assigned to the stretching mode in the graphite sheet (Li at al., 2007).

The result from Raman spectra (Figure 3-5) shows that the D peak appears for the annealed CB powder at HT500 and HT750. However, the D peak disappeared at heat treatment temperature 1000°C and above. Simultaneously, the G peak did not appear for heat treatment temperature below 750°C . This peak starts to show for heat treatment temperature at 1000°C and above. It is also clearly shown in the Raman spectra that a wide region of Raman lines lay between 1000 - 1300 cm^{-1} . This is related to the chemical structure of C – O, C = O, C – O – C and C = C bond described in reference (Saleha et al., 2014).

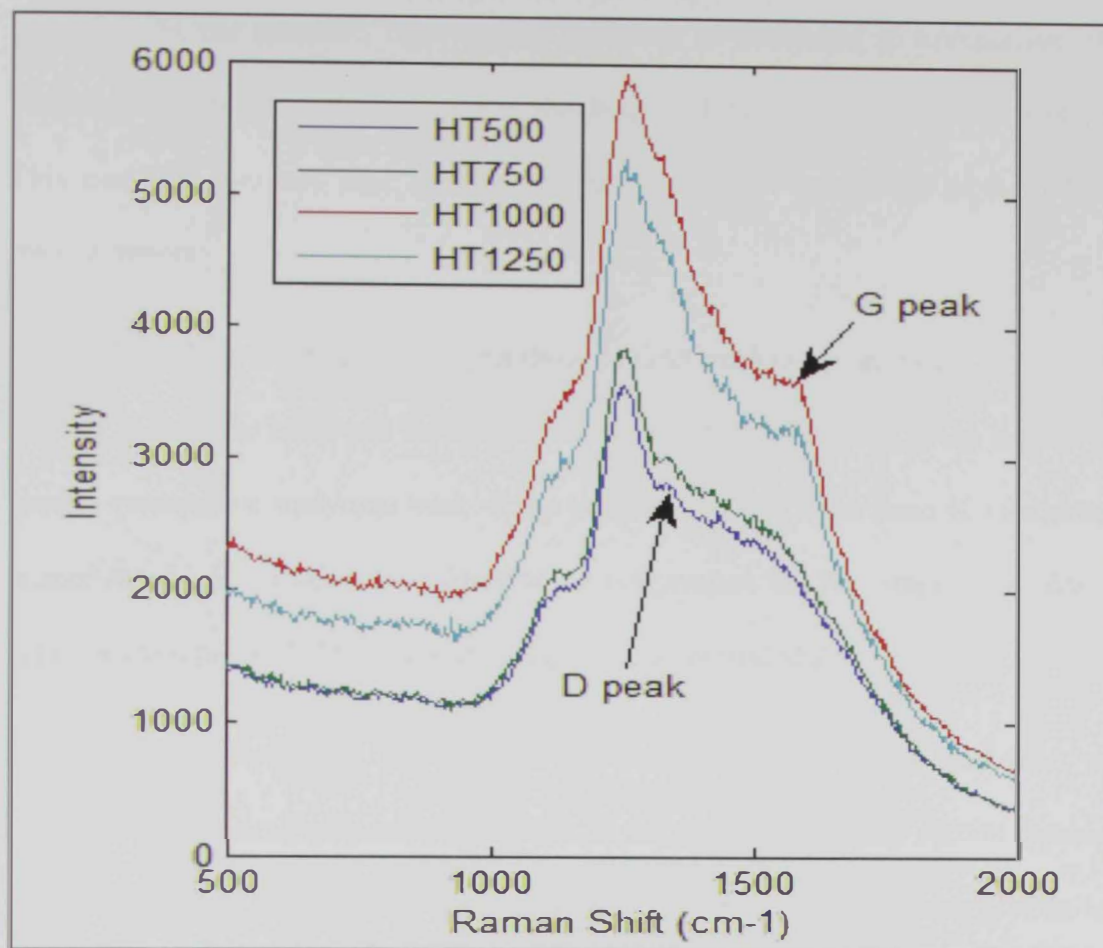


Figure 3-5: Raman spectra for waste CB under different heat treatment temperatures

3.4 Thermo-gravimetric analysis (TGA)

Thermal analysis consists of different techniques in which an investigated sample is examined under heat and time at specified atmosphere. Such commercialized machines perform different methods of thermal analysis that allow the chemical reactions associated with heating or cooling. The chemical reactions include decomposition, pyrolysis, ignition, phase changes, calorimetry, etc. Thermal analysis can be performed on small amounts samples. There are two types of thermal analysis machines: horizontal and vertical balance. Thermo-gravimetric analysis (TGA) can be performed using the vertical balance in which the specimen pan is

hanged from the balance. This type of machine is calibrated to compensate the buoyancy effects due to the variation in the density of the purge gas with temperature. This machine does not have a reference pan and is not capable to perform DSC measurements.

3.4.1 Thermo-gravimetric Analysis (TGA) working principle

TGA is the basic and the simplest thermo analytical method. TGA is used for routine quantitative analytical work. It is a technique in which the mass of a substance is monitored with relation to a function of temperature as the sample specimen is subjected to a controlled temperature program in a controlled atmosphere.

TGA is performed in oxidative atmosphere (air or oxygen and inert gas mixture) with a linear temperature gradient. In the particular case of carbon material, the sample is first heated in nitrogen gas in order to dry it and to expel any volatiles, and then the atmosphere is switched to oxygen and the carbon content is burnt to CO_2 . Finally, the residual weight and oxidation temperature are obtained. The weight loss in an atmosphere is typically due to carbon dioxide and the weight gain due to oxidation of residual metal catalyst into solid oxides. The residual weight is obtained assuming that all chemical reactions are completed. The maximum temperature is selected by the user so that the sample weight is stable at the end of the experiment. Finally, the output from data acquisition can extract the needed information for residual weight and oxidation superposition of the weight loss due to the oxidation of carbon (Figure 3-6).

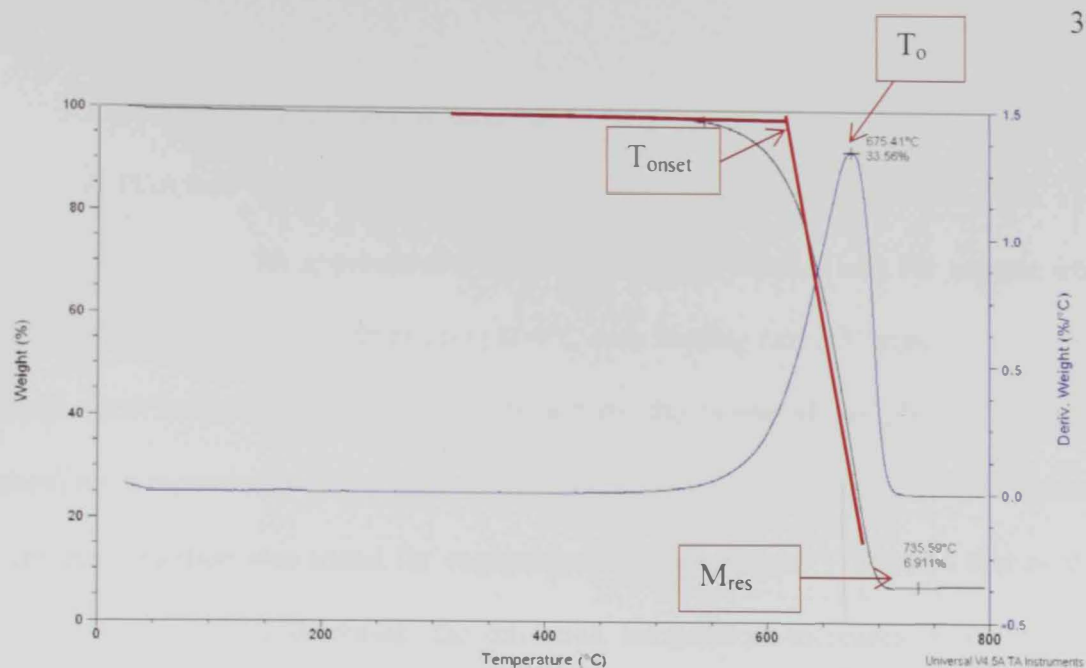


Figure 3-6: TGA graph of carbon based material

The oxidation temperature (T_o) is defined as the maximum in the weight loss. This can be obtained by taking the first derivative of the TGA graph (dm/dT_{max}). Figure 3-6 shows yet another definition which is the temperature when oxidation starts and the weight loss starts to increase sharply which is called T_{onset} . $T_o = dm/dT_{max}$ is preferred for two reasons. T_{onset} cannot be determined precisely due to the initial gradual transition. A sample such as carbon based material contains some amount of impurities such as carbonaceous that may oxidize at a temperature lower than the base material. Second, the increase in weight due to catalyst oxidation at low temperature will overlap the weight loss due to oxidation. This will result in upward fluctuation of the TGA graph prior to the bulk weight loss which will lead to more difficulty in obtaining T_{onset} . Hence, $T_o = dm/dT_{max}$ is relatively precise and was adopted in this study.

3.4.2 Thermo-gravimetric analysis (TGA) result

A TGA test was performed using a TA Q50 (from TA instruments, USA). The balance was filled with approximately 10 mg of carbon black. Then, the sample was heated from ambient temperature up to 800°C with heating rate 5°C/min.

Thermo-gravimetric analysis was performed on the prepared samples at different annealing temperatures (500, 750, 1000 and 1250°C). One sample for each heat treatment condition was tested for each annealing case. Figure 3-7 shows that as the annealing temperature increases, the oxidation temperature increases in a linear fit function.

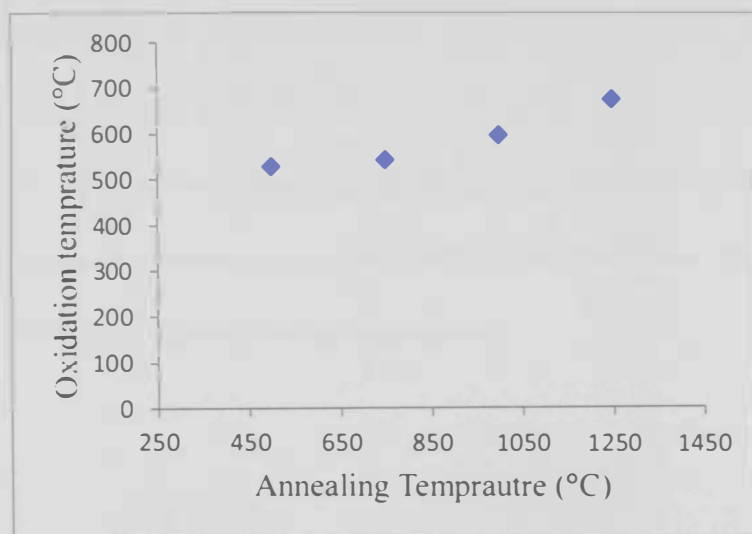


Figure 3-7: Oxidation temperature obtained from TGA for different annealing temperatures

Furthermore, Figure 3-8 shows that as the amount of residual mass slightly decreases, as the annealing temperature increases up to 1000°C. This can be contributed to the reduction of the amount of carbonaceous deposits on the surface of CB. One sample was tested for each annealing case. However, three different samples were tested for

the annealed waste CB at 1250°C. It is also reported in the EDX result (section 3.6) that the amount of additives decreases at annealing temperature 750°C and above. Moreover, at annealing temperature 1250°C, it has been noticed that the amount of residual mass decreases dramatically for annealing at 1250°. This can be due to the restructuring of crystalline ZnS from the powder which is reported in XRD result taking into account the reduction of carbonaceous material. The thermogravimetric graphs of each annealing case are listed in Appendix A.

Generally, TGA results demonstrated that the higher the temperature of the heat treatment, the more thermally stable is the CB obtained from waste tire. In addition reduction of the residual mass will increase the contact surfaces between the CB particles. This is due to the reduction of the carbonaceous deposition on the surface of CB particles and because of the reduction of the additives. Hence, increasing the chances of creating electron tunnel and provide the ability of electrons to jump between closely spaced carbon aggregates.

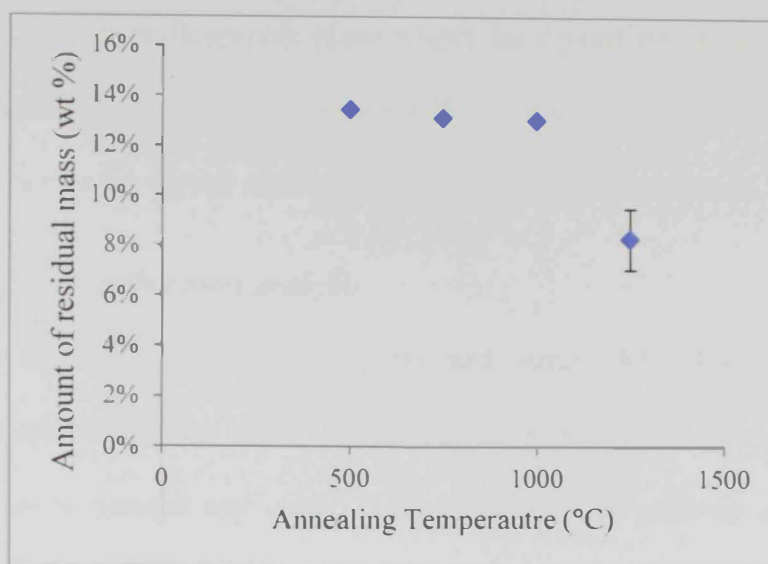


Figure 3-8: Amount of residual mass (wt. %) obtained from TGA for different annealing temperatures

3.5 X-ray diffraction technique (XRD)

The solid material can be classified into two categories, amorphous and crystalline. The atoms in amorphous material are arranged in a random way and short range orders. While in crystalline material, the atoms are arranged in long range order of repeated unit cells. The unit cell is the smallest volume element by repetition in three dimensions. X-ray diffraction technique provides information about the bulk structure and the finger print of the crystalline material (Callister et al, 2008).

3.5.1 X-ray diffraction principle

The sample was mounted in the center of a rotary counter and is exposed to a source of X-rays. The source of X-rays is used as the wavelength size is comparable with the atoms. The counter is rotating with constant angular velocity and plots the diffraction beam intensity as a function of diffraction angles (2θ) that is received by the detector. The high intensity at specific diffraction angle means that the material

contains a specific crystallographic plane within the crystal structure. In most of the cases, the crystalline material will contain different intensities at different diffraction angles that describe the crystal structures of the material (Callister et al, 2008).

3.5.2 X-ray diffraction analysis

X-ray diffraction analysis was performed using XRD 6100, Shimadzu. An aluminum sample holder was filled with the powder sample and was pressed properly with wax paper to prevent any voids. Then, the diffraction patterns of the powders were performed using Cu K α radiation. The scan range was from $2\theta=20^\circ$ to $2\theta=80^\circ$ with step $2\theta=0.02^\circ$ and a scan speed of 2 degree/minute. One sample was tested for each annealing case.

The X-ray diffraction (XRD) results in Figure 3-9 show a peak at $2\theta=25.2^\circ$ which is associated with amorphous carbon which is present in all the annealing cases. This peak is a confirmation that the material contains a large amount of disordered material in the form of amorphous carbon. This peak is present in all the different annealing conditions with the same intensity except for annealing condition at 1250°C . In this case the peak is shifted backward with 0.2° difference with increasing the intensity as is shown in Figure 3-15 .

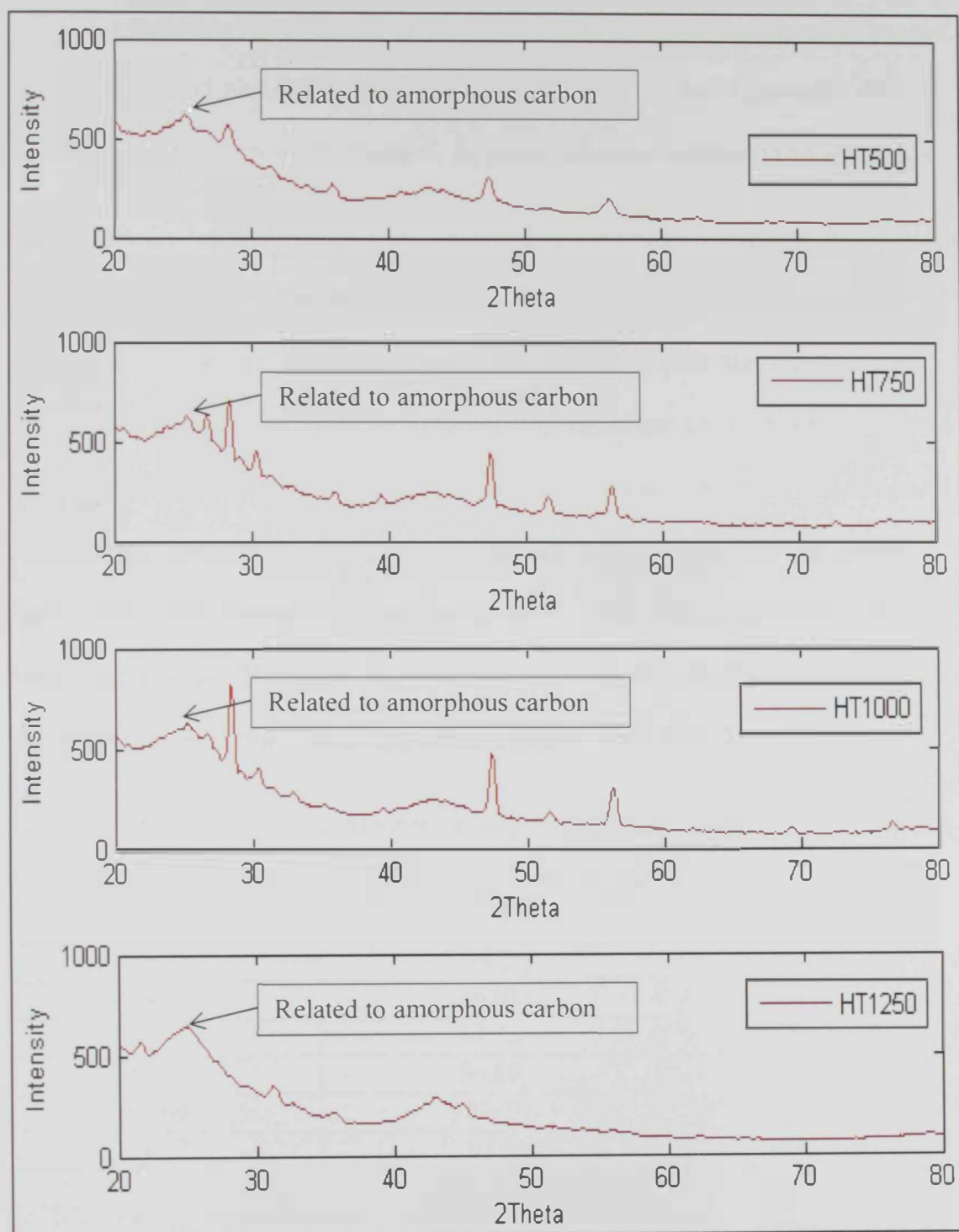


Figure 3-9: Diffractograms of post heat treatment CB powder at different heat treatment

Furthermore, the result shows that the crystalline compositions mainly consist of zinc sulfide and zinc oxide. Although the intensity of the peaks generally differ as the heat treatment temperature changes, the main difference is found to be as follows: For HT500, the result in Figure 3-10 illustrated that the main crystalline composition consists of zinc oxide. The characteristic peaks for zinc oxide (ZnO) were obtained from Undria et al. (2013). They were also compared with the obtained peaks, comparisons are listed in Table 3-1. The peaks obtained are approximately matching with the reference values. On the other hand, the result demonstrated that the small characteristic peaks related to ZnS are also presented in HT500 as shown in Figure 3-11. The characteristic peaks intensity for zinc sulfide (ZnS) were obtained from Undria et al. (2013) and they were also compared with the peaks that were obtained experimentally. The comparison is listed in Table 3-2.

Table 3-1: ZnO XRD peaks comparison between the reference and the peaks obtained

Peaks listed in Ref. Andrea	Peaks obtained by this study
31.85	31.5
34.55	34.2
36.36	36.02
47.7	47.32
56.75	56.26
63.09	62.7
68.17	67.9

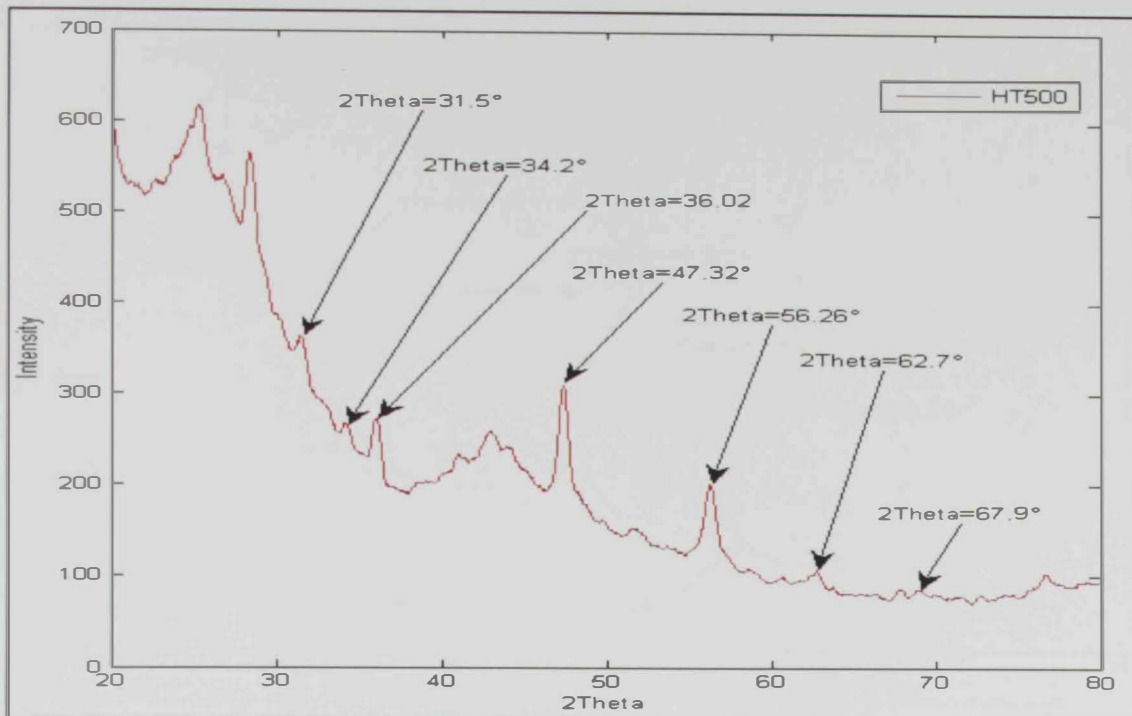


Figure 3-10: XRD peaks related to ZnO for waste CB annealed at 500°C

Table 3-2: ZnS XRD peaks comparison between the reference and the peaks obtained

Peaks listed in Ref. Andrea	Peaks obtained by this study
26.81	26.7
28.41	28.3
30.42	30
39.47	39.06
47.36	47.32
51.58	51.56
56.16	56.26
57.33	57.3

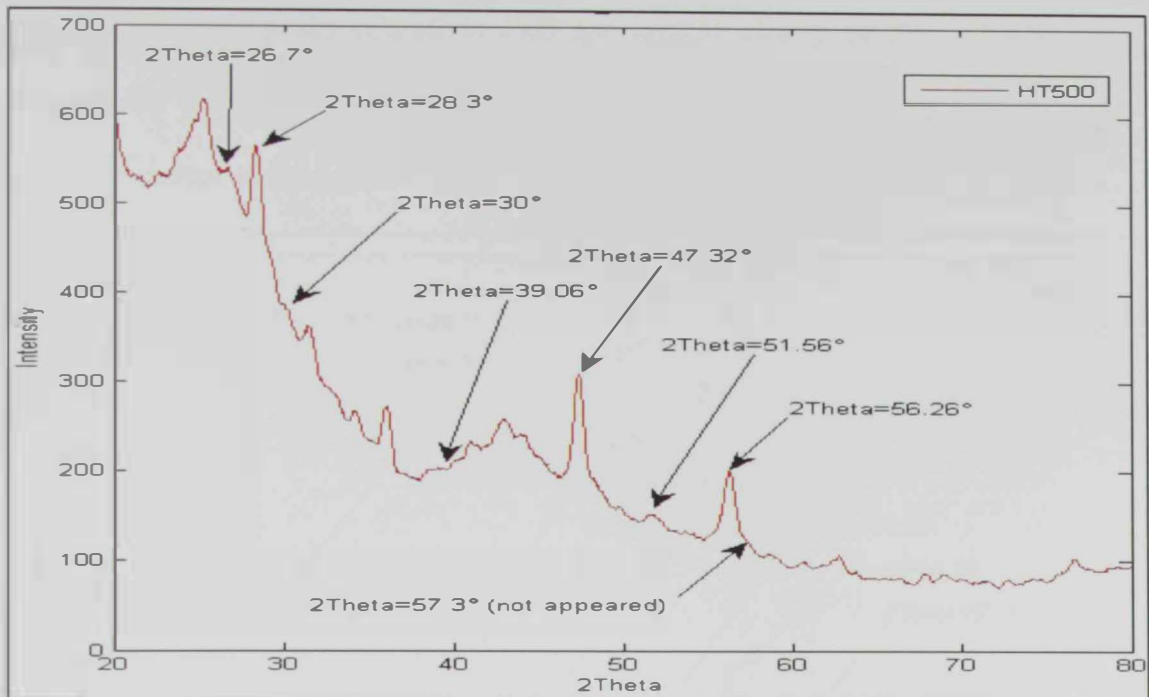


Figure 3-11: XRD peaks related to ZnS for waste CB annealed at 500°C

For HT750, the characteristic peaks related to ZnO decreased. Meanwhile, the characteristic peaks for ZnS increases as is shown in Figure 3-12.

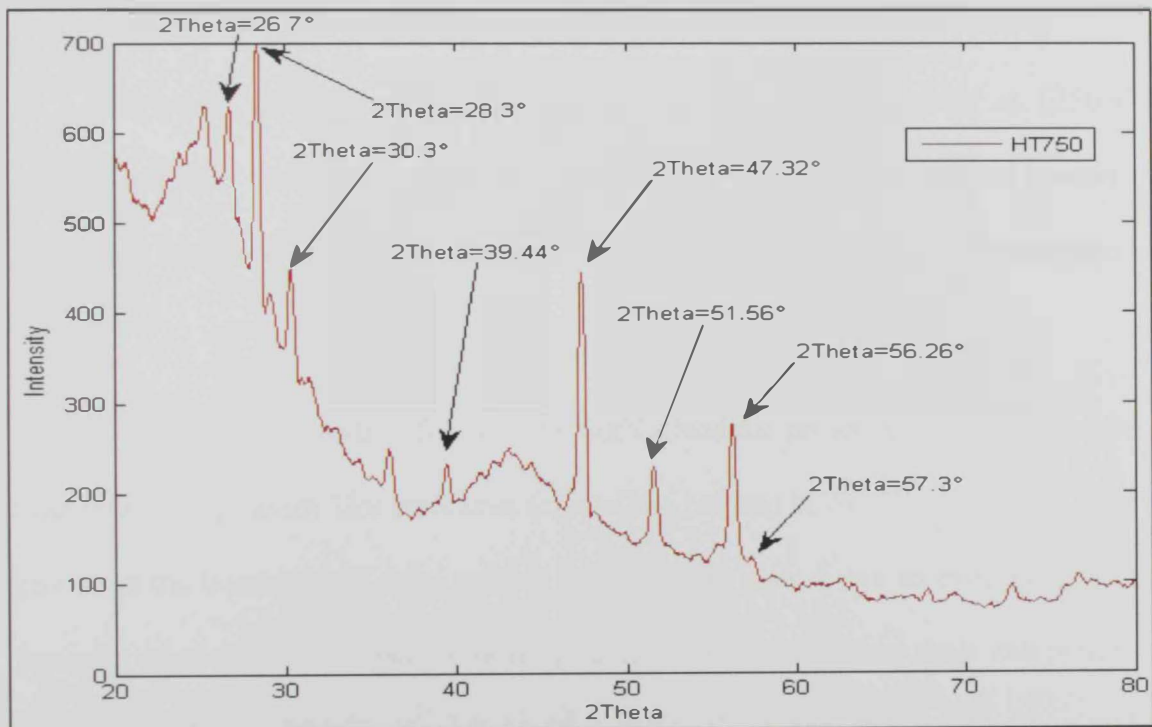


Figure 3-12: XRD peaks related to ZnS for waste CB annealed at 750°C

For HT1000, the peaks related to ZnS are present clearly in the diffractogram. Meanwhile, the peaks related to ZnO almost disappeared suggesting that the ZnO react with sulfur and produce a crystalline composition of ZnS.

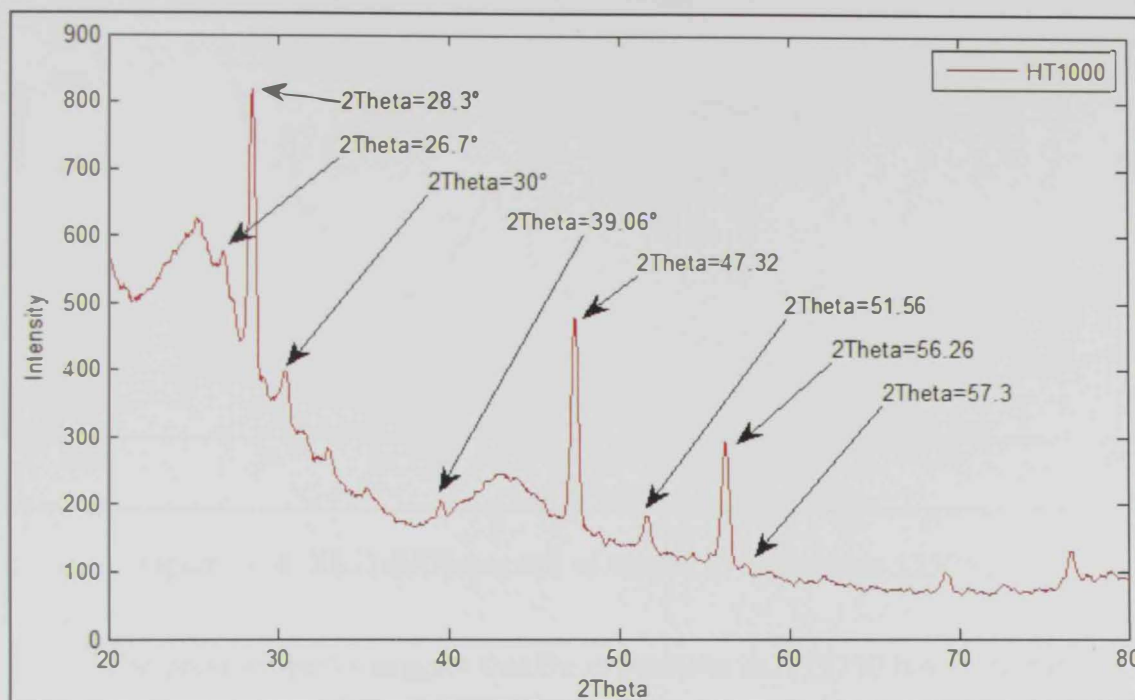


Figure 3-13: XRD peaks related to ZnS for waste CB annealed at 1000°C

However, the diffractogram of post heat treatment CB powder at 1250°C pointed out that the characteristic peaks for both ZnO and ZnS are not present. Moreover, Undria et al. (2013) noted that the peak at 25.1 is related to amorphous carbon.

The diffraction pattern for HT1250 highlighted the presence of a characteristic peak related to graphite like structures (crystalline carbon) at $2\theta=25^\circ$ (002) with extra growth in the intensity. An extra peak at $2\theta=43^\circ$ (100) also shows an extra growth of intensity compared to the lower annealing cases. At HT1250, a new peak was present at $2\theta=44.9^\circ$ (010) which is associated with turbostratic carbon, that is also associated with the peak at $2\theta=44^\circ$ (Xu et al., 2009).

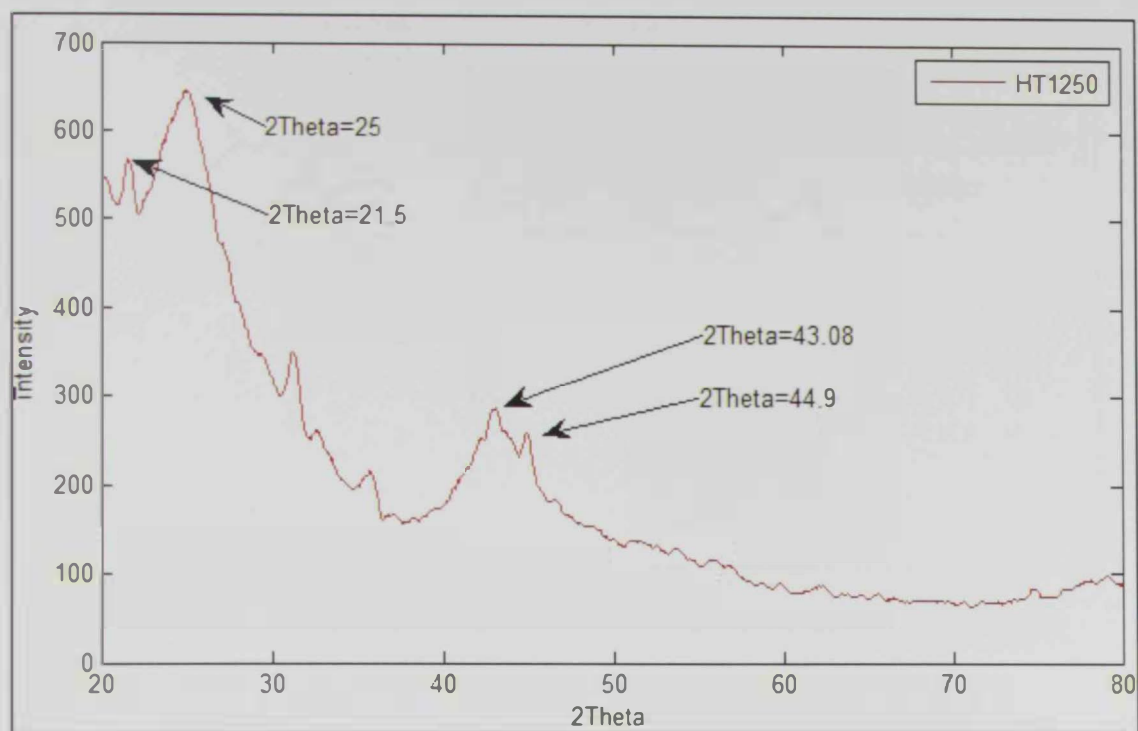


Figure 3-14: XRD diffractogram of waste CB annealed at 1250°C

The previous peaks suggest that the crystallites in HT1250 have intermediate structures between graphite and the amorphous state called turbostratic structure or random layer lattice structure. Turbostratic carbon consists of disordered graphene layers with different stacking distances and stacking ordering degrees (Manoj et al., 2012).

It is also noticed that the intensity of the peak $2\theta=25.2^\circ$ is higher at annealing temperature 1250°C. This peak is also slightly shifted backward 0.2° as shown in Figure 3-15. This shift and intensity change are originated due to the re-arrangement of the graphene stacking structure (Xu et al., 2009; Manoj, 2012; Li et al., 2007).

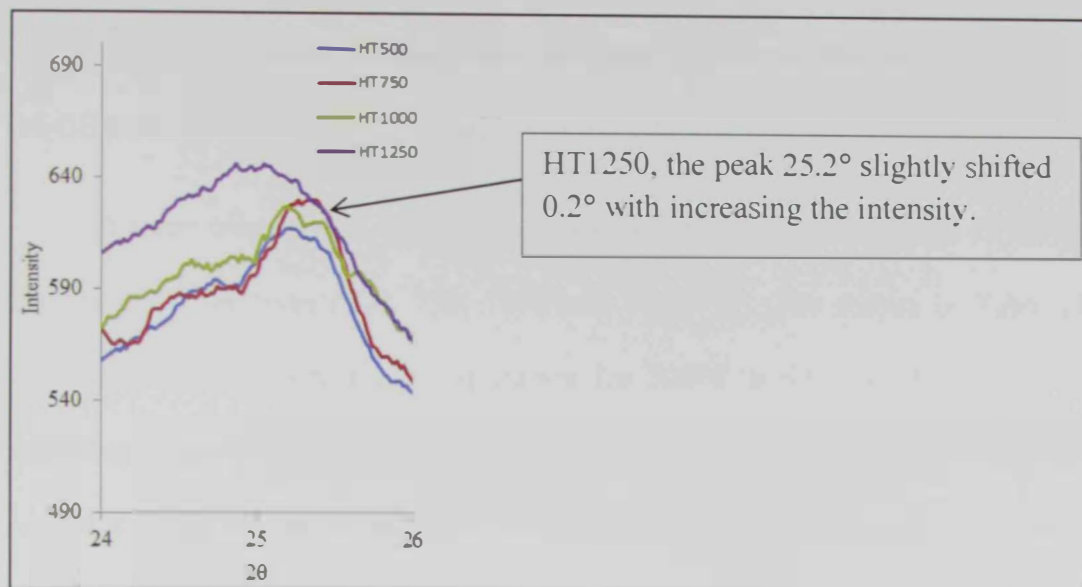


Figure 3-15: The common peak at $2\theta=25.2^\circ$ for all the annealing condition

As the heat treatment temperature of CB powder increases up to 1000°C , the characteristic peak intensities for zinc oxide (ZnO) starts to decrease. At the same time, the characteristic peaks for zinc sulfide (ZnS) increase. It is worth mentioning that the characteristic peak (002) at 25.2° was present in all the annealing cases with the same intensity. This peak is slightly shifted backward with 0.2° and higher intensity. Moreover, extra growth of the peak (100) and the new peak (010) are present for annealing condition at 1250°C . As a result, the disordered graphene layers in the turbostratic structure enhanced this annealing temperature.

3.6 Scanning electron microscope and EDX

SEM and EDX were performed on waste CB powder using JSM-5600 (from JEOL, Japan) to investigate the morphology of the powder. A sufficient amount of the carbon black was placed on the sample stub to be scanned under the SEM. The investigation was performed at 15 kV using electro probe microanalyzer. Then, digital micrographs are captured and stored on the computer. The attached EDX

system is used to obtain the analytical elemental analysis of the prepared waste CB for different annealing temperatures.

Energy dispersive X-ray was performed on the waste CB samples for different annealing temperatures (500, 750, 1000 and 1250 °C). The results in Table (3-3) illustrate that the concentration of carbon for 500°C is 93.5 wt. %. However, at annealing temperature 750°C, the concentration increases to 97.5 wt. % with slight reduction in the amount of additives remaining from the pyrolysis process. Also, the results show that there is no significant change in the carbon concentration and other additives under the effect of increasing the annealing temperature above 750°C. The presence of other metallic and nonmetallic elements in the CB powder obtained from waste tires can be contributed to the additives added during tire production.

Table 3-3: Energy dispersive X-ray for different post heat treatment temperature.

Temperature (C°)	Elemental Percentage (wt. %)								
	C	Al	Si	S	Mn	Fe	Cu	Zn	Sn
500	93.38	0.1	1.9	2.85	0	0.13	0.54	2.61	-0.29
750	97.52	0.06	0.34	0.79	0	0.1	0.66	0.53	0
1000	97.46	0.1	1.14	0.93	0	0.08	0.02	0	0.6
1250	96.76	0.26	0.4	0.62	0.18	0	0.45	0.21	0.25

Moreover, Table 3-3 demonstrates the presence of high concentrations of Cu and Zn elements with respect to other additives that are present in the waste CB. This can be rooted to the presence of brass alloy during the production of the tire. This is usually used to increase the adhesion property between the elastomeric polymer and

the reinforcement metallic wires. Also, Si and S are present in large amounts with respect to other additives. Si can be present in the form of silicates but they are in amorphous condition as they are not evidenced in XRD result. While, sulfur is present because it is added during vulcanization process which is performed during tire production to increase the durability of tire production. XRD result in section 3.5.2 reported that the Zn is present in the form of ZnO and starts to react with S to form ZnS. The Zn in the form of ZnO and ZnS disappeared at annealing temperature 1250°C. Note that they may be absent as they are in the amorphous form. But from EDX analysis, the result shows that the concentration of Zn and S is lowered at annealing temperature 750° and above. Another issue which can be reported is that some minor elements (Al, Mn and Sn) are evidenced by EDX (Undria et al., 2013). Undria et al., (2013) also reported some differences in the presence of different minor additives such as (Cr, Mg, Co and Cr) in which they are not evidenced in this paper. This can be contributed to the different elements and additives added during tire production and will mainly depend on the usage of different tire brands.

SEM images for different annealing conditions are shown in Figures 3-16, 3-17, 3-18 and 3-19. The deposition of carbonaceous on the waste CB particles is clearly visible in the SEM images. No significant morphological changes occur at different annealing temperatures. The CB aggregate size ranges between 50 to 100 micrometers. Moreover, the macrospore structure of waste CB cannot be observed because of carbonaceous deposition and because of the additives that might be related to organic or/and inorganic compounds. When the annealing temperature of waste CB increases to 750°C and above, the amount of additive deposited with CB

particles decreases or they react with each other to form amorphous compound that cannot be observed in XRD. It was also observed in all the SEM images with magnification x15000 that the amount of carbonaceous deposition was significantly reduced at annealing temperature 1250°C.

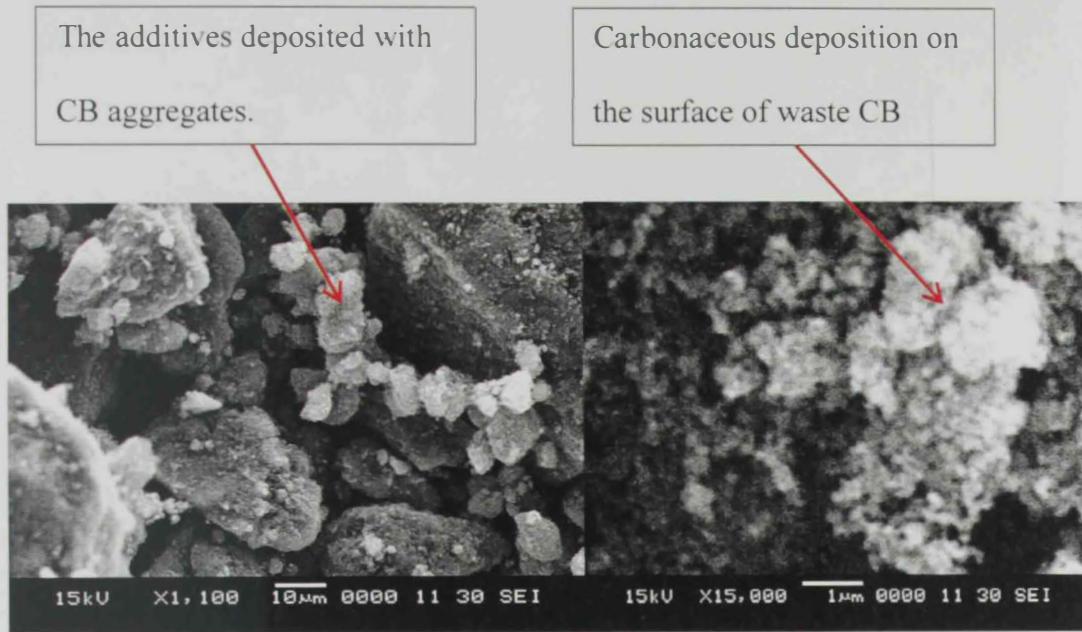


Figure 3-16: SEM images for HT500

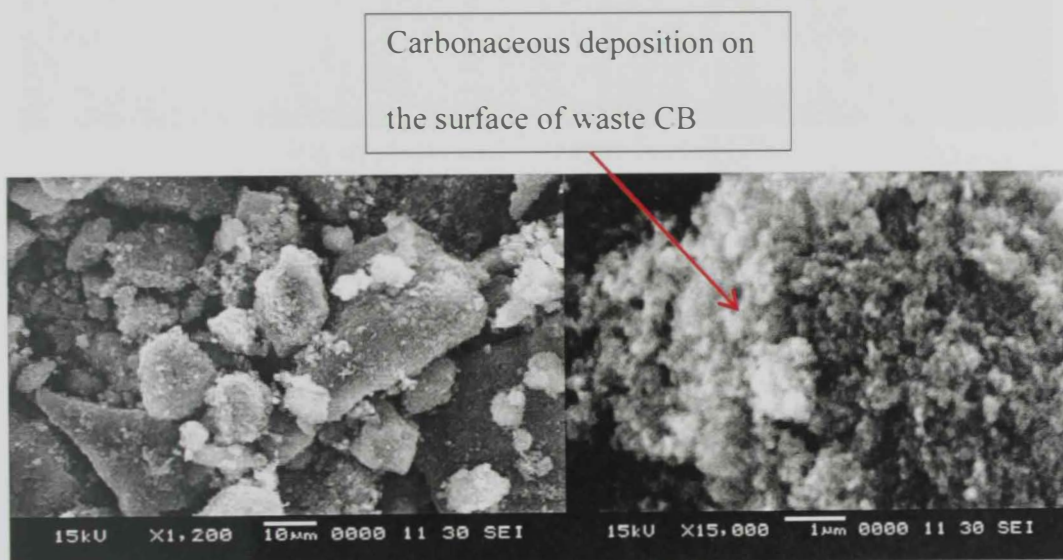


Figure 3-17: SEM images for HT750

Carbonaceous deposition on
the surface of waste CB

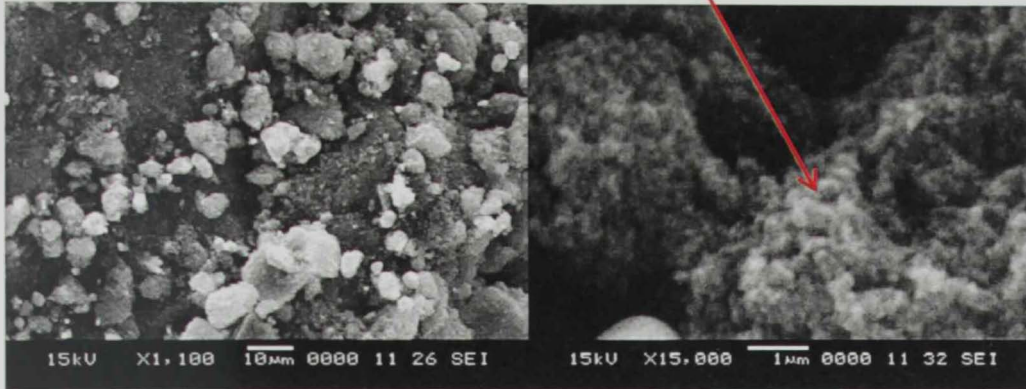


Figure 3-18: SEM images for HT1000

Carbonaceous deposition on the
surface of waste CB was reduced

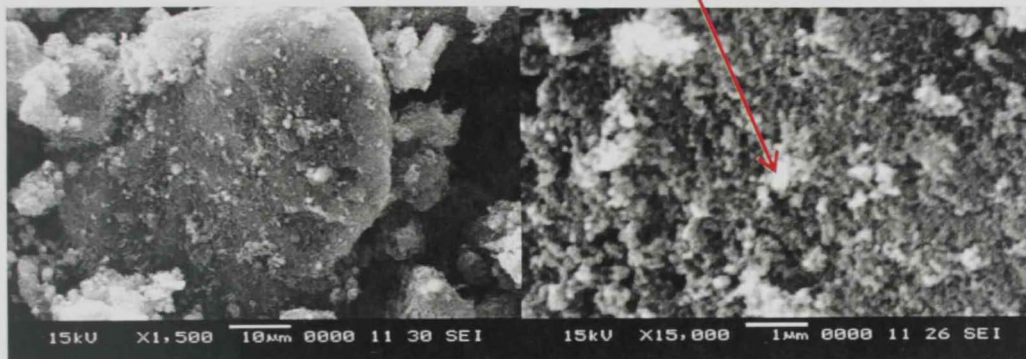


Figure 3-19: SEM images for HT1250

CHAPTER FOUR

CHARACTERIZATIONS RESULT OF CARBON BLACK WITH EPOXY RESIN

This chapter describes the work done in producing solid conductive polymer composite by utilizing the waste CB annealed at 1250°C. Annealed waste CB at 1250 °C was added to epoxy resin with low and different wt. percentages (0%, 3%, 6%, and 9%) to investigate the possibility of producing conductive polymer composite. Preparation and characterizations result of DSC, TGA, nano-indentation and FTIR are also reported in this chapter. Electrical conductivity was measured indirectly using Network Analyzer. Then, DC electrical conductivity of high loading of waste CB (30% and 40%) that reaches to critical pigment volume concentration (CPVC) was investigated.

4.1 Preparation of composite made of epoxy loaded with low wt. % of waste CB

The epoxy resin used was from type ARALDITE® AY105 IN form HUNTSMAN (see table (4-1) for material specification). Furthermore, the hardener was Aradur® 42 form HUNTSMAN which is basically polyamine. The cross linking reaction is based on the primary amine groups in polyamine that are converted to secondary and tertiary amines (Nikolic et al., 2010).

Waste carbon black was produced by pyrolysis process followed by post heat treatment at 1250°C to improve the electrical conductivity of the waste carbon black as described in the previous chapter.

Table 4-1: Technical data of ARALDITE® AY105 IN epoxy resin (according to HUNTSMAN)

Epoxy index (ISO 3001)	5.30-5.45[eq/kg]
Epoxy equivalent (ISO 3001)	183-189 [g/eq]
Viscosity at 25°C (Falling-ball. ISO 12058-1)	10000-12000 [mPas]
Vapour pressure at 20 C (balance)	≤0.01 [Pa]
Density at 25 C (ISO 1675)	1.13 [g/cm ³]

Sixty grams of epoxy resin was filled in a container. The container was placed on magnetic stirrer supported with heater. The temperature was raised up to 80°C to reduce the viscosity of the epoxy and facilitate the stirring which consequently provide uniform distribution of waste carbon particles in the resin. After that, Waste carbon black with the target weight was added to the epoxy. The mixture was kept under stirring for one hour. Then, the hardener was added to the final mixture with resin to hardener ratio equal to 4:1. Afterward, the final mixture with hardener was stirred manually for 15 minutes. Finally, the mixture was casted in a waxed plastic container (mold). The sample was cured at room temperature for at least 6 hours. Different samples with different Wt. % of waste carbon were prepared and listed in the table (4-2) below.

Table 4-2: Different weight % of waste CB loaded in epoxy resin

Sample No.	CB wt. %
1	0%
2	3%
3	6%
4	9%

4.2 Thermal properties

4.2.1 Thermo-gravimetric analysis (TGA)

Thermo-gravimetric analysis (TGA) was used to investigate the thermal decomposition of the cured epoxy composite. Thermal stability of conductive polymer composite is necessary in the application where the material is exposed to heat generation in electronic application.

The TGA test was performed in an instrument Q50 (TA instrument, US) to determine the thermal decomposition temperature and the residual wt. %. The balance was filled with approximately 10 mg of the prepared composite sample. The sample was heated from ambient temperature up to 800°C with heating rate 10° C/min (U.G.Rane, A. A. Sabnis, and V. V. Shertukde-2014). The TGA thermo-grams for various waste CB wt. % are shown in Figure 4-1. One sample for each specific wt. % of waste CB was tested. All the other graphs are listed in Appendix B. The rate of weight loss is the same for all the conditions.

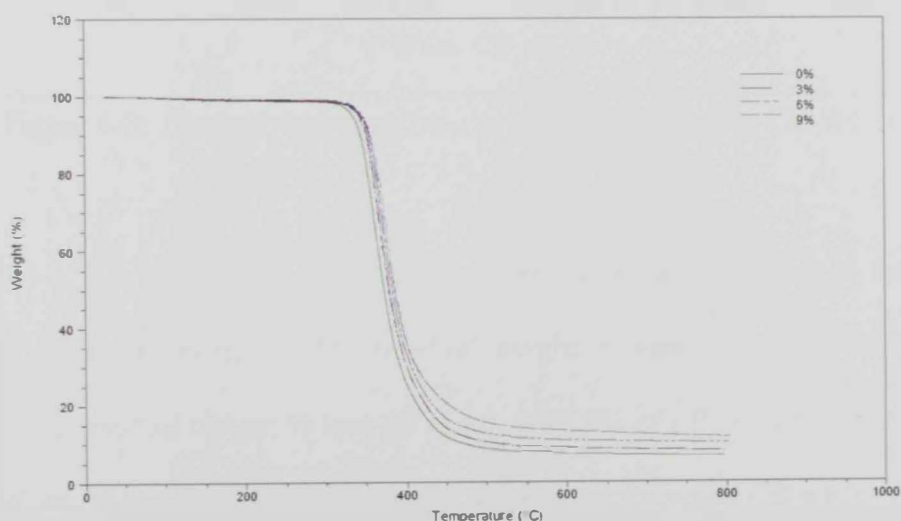


Figure 4-1: TGA thermo-gram epoxy mixed with different wt. % of waste CB

Figure 4-2 illustrates the thermal decomposition temperature as a function of waste CB wt. %. It was also noticed that the thermal decomposition temperature of the cured epoxy is slightly decreased as the wt. % of waste CB increase up to 9%. The decomposition temperature for neat epoxy is 362°C. However, the decomposition temperature for epoxy with 9% of CB is 359.5°C. By this, it can be revealed that waste CB slightly negatively affected the thermal stability of epoxy resin with reduction of only 1%.

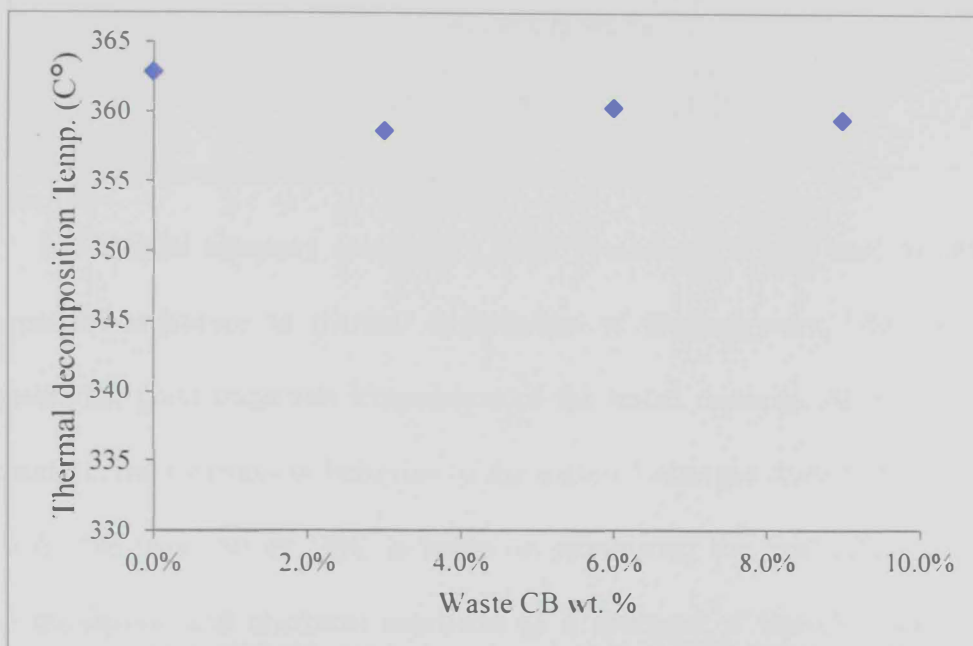


Figure 4-2: Thermal decomposition as a function of waste CB Wt. %

In Figure 4-3, it is shown that the amount of residual weight increases as the loading wt. % of waste CB increases. The residual weight % loss for neat epoxy is 6.8%. However, the residual weight % loss for epoxy with 9% of CB is 11.8%. The increase in residual wt. % is due to the increasing of the amount for waste CB additive.

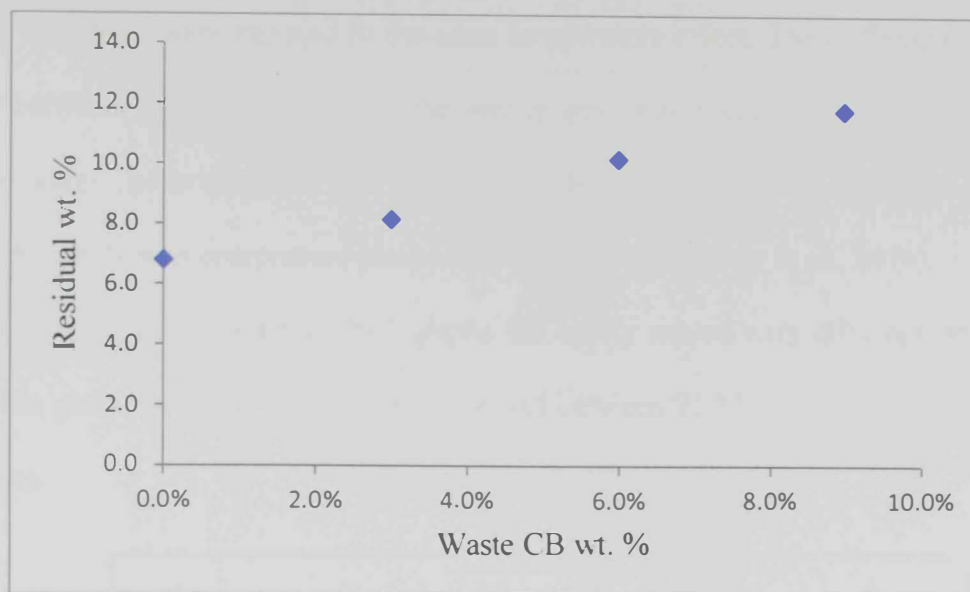


Figure 4-3: Residual Wt. % vs. Waste CB Wt. %

4.2.2 Differential scanning calorimetry (DSC)

Differential scanning calorimetry (DSC) technique is also used to determine the material resistance to thermal degradation of the polymers. DSC is used to determine the glass transition temperature of the tested material. At glass transition temperature, the mechanical behavior of the material changes from brittle to rubbery and soft. The principal of DSC is based on monitoring the heat effects caused by phase transitions and chemical reactions as a function of linearly increasing the temperature. The temperature increased at a constant rate defined by the user. DSC analysis can be performed using the horizontal balance machines that contain two pans (one for the examined sample and the other for the reference).

The glass transition temperature of the composite was obtained by differential scanning calorimetry (DSC) model: Q200 (from TA instruments, US). The test was performed for different wt. % of waste CB in epoxy resin. The sample was put into an aluminum pan with known mass. Another empty pan was placed near the filled pan.

Then, both pans were exposed to the same temperature effect. The difference in heat flow between the filled pan and the empty pan was recorded as a function of temperature. The heating rate was $10^{\circ}\text{C}/\text{min}$ under nitrogen flow of $50\text{ml}/\text{min}$. 10 mg of each sample was compressed inside the aluminum pan (Rane et al., 2014).

Figure 4-4 shows the DSC graphs for epoxy mixed with different wt. % of CB. The glass transition temperature is located between 71.8°C and 75.4°C for all the samples.

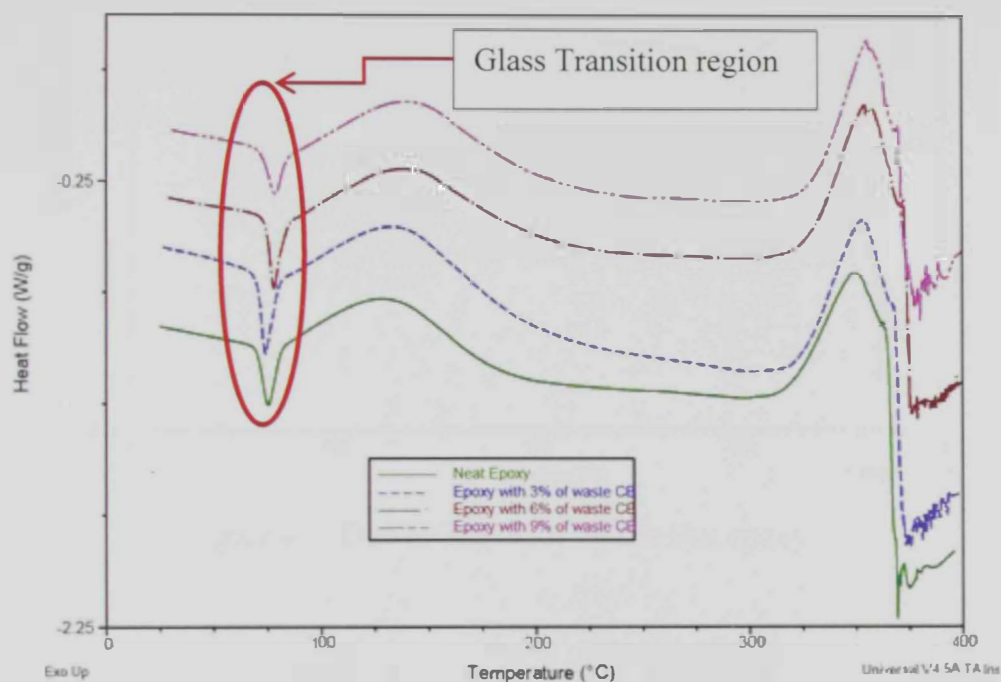


Figure 4-4: DSC graphs for epoxy mixed with different wt. % of waste CB

Figure 4-5 demonstrates that the glass transition temperature is around 75.4°C for neat epoxy. This means that this epoxy can be used in applications exposed to an environment below this temperature. However, the graphs for the epoxy mixed with CB in Figures: 4-6, 4-7, 4-8 and 4-9 show a slight decrease in glass transition temperature. The decrease reaches to approximately 72.6°C . The reduction in the

glass transition temperature is due to the blending of waste CB. A possible chemical reaction between the carbon black with the amine group from the hardener occurred. Thus, the crosslinking of the epoxide groups will be reduced. Figure 4-9 shows the glass transition temperature as a function of waste CB Wt. % blended in epoxy resin.

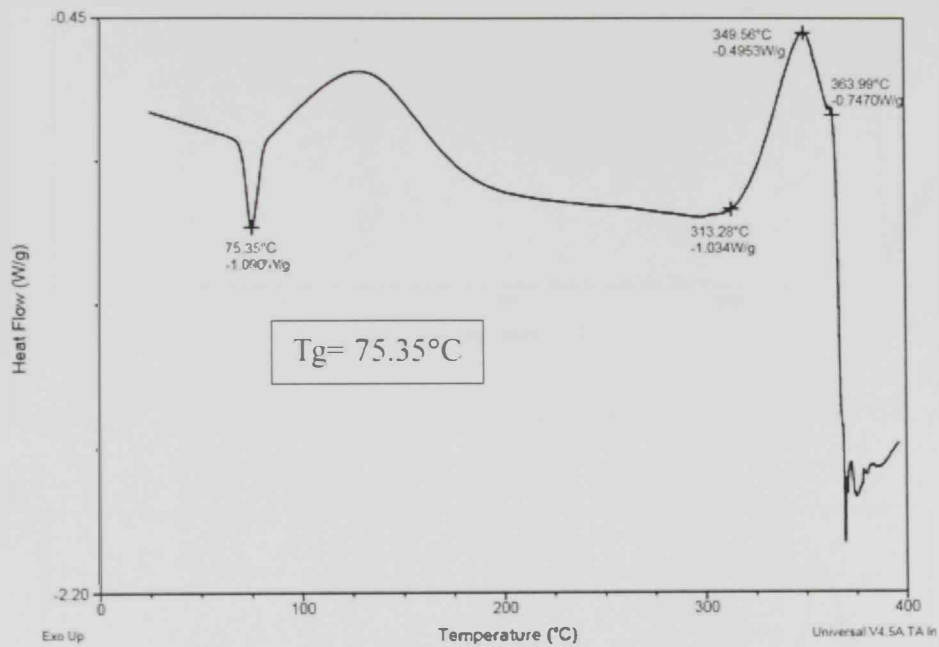


Figure 4-5: Determination of Tg for neat epoxy

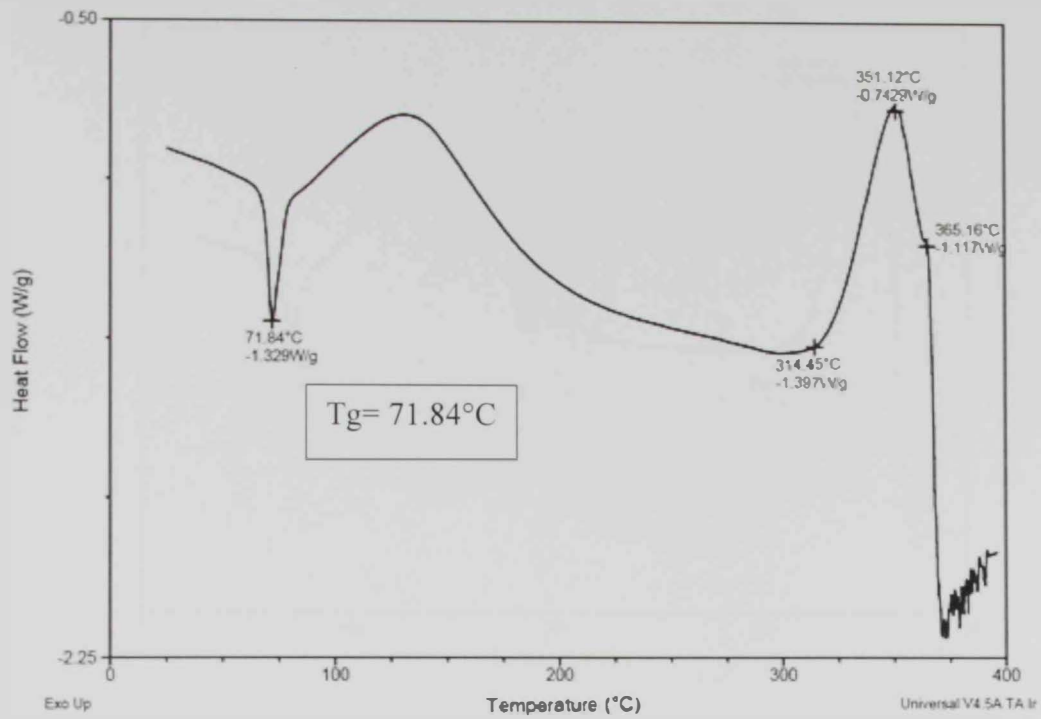


Figure 4-6: Determination of T_g for epoxy mixed with 3 wt. % of CB

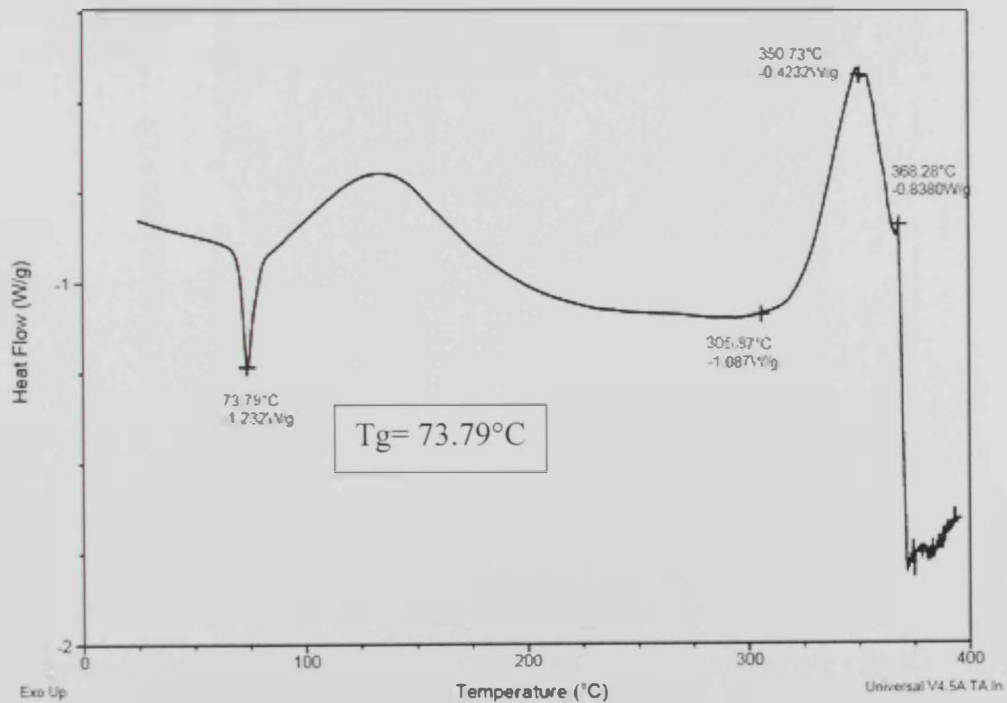


Figure 4-7: Determination of T_g for epoxy mixed with 6 wt. % of CB

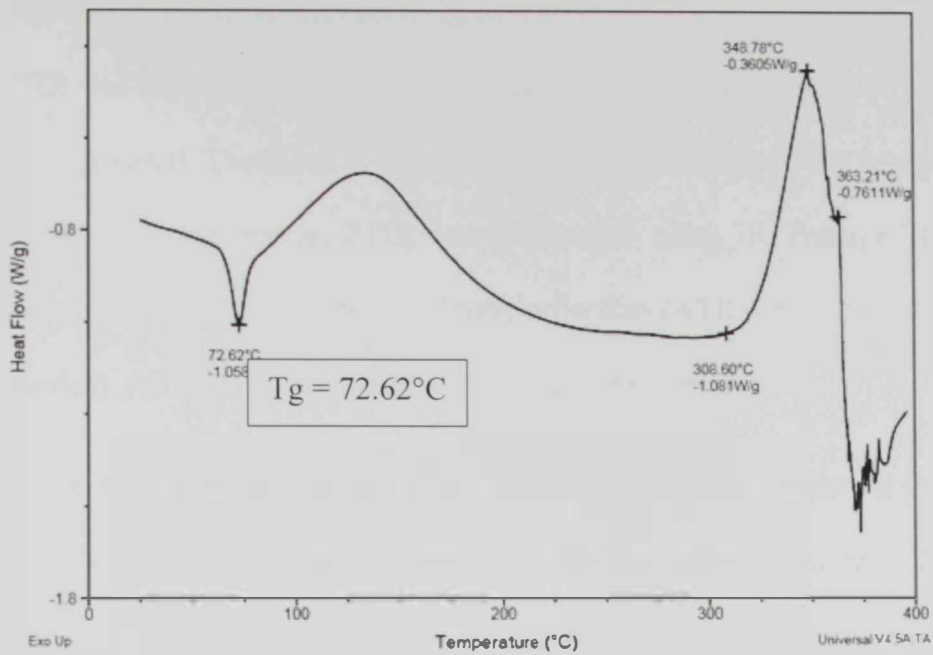


Figure 4-8: Determination of T_g for epoxy mixed with 9 wt. % of CB

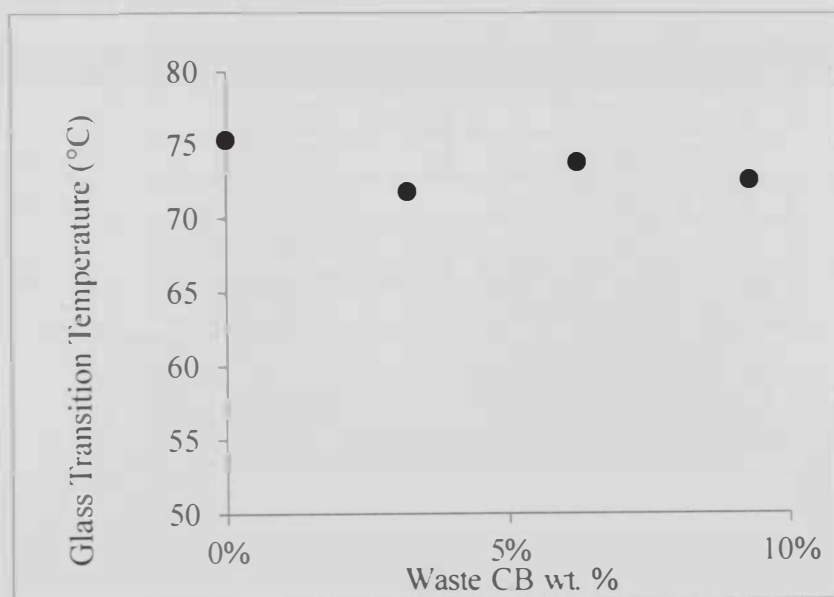


Figure 4-9: Glass transition temperature as a function of waste CB Wt. %

4.3 Fourier transform infrared spectrum ((FTIR)

FTIR was used to investigate the presence of specific and important chemical groups in the material. Therefore, it will investigate the possibility of the formation of carbon bonds with the matrix. FTIR was performed using IR Prestige-21 FTIR Spectrophotometer support by attenuated total reflection (ATR) (from SHIMADZU, North America). All the spectrum graphs are listed in Appendix C.

Figure 4-10 demonstrates the FTIR spectra for samples consisting of epoxy mixed with different percentage of waste CB. All the major peaks related to the epoxide groups were observed. The common absorption peaks that are related to the epoxide groups are: $\sim 825\text{ cm}^{-1}$, $\sim 910\text{ cm}^{-1}$, $\sim 1250\text{ cm}^{-1}$ which are listed in Table 4-3.

Table 4-3: Epoxide group FTIR peaks

Waste CB wt. %	Peak No. 1	Peak No. 2	Peak No. 3
0%	825.5 cm^{-1}	910.4 cm^{-1}	1242.2 cm^{-1}
3 wt. %	825.5 cm^{-1}	Not shown	1244.1 cm^{-1}
6 wt. %	825.5 cm^{-1}	906.6 cm^{-1}	1236.4 cm^{-1}
9 wt. %	Overlap due to generation of new peak	Overlap due to generation of new peak	1259.6 cm^{-1}

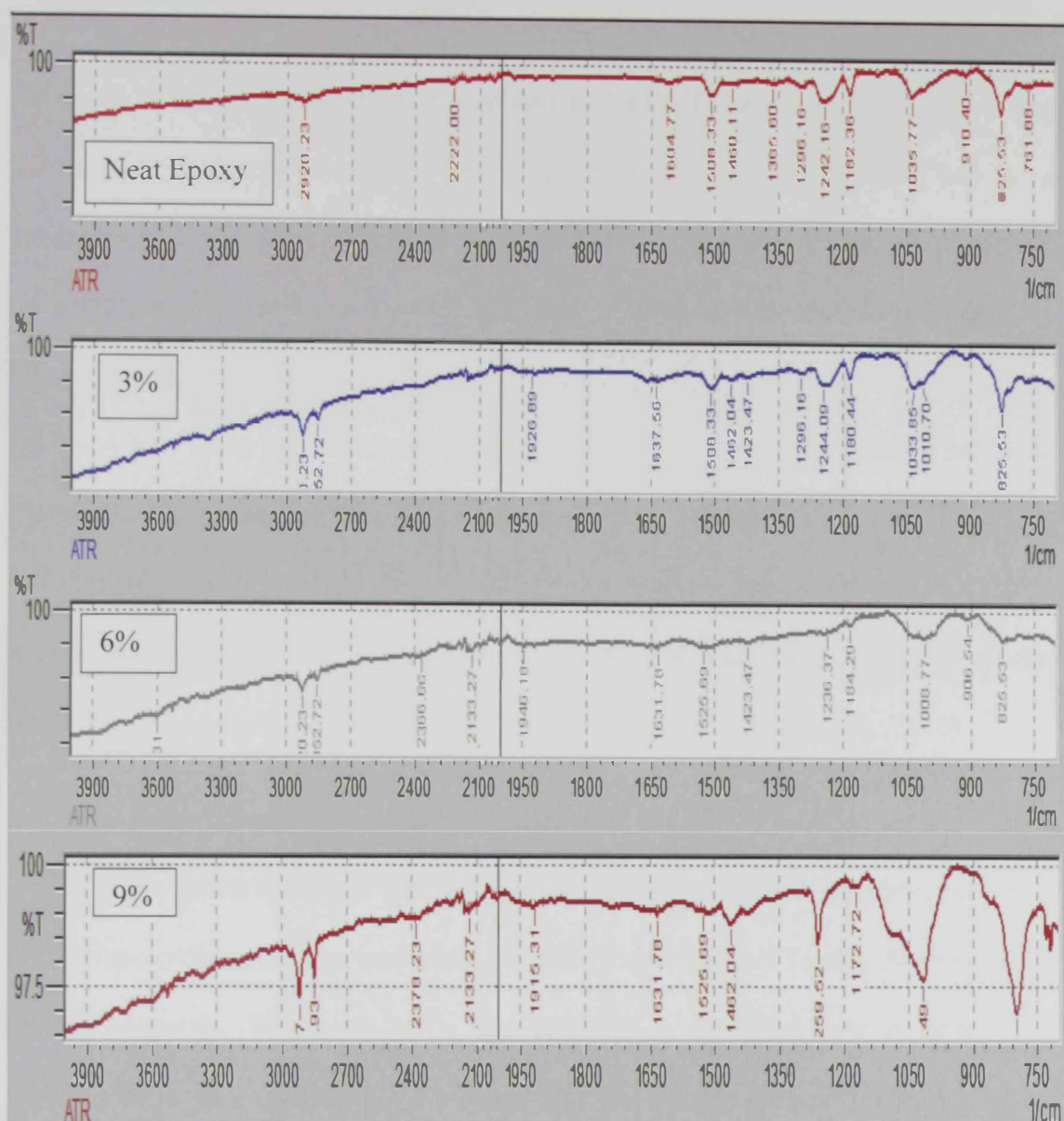


Figure 4-10: FTIR spectra for epoxy mixed with different wt. % of waste CB

Moreover, an absorption peak at around 1510 cm^{-1} was observed in all the samples with different wt. % of waste CB and it was related to the stretching of $-C-O-C-$. A small absorption peak at 1631.8 cm^{-1} was observed for most of the samples and it was related to the stretching mode of cured resultants. The hydroxyl group $-O-H-$ band does not show in any of the spectra (Rane et al., 2014).

A vibrational band was observed for neat epoxy and epoxy mixed with CB. This peak is around 2920 cm^{-1} and is related to the C–H stretching. By adding waste CB to epoxy, a new vibrational peak was observed around 2133 cm^{-1} and it is attributed to –C–O group (Ahamad et al., 2014). Also, a new vibrational peak was observed around 2853 cm^{-1} which are also related to also the C–H stretching (Mohanty et al., 2013).

A new sharp and high intensity peak was observed for epoxy with 9 wt. % of CB at 798.53 cm^{-1} and at 1016.5 cm^{-1} . This might be related to the stretching of the C–O group. This suggests a possible interaction between the carbon and the epoxy matrix. As mentioned previously, a possible chemical reaction between the carbon black with the amine group occurred (Mohsin et al., 2011; Nikolic et al., 2010).

4.4 Nano-indentation of epoxy and waste carbon black

Nano indentation is a tool for measuring the mechanical properties at small scale. Nano indentation was performed by Nano Test Materials Testing Platform Two (Micro Materials, Wrexham, UK). The platform is equipped with a three-sided pyramid Berkovich type diamond indenter tip. The sample is fixed on the top of an aluminum fixture to enable the indentation.

The nano-indentation loading-unloading curves of epoxy loaded with different wt. % of waste CB are shown in Figures 4-11, 4-12, 4-13 and 4-14. The Hardness was extracted from the curves it is a measure of material strength.

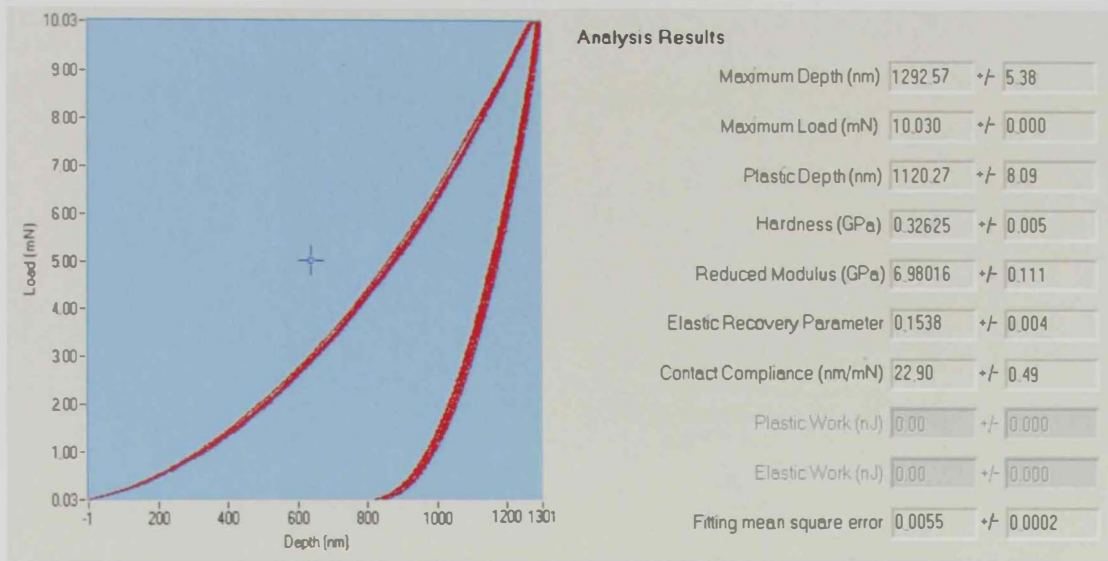


Figure 4-11: Loading-unloading curve for neat epoxy

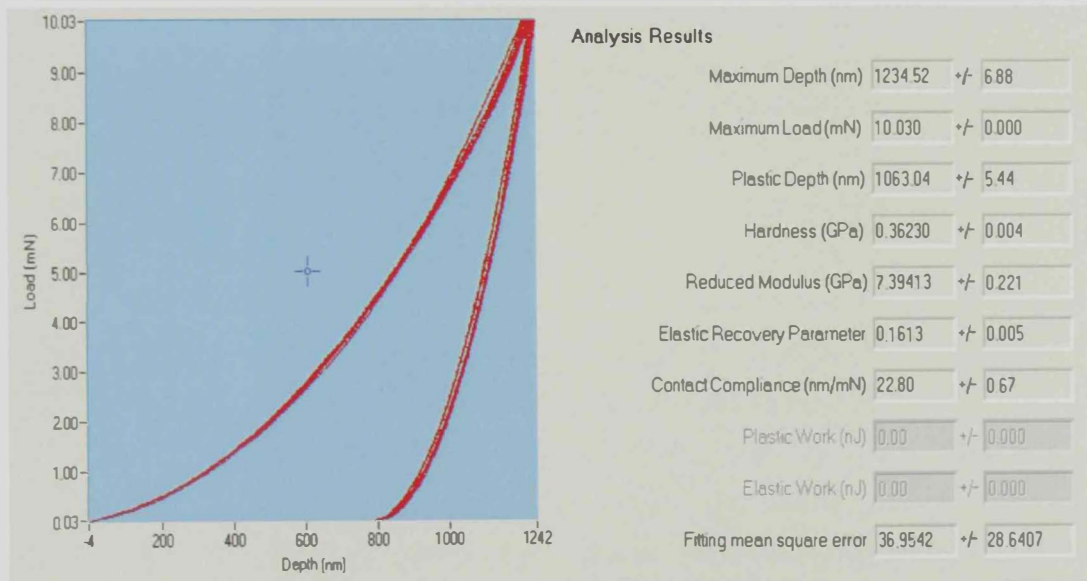


Figure 4-12: Loading-unloading curve for epoxy mixed with 3 wt.% of waste CB

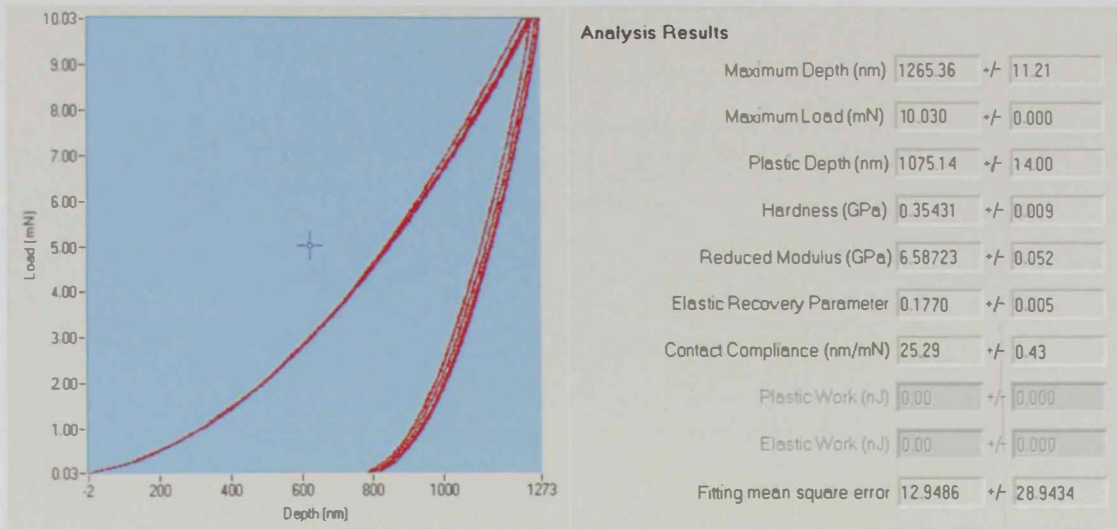


Figure 4-13: Loading-unloading curve for epoxy mixed with 6 wt. % of waste CB

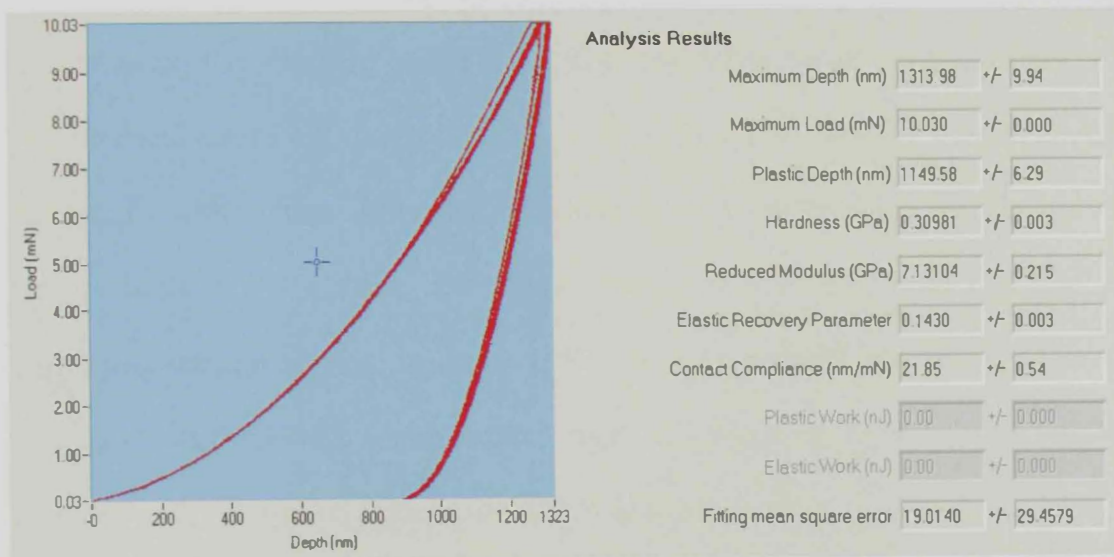


Figure 4-14: Loading-unloading curve for epoxy mixed with 9 wt. % of waste CB

The result of the hardness is listed in Table 4-4. It is noted that the hardness slightly increases when the epoxy is loaded with 3 wt. % of waste CB. As the waste CB wt. % increases, the hardness slightly decreases.

Table 4-4: The result of nano-indentation of epoxy loaded with different wt.% of waste CB

Waste CB (wt. %)	Hardness (GPa)
0%	0.3263
3%	0.3623
6%	0.3543
9%	0.3098

4.5 Electrical conductivity

Electrical conductivity was investigated by using DC Source Measure Unit KETHLEY 236 (from KETHLEY, US). The measurement was done on small sample size because the expected result is a high resistance value. Unfortunately, the unloaded and loaded epoxy with 3%, 6% and 9% did not pass any DC current through the sample with voltage differences reaching to ± 100 volt between the top and the bottom surfaces. As a result, the sample was considered an insulator. Then, the electrical conductivity was measured indirectly by a network analyzer. Moreover, new epoxy samples with highly loaded waste CB reaching 30 and 40 wt. % was prepared and investigated again by the DC Source Measure Unit.

4.5.1 Electrical conductivity using network analyzer

Vector Network Analyzer (from ROHDE & SCHWARZ, Germany) was used to measure indirectly the electrical conductivity of epoxy mixed with different/low weight percentage of waste CB.

The principal is to transmit electromagnetic waves with variable frequencies into the sample (range: 9kHz to 14 GHz). Different epoxy samples with different waste CB wt. % were prepared in cylinder geometry. The diameter was 1 inch and the length was selected to be 4 inch to provide semi-infinite geometry to ensure the transmission and reflection only through the sample. The preparation was achieved by following the procedures described in section 4.1.

A dielectric assistance kit probe 3.5 (DAK Coaxial probe) with 1 inch diameter was used to transmit and receive the reflected electromagnetic waves through the sample. Based on the radiation coefficient (S_{11}), the DAC software will provide the permittivity of the samples in real and imaginary values and the conductivity as a function of electromagnetic frequency. The real value of permittivity (ϵ') is a measure of how much energy is stored in a material from the electromagnetic field. The imaginary value of permittivity (ϵ'') is a measure of how lossy is the material to electromagnetic field. Figure 4-14 shows the result of electrical conductivity as a function of electromagnetic frequency for epoxy mixed with different wt. % of waste CB (0%, 2%, 5% and 10%). It is noted that the conductivity does not change significantly by adding 2wt. % and 5 wt. % of waste CB. However, epoxy with 10wt. % of waste CB shows a higher trend of electrical conductivity. This suggests a percolation threshold occurrence within this loading level of waste CB. The dielectric constant vs. frequency graphs are attached in Appendix D. Also, reflection coefficient S_{11} vs. frequency graphs are attached in Appendix D. It is also noted that the conductivity of epoxy with low loading of waste CB (2 wt. %, 5 wt. % and 10 wt. % of waste CB) is dependent on the frequency and the dielectric constant. This

reveals that epoxy loaded not more than 10 wt. % of waste CB is not suitable for DC conduction. The conductivity of the medium subjected to electromagnetic radiation is given by equation (4).

$$\epsilon_c = \epsilon \left[1 - j \frac{\sigma}{\omega \epsilon} \right] \quad (4)$$

where ϵ_c is the complex permittivity

$$\text{since } \epsilon_c = \epsilon' - j\epsilon''$$

$$\text{and } \epsilon' = \epsilon$$

$$\text{then, } \epsilon'' = \sigma/\omega$$

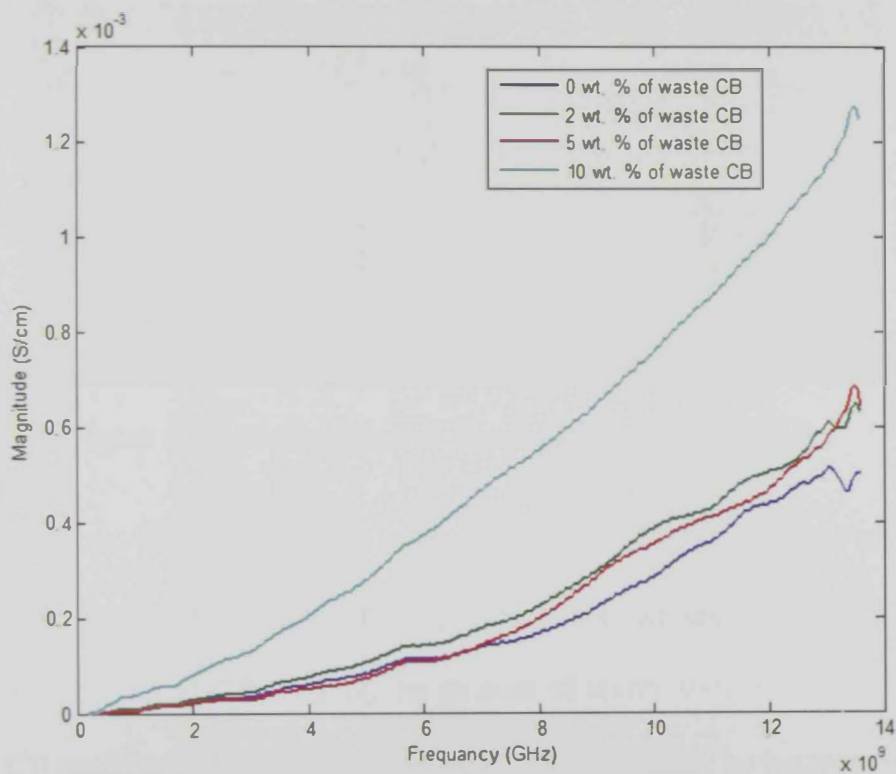


Figure 4-15: Conductivity as a function of electromagnetic frequency for epoxy with different waste CB wt. %

4.5.2 Electrical conductivity of highly loaded epoxy with waste CB

Electrical conductivity of the epoxy mixed with high wt. % of waste CB was investigated as a function of wt. % of CB in the epoxy matrix. The test was performed using DC Source Measure Unit KETHLEY 236 (from KETHLEY, US). The measurement was done on small sample size because the expected result is a high resistance value of the material. The dimensions of the measured samples are $15 \times 15 \times 3 \text{ mm}^3$. The sample was sandwiched between two electrodes connected to the source measure unit as is shown in Figure 4-15.

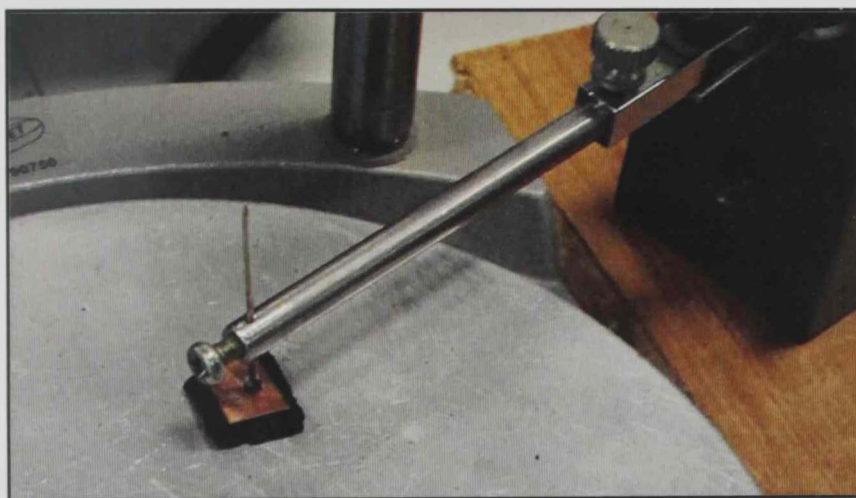


Figure 4-16: Placing epoxy/CB sample between electrodes

Therefore, it was decided to increase the waste CB wt. % to be above 30%. However, the mixing will be manually by hand as the mixture before curing will be highly viscous. At high CB loading, the amount of epoxy starts to be fully engaged with the CB particles in which the stirring will not be possible by magnet stirrer. The sample preparation steps are as follow:

1. 60 grams of epoxy was filled into glass container.

2. The required wt. % of the waste CB was added to the epoxy (40 grams for 40 wt. % CB and 25.7 grams for 30 wt. % CB).
3. 30ml of acetone was added as a solvent and to facilitate the stirring.
4. Stirring was performed by hand for 10 minutes.
5. The mixture was heated for 30 minutes at 80°C to evaporate the acetone.
6. The hardener was added with ratio 4 to 1 followed by hand stirring for 20 minutes until the mixture became very viscous in order to ensure the waste CB will not settle.
7. The mixture was casted into plastic disk cavity.
8. Samples were cured at room temperature for not less than 6 hours.

Figure 4-12 shows the cross sectional area comparison for different loading of waste CB. While Figure 4-12 (a) demonstrates the epoxy sample with 9 wt. % of CB that was prepared in the previous investigation section 4.1. Figure 4-12 (b) illustrates the epoxy sample with 30 wt. % of CB. Figure 4-12 (c) shows the epoxy sample with 40 wt. % of CB. It was clearly shown in the highly waste CB loading, that the waste CB particles are more compact and hence the chance of creating electron network channels is higher. It was observed during the sample preparation that the 40 wt. % of CB approximately reaches the critical pigment volume concentration (CPVC). This means that above this percentage, there will not be enough epoxy to bind the rest of waste CB powder. However, an extra rich layer of polymer around 0.1mm in thickness on the top and the bottom surfaces was observed even in the case of CPVC. This layer was removed by using sandpaper.

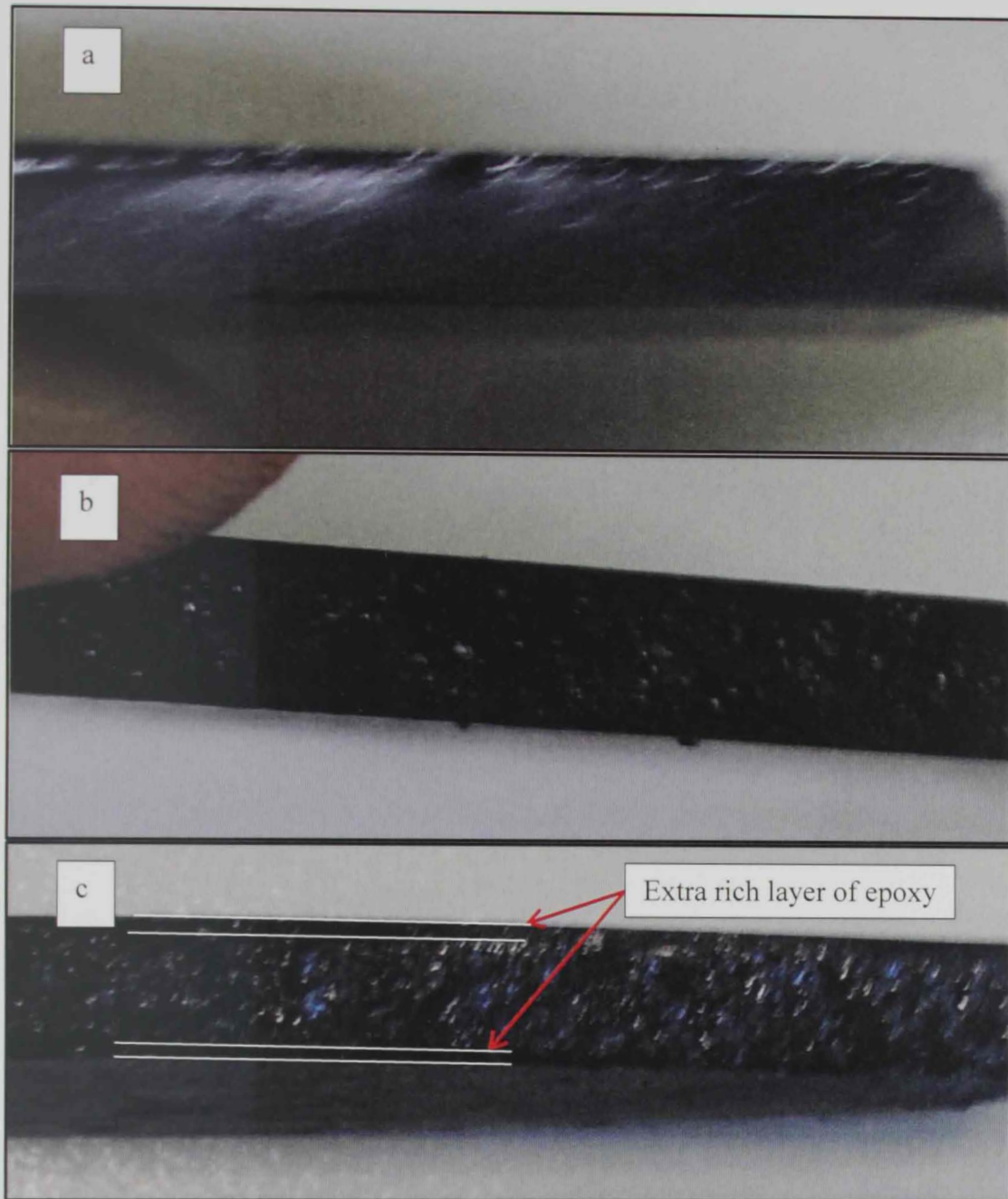


Figure 4-17: Cross section area of the prepared epoxy/CB samples

An investigation on the electrical conductivity of epoxy sample that is highly loaded with waste CB (30% and 40%) was conducted with the same setup that was described in Figure 4-11. It was observed that the samples can pass DC current source that reaches to 0.001 Amp. by applying voltage range -10 to +10 volts. Figure 4-13

shows the plot of I-V for 30 wt. % sample and Figure 4-14 represents the plot of I-V for 40 wt. % sample. The resistance was extracted from I-V plots to determine the electrical conductivity. The values are summarized in Table 4-4.

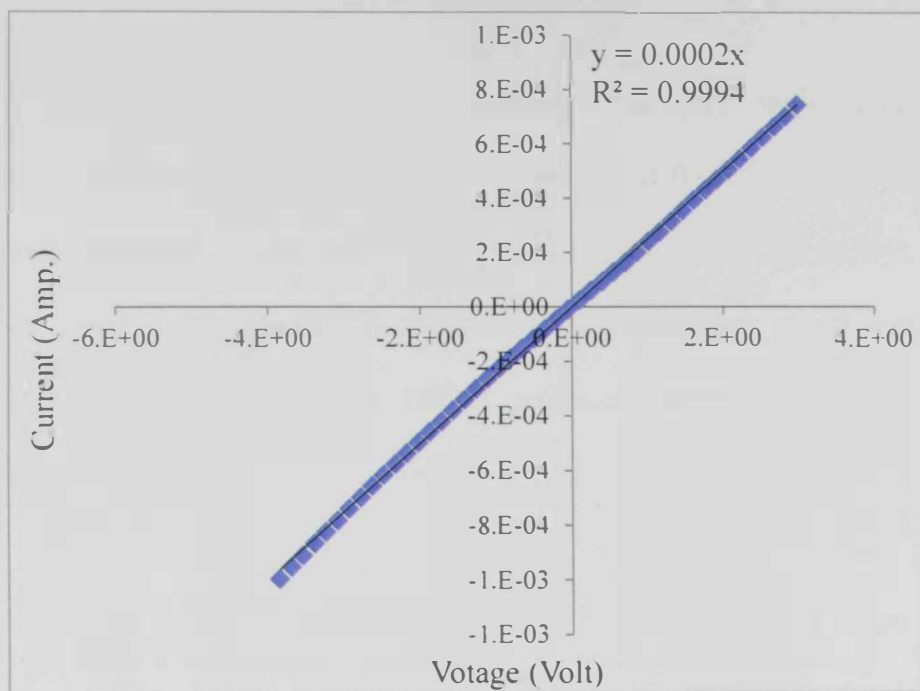


Figure 4-18: I-V plot for epoxy with 30 wt. % of waste CB

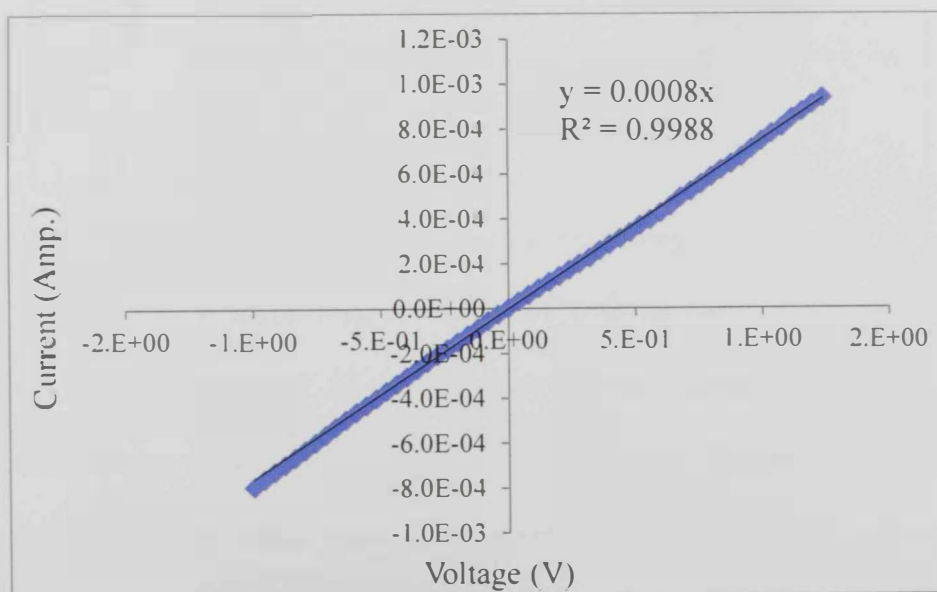


Figure 4-19: I-V plot for epoxy with 40 wt. % of waste CB

Table 4-5: Conductivity measurement for epoxy loaded with high % of waste CB

Waste CB wt. %	R (Ohms)	Thickness (cm)	Area (cm ²)	Resistivity (Ohm.cm)	Conductivity (σ /cm)
30%	5000	0.34	0.072	1058.8	0.0009
40%	1250	0.31	0.072	290.3	0.0034

Figure 4-19 shows the electrical conductivity of epoxy with high loading of CB. The electrical conductivity of 40% of waste CB is 0.0034 σ /cm. This value is very small compared to the other work done on producing conductive polymer composite using epoxy. Du (2008) obtained 1 S/cm for epoxy mixed with 40% of synthetic graphite. Moreover, Du (2008) produced epoxy mixed with 40% of expanded graphite with conductivity value reaching 100 σ /cm.

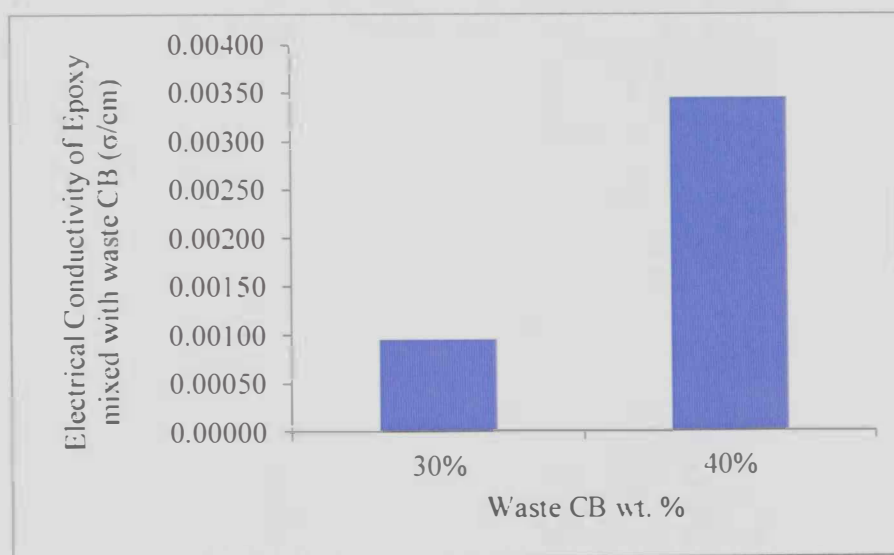


Figure 4-20: Result of electrical conductivity of epoxy/CB

From these investigations, epoxy mixed with annealed waste CB at 1250°C does not have a potential as conductive polymer composite. The electrical conductivity is very low compared to the other work done by using graphite source. This composite is very brittle, hence, extra investigation in mechanical properties was not performed due to breakage of the sample during the de-molding. The mechanical

properties using a carbon fiber has proven to be enhanced in comparison with the polymer. the following study, presented in chapter five, investigates the effect of impregnating carbon black as a filler with carbon reinforced polymer composite and the effect on the electrical conductivity and mechanical properties.

CHAPTER FIVE

CARBON BLACK MEDIATED CARBON FIBER REINFORCED EPOXY CONDUCTIVE POLYMER COMPOSITE

This chapter presents the alteration of properties as a result of loading waste carbon black into carbon fiber reinforced composite with epoxy resin (CFRP). The properties have been investigated at different loading capacities based on weight percentage from the total weight. The surface and through plane electrical conductivity were investigated. Furthermore, the through-plane thermal conductivity and flexural properties were determined.

5.1 Preparation of polymer matrix loaded with waste carbon black

Waste carbon black was produced by a pyrolysis process followed by post heat treatment at 1250°C to improve the electrical conductivity of the waste carbon black. The reinforcement of CFRP by waste carbon black powder was done by mixing this powder with the epoxy resin; 100 grams of epoxy resin mixed with variable weights of waste carbon black. The mixture was heated at 80°C to reduce the epoxy viscosity. Then, the mixture was uniformly mixed on a magnetic stirrer while keeping the temperature of the mixture at 80°C for three hours to facilitate a uniform dispersion. Then, the hardener was added to the resin mixture with epoxy to hardener ratio 4:1. The epoxy resin type was ARALDITE® AY105 IN form HUNTSMAN (see table (4-1) for material specification). While, the hardener is ARADUR® 42 which is a polyamine. The crosslinking reaction is based on the primary amine groups

in polyamine. Polyamine is converted to secondary and tertiary amines to create cross linkage and curing (Nikolic et al., 2010).

5.2 Fabrication of fiber reinforced polymer

The carbon fiber used is 10.9 oz/sq yd, 0.024" thick, 6K; 5HS weave construction (see Table 5-1 for material specification according to the supplier). Different weight percentages of, the post heat-treated, waste carbon black powder of the carbon fiber composite have been prepared. The fiber is cut into square pieces 20x20 cm. Where the number of carbon fiber is 4 layers with zero degree orientation for all the layers.

Table 5-1: Technical data of 6K, 5HS Weave Carbon Fiber (according to Fiber Glast Development Corporation)

Warp Raw Material	6K –Multifilament Continuous Tow
Filling Raw Material	6K –Multifilament Continuous Tow
Weave Pattern	5 HS
Fabric Areal Weight	10.8-11.5 oz/yds ²
Nominal Thickness	.024 inches
Tensile Strength	610-700 KSI
Tensile Modulus	33-34.9 MSI
Elongation	1.4-1.95%

The lamination was performed on waxed with low roughness stainless steel plate. The mixture of epoxy and waste CB was uniformly distributed on the carbon fiber cloth by using a wiper to eliminate the extra epoxy mixture between the carbon fiber layer and the stainless steel plate. After lamination, the composite was covered by another waxed stainless plate and placed in hot press machine (Figure 5-1) with parameters listed in Table 5-3.

Table 5-2: Hot press machine pressing parameters

Parameter	Value
Platen temperature	350K
Load	8000 lbf
Total surface area of prepared composite	62 in ²
Pressing time	15 minutes



Figure 5-1: Hot press machine (CARVER 3893, USA)

In order to determine the weight percentage of resin and waste CB from the final laminate, the weight of 4 carbon fiber layers was measured before lamination. After hot pressing (curing), the total weight was measured to obtain the weight of resin and waste CB in the laminate. It was difficult to control the wt.% of the waste CB and resin mixture with respect to fiber for all samples using the hand lamination/hot press technique. This problem was noticed by weighing the samples after pressing and curing. Also, the thickness of the final laminate increased as the resin weight fraction increased as it is shown in Figure 5-2, for the sample that

contain waste CB at 16 wt.%. This can also be contributed to the fact that the high wt. % waste CB in the epoxy matrix cannot be fully immersed between the fibers and hence, will settle on top of the laminate which will have a negative effect on the properties of the prepared composite material: especially the electrical conductivity values for the higher wt. % of CB.

Table 5-3: Determination of waste CB weight% after curing

CB wt. % ratio to resin	Carbon fiber total weight of layers (grams)	Final weight after hot press (grams)	Resin + CB wt. %	CB wt. % ratio of total composite	Thickness of laminate (mm)
0.0%	66	92	28.3%	0.0%	1.37
5.4%	63	94.5	33.3%	2%	1.47
14.6%	65	94.5	31.2%	5%	1.45
22.2%	67	102	34.3%	8%	1.6
30.0%	66	139	52.5%	16%	2.6

It has been noticed that the thickness of the prepared composite material was stable with waste CB loading from 0% to 8%. The thickness at these loadings was approximately 1.5mm. On the other hand, at high waste CB loading (16%), the thickness of the composite laminate reaches to 2.6mm. It means that there was an extra built up polymer 1.1mm in thickness at loading equal to 16 wt. % of waste CB.

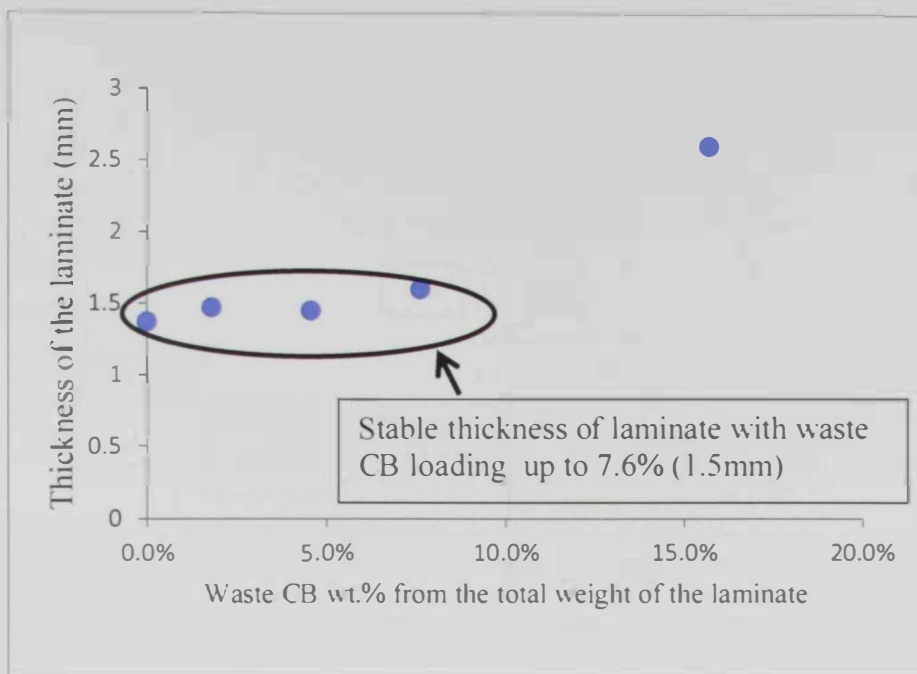


Figure 5-2: Waste CB wt. % vs. sample thickness

Figure 5-3 shows that the amount of weight % of resin from the total composite weight was stable at waste CB loadings equal/below 8%. The resin weight percentages for these loading are between 28% and 34%. However, the resin mixture weight percentage from the total reached to a high value. The value reaches to 52% for the waste CB loading of 16%. This also confirmed that the rich interlayer generated between the carbon fiber plies. These interlayers consist of epoxy mixed with waste CB.

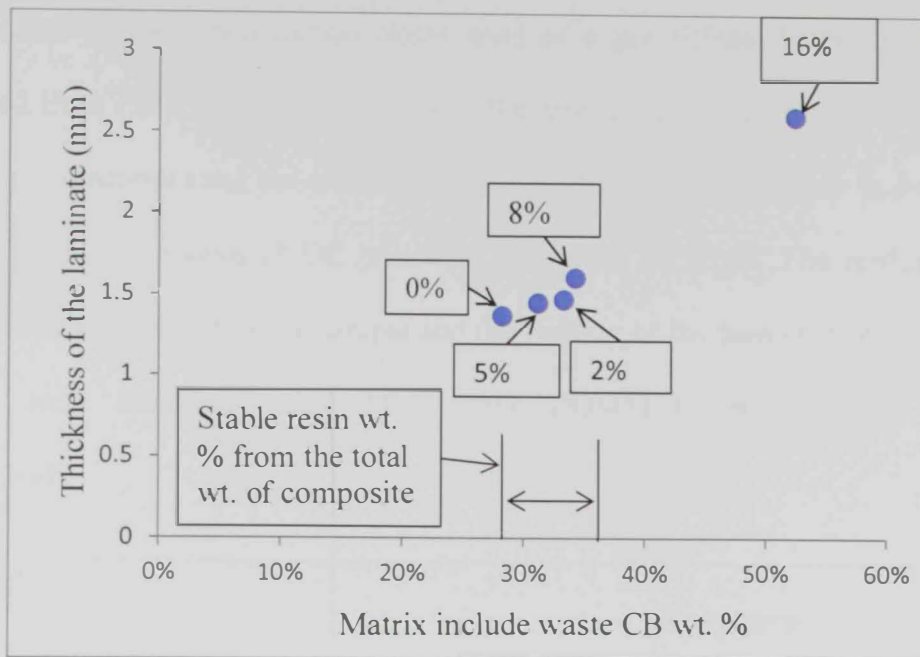


Figure 5-3: Wt. % of the matrix included waste CB vs. sample thickness

5.3 Through plane conductivity of solid material

5.3.1 Through plane conductivity of solid material

The through plane conductivity was measured using an experimental setup shown in Figure 5-4. The setup has been built according to the Department of Energy (DOE) specifications. This is because the setup has been used in evaluating the through plane conductivity of the composite polymer that can be used as a bipolar plate in PEMFC. A compression pressure of 1.5 MPa was applied on the sample and the setup is as specified in DOE target (Kim et al. 2012; Kim et al., 2014; Antunes, 2011; Alayavalli et al., 2010; Du, 2008; Kumar, 2003).

Testing the through plane electrical conductivity of carbon fiber reinforced composite filled with different percentages of waste carbon black was performed by using a D.C power source at room temperature by following the procedure in Kim et al. (2012). Figure 5-4 shows the electrical conductivity setup. The sample was

sandwiched between two carbon cloths used as a gas diffuser layers in fuel cells supplied from FREUDENBERG to lower the interfacial contact resistance between the copper electrodes and the composite sample. The 2 inches electrode in diameter is gold coated. The source of DC power is PowerFlex CPX200. The reading of the micro-voltage drop across the sample and the reading of the pass current through the circuit were measured using Multimetrix DDMM240 and Agilent 34405A, respectively.

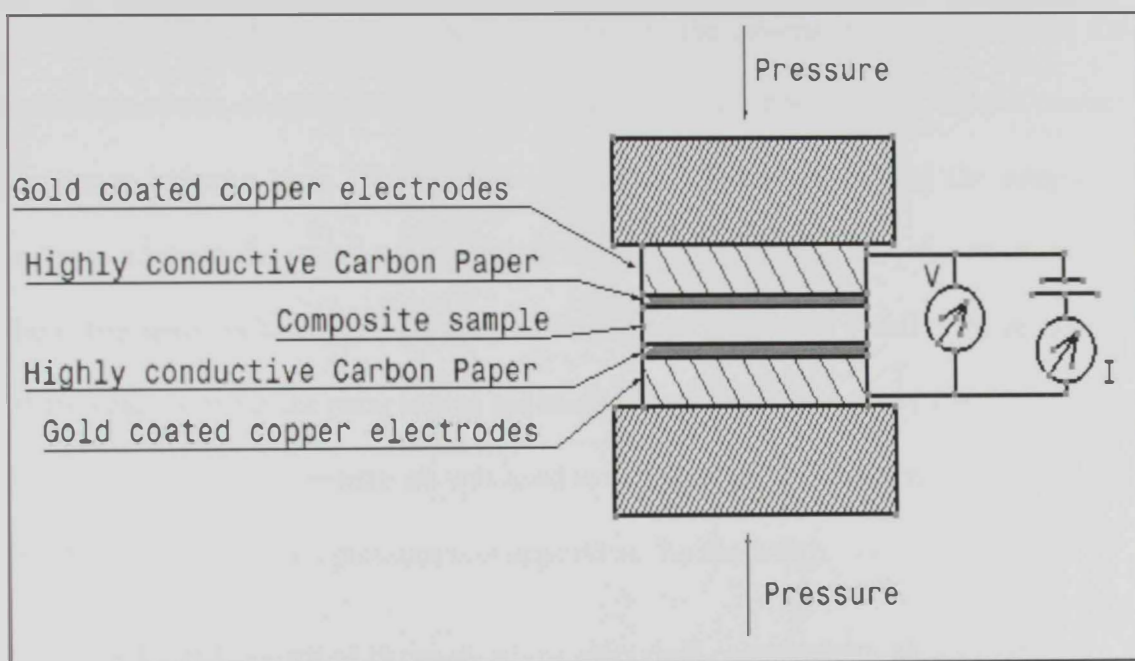


Figure 5-4: Through plane electrical conductivity measuring setup

The conductivity of the solid samples is measured using the calculation procedure described in section 3.2.1 and is given by equation (1) page 30:

$$\sigma = \frac{l}{R * A}$$

where R is the electrical resistance in Ω . A is the surface area of the composite sample. The resistance of the measured samples was determined by Ohm's law. For each run, R is measured by taking the slope of V vs. I .

10 different voltage readings were applied to the system with maximum current of 1 Amp to avoid the heating that may affect the resistance value of the sample. All the samples show slopes with R-squared value=0.999 which reveals good ohmic contact between the sample and the entire carbon papers.

Before installing the sample in the testing fixture, the system resistance includes the resistance of two copper electrodes, the two conductive carbon papers and the contact resistance between them (Figure 5-4) is measured without installing the sample in order to subtract the resistance generated through the circuit. Then, the resistance of the entire setup including the composite sample was measured. Finally, the resistance of the setup without the sample was subtracted from the resistance of the entire setup (setup + sample). This resistance was used to calculate the conductivity of the sample. A 1.5 MPa compression pressure was applied on the sandwich.

5.3.2 D.C result of through-plane electrical conductivity of composite sample

The through plane electrical conductivity of the prepared composite showed that as the weight percentage of the waste carbon black increases, the electrical conductivity increases up to an optimum point that equal to 5%. Then, the electrical conductivity for the composite material started to decrease as the loading of waste CB increased above this value. It was also noticed that the electrical conductivity for waste CB was lower than the carbon fiber electrical conductivity. Furthermore, the

extra filler mixed with the resin was dispersed on the top of each layer which generates extra thin layers between the fiber laminates with electrical conductivity lower than the laminate conductivity. This was confirmed with the thickness of the sample section 5.1. For higher loading (at 16 wt. % of waste carbon black), there was a generation of epoxy/waste carbon black layers between the carbon fiber laminates that will have built up extra resistance between the carbon fiber laminates.

The percolation threshold cannot be predicted in through plane conductivity because the composite material is already loaded with carbon fiber that makes the through plane electrical conductivity above the percolation threshold.

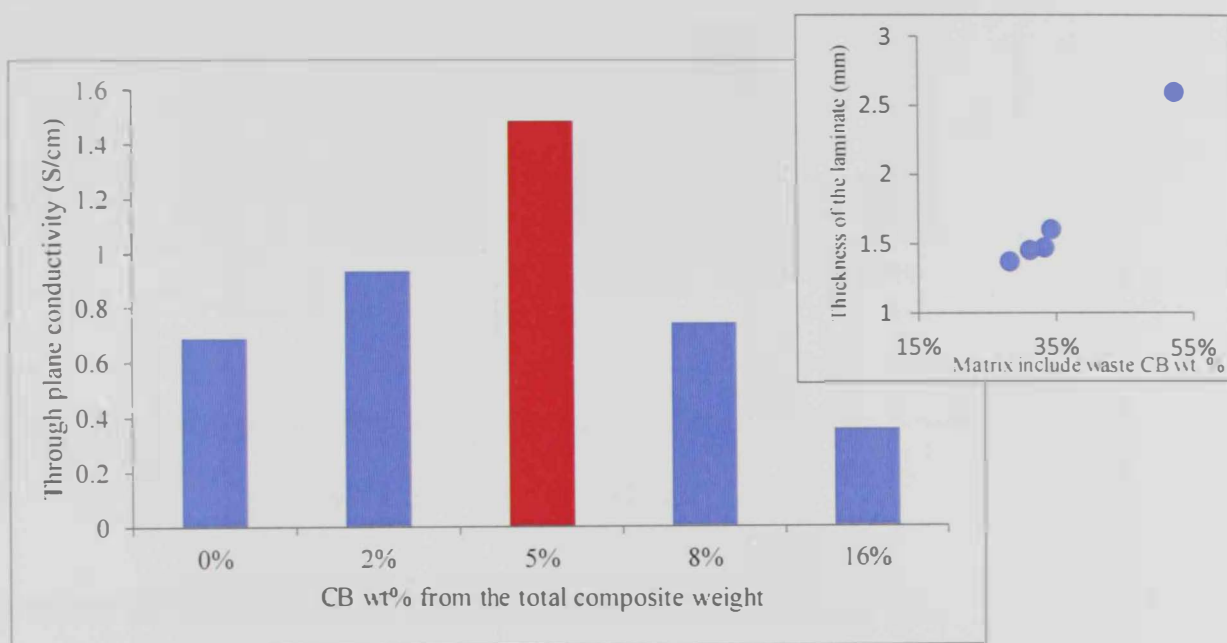


Figure 5-5: Through plane electrical conductivity result

It is advised by Kim et al. (2012) and Kim et al. (2013), to compare the result of through plane conductivity of the composite material with the area specific resistance. The area specific resistance (ASR) is defined as:

$$ASR = R \times A$$

where R is the resistance of the entire system including the bulk resistance of the sample and interfacial contact resistance between the sample and the carbon papers (GDLs). The result shows that the minimum ASR was obtained at 5% loading of waste carbon black.

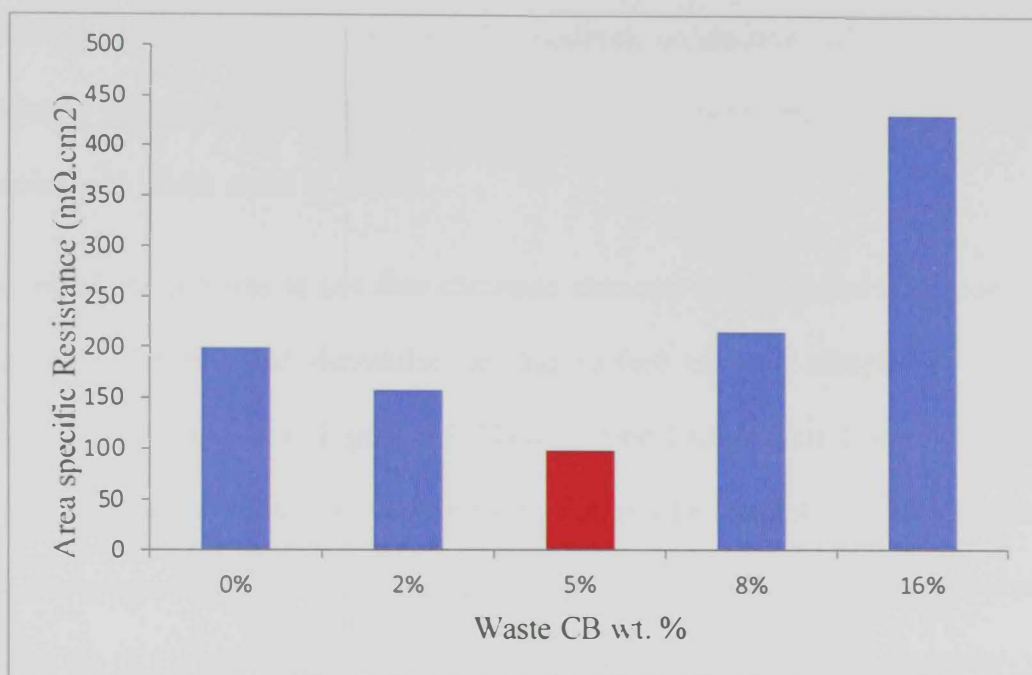


Figure 5-6: Area specific resistance (ASR) of carbon fiber composite at different waste carbon black loadings

5.4 In-plane electrical conductivity of solid material

The surface conductivity (or in-plane conductivity) was studied to investigate the effect of adding waste CB in the carbon based polymer composite. The objective is to increase the surface electrical conductivity as the Wt. % of waste CB increases.

5.4.1 Surface electrical conductivity of solid material measuring technique

The in-plane electrical conductivity has been performed using ASTM 4496 for moderately conductive, which suits the fiber reinforced polymer composite with four point probes technique. The standard ASTM 4496 is used to determine the electrical resistivity for materials that are generally moderate conductive and are neither good insulators nor good electrical conductors. The test was performed on rectangular flat samples with width equal to 15mm.

The initial attempt was to use four electrode channels (non-guarded electrodes) that were produced by gold deposition on the surface of each sample with known dimensions as is shown in Figure 5-7. Then, electrical wires were fixed on the top of the gold channels by silver conductive paint. The second attempt was more successful than the previous attempt. In this case 4 strips of copper electrodes were stacked on the surface of the sample as shown in Figure 5-8. The sample and the electrodes were exposed to a compression load equal to 40 MPa by utilizing the known mass used in weight balance.

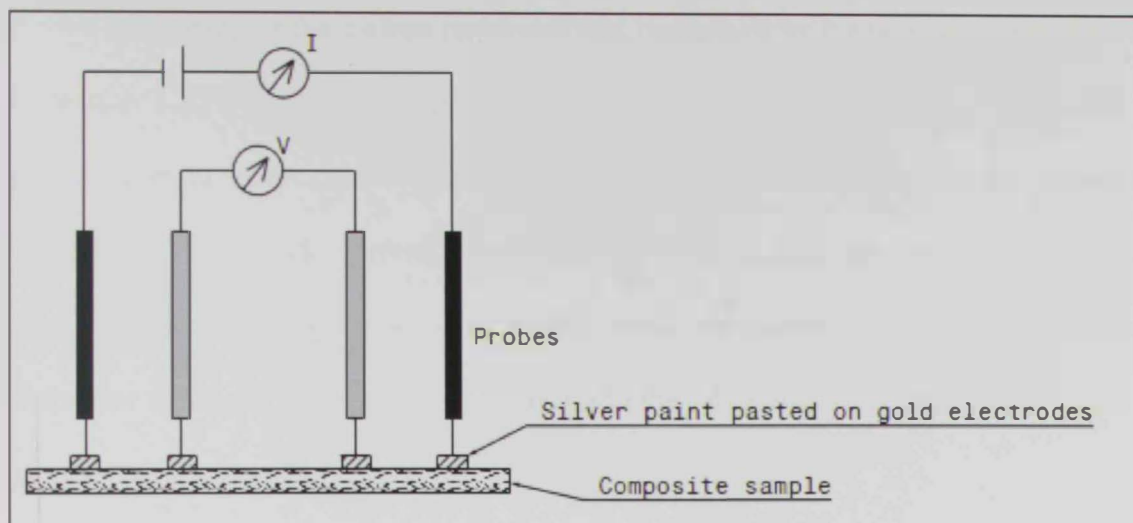


Figure 5-7: Surface electrical conductivity (four points' probes.) setup using conductive paste

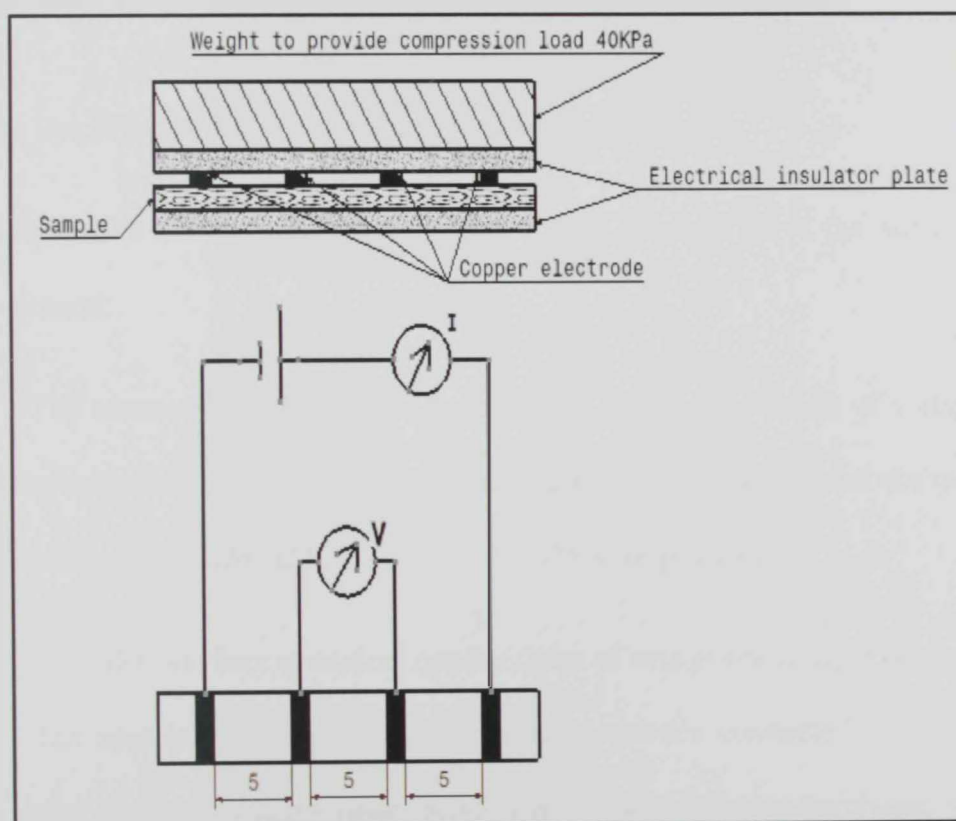


Figure 5-8: Surface electrical conductivity (surface conductivity) using copper strips as electrodes under compression load

Measuring of the surface resistance was performed by the procedure described in section 3.2.1. Voltage readings were taken in the range between 0 to 0.1 V with passing current lower than 1 amp to avoid the influence of heating on the sample resistance. Voltage vs. current slope was obtained to find the resistance of the measured sample. Electrical conductivity was calculated by normalizing the resistance with sample dimensions according to the following equation.

$$R_s = \frac{V}{I} \quad (3)$$

where R_s is the surface resistance, Ω .

The surface resistivity is given by:

$$R_s * \frac{W}{L} \quad (4)$$

L is the length between the two voltage measuring electrodes.

W is the width of the measuring sample. L and W must have the same unit of measurement.

The source of DC power is PowerFlex CPX200. The reading of voltage drop along the sample and the reading of the pass current through the circuit are measured using Multimetrix DDMM240 and Agilent 34405A, respectively.

5.4.2 D.C surface electrical conductivity of composite sample result

The approach was to make four gold electrodes connected with electrical wires using silver conductive paste. Silver conductive paste was purchased from RS electronics. The gold electrodes were produced by vacuum deposition of gold on the

surface of the sample. A metallic mask containing multiple slots with 3mm width was stacked on the sample in order to deposit the gold on the sample through the slots and hence produce the gold electrodes. The electrodes width is 3mm. The distance between each electrode is also 3mm. Finally, the silver paint was carefully applied on the gold electrode.

The circuit was built based on the four points probe technique. The two middle wires were connected to a micro-voltmeter to read the voltage drop across the distance between the two electrodes (equal to 3mm). The sides of electrodes are connected to the power source circuit which is connected with a digital multi-meter to read the current passed through the entire system.

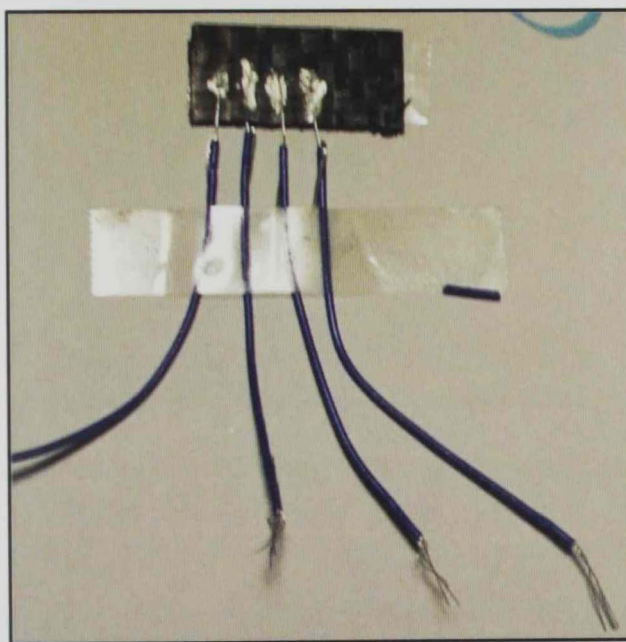


Figure 5-9: Four point connections using silver conductive paste for in-plane conductivity test

However, the result using the silver conductive paint was not stable for majority of the samples and the effect of increasing the Wt. % of waste CB on the surface electrical conductivity was not achieved by using the silver paint connection method. The reason for this was because the paint might contain solvents that are absorbable by the material under test. Thus, it will affect the conductance performance of the sample in an irreversible manner.

Another approach in Figure 5-10 was used to eliminate the silver paste by using a removable copper electrode with 3mm wide strips. The distance between each two electrodes is 5mm. The result is more stable once we applied same load on each sample.

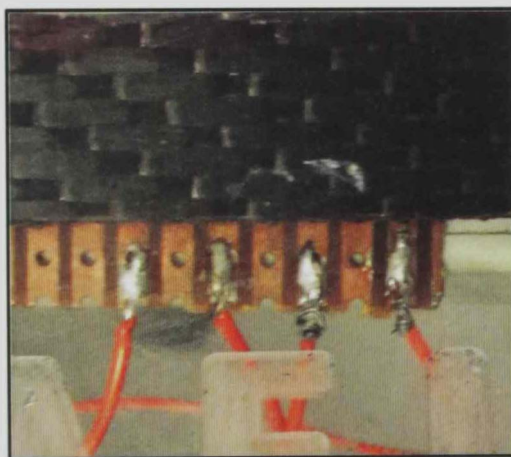


Figure 5-10: Four point connections using copper electrodes for surface conductivity test

The measurement of electrical conductivity was performed by following the procedure mentioned in section 3.2.1. Each Wt. % of waste CB was measured with three different samples that were randomly selected from the prepared samples. However, the samples with contamination or moisture were replaced by other samples. Moreover, the measurement setup was repeated three times, for which the

results are listed in Table 5-5. It shows that the surface electrical conductivity of the sample without adding waste CB is equal 2.5σ (per square). The trend of surface conductivity as a function of waste CB loading is shown in Figure 5-11. Loading the composite material with 2 Wt. % of waste CB results in increasing the surface conductivity that reached an average value equal to 13.2σ (per square). This value is 5 times greater than that of the sample without waste CB. After that, the surface electrical conductivity became stable with no significant fluctuation at loading levels above the 2 %. Adding waste CB to the resin resulted in creating a conductive carbon network and hence decreased the effect of the extra rich polymer layer on the surface of the composite. The average surface conductivity at 2% and above was equal to $13 \pm 3.9 \sigma$ (per square).

Table 5-4: The result of surface conductivity

CB wt. %	Conductivity σ (per square)	Conductivity σ (per square)	Conductivity σ (per square)	Average surface conductivity σ (per square)	Standard Deviation
0%	1.85	3.66	1.87	2.46	1.04
2%	8.73	14.06	16.34	13.04	3.91
5%	14.52	10.76	10.76	12.01	2.17
8%	10.2	10.6	11.25	10.68	0.53
16%	9.59	9.59	12.09	10.43	1.45

It is observed that the three different readings of surface conductivity contain some reading variation due to the following measurement errors :

1. Non uniform distribution of waste CB in the epoxy resin.
2. Difficulty in controlling the volume fraction between carbon fiber and epoxy resin.

3. The resistance of the entire system is sensitive especially at the wire connections. Moreover, the resistances of the samples are small due to low voltage drop across the samples in which the readings are in micro volt. The low values make the measurement system very sensitive to any external source of electrical resistance.
4. The roughness and geometrical flatness of the samples.
5. Misalignment of the sample on the copper electrodes due to anisotropic properties of the material.

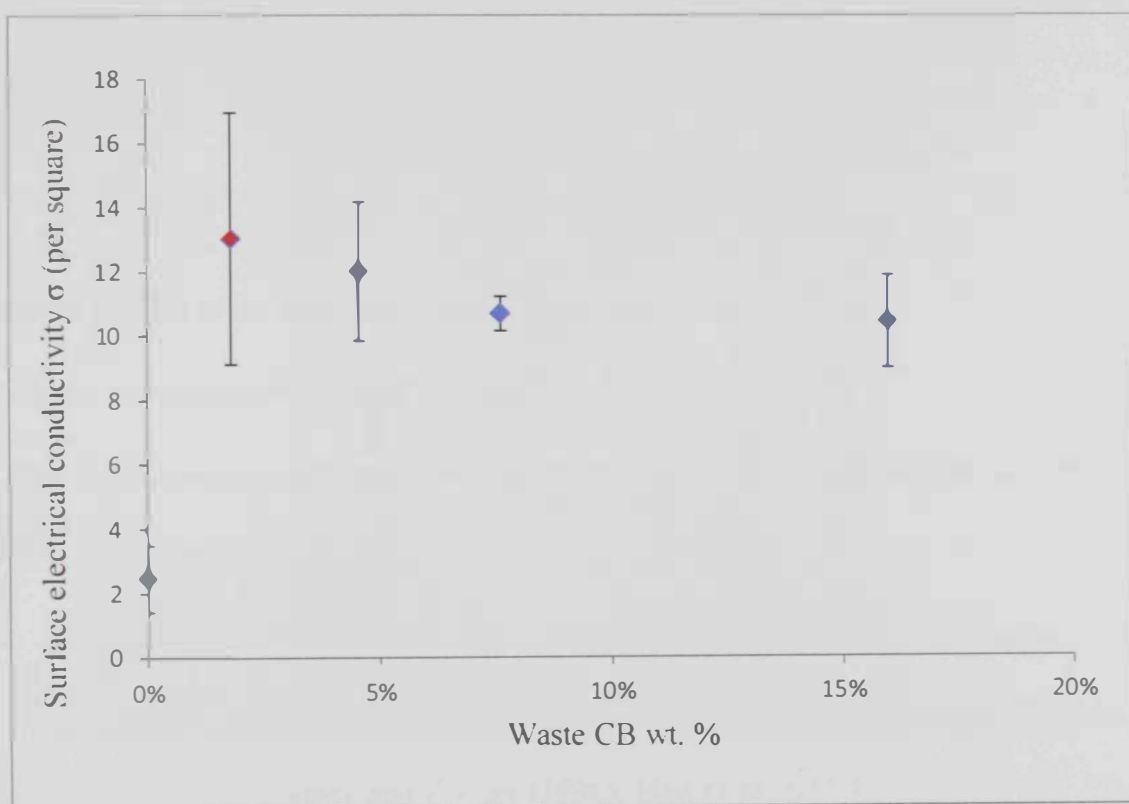


Figure 5-11: Surface electrical conductivity σ (per square) vs. waste CB wt. %

5.5 Through plane thermal conductivity

Thermal conductivity is a property of a material which is defined as the ability to conduct heat and is called the thermal conductivity coefficient. It is an important

property in material science, research and electronics especially for the parts exposed to high operation temperatures. High energy generation within any machine requires a material selection with high thermal conductivity, e.g., highly conductive material like copper is used in heat exchangers and material with low thermal conductivity can be used for insulation purposes.

The thermal conductance is defined as the quantity of heat ΔQ transmitted during time Δt through a thickness L in a direction normal to a surface of area A due to a temperature gradient within ΔT as is shown in equation (5):

$$Q = k A \frac{dT}{dx} \quad (5)$$

The unit measurement of thermal conductivity is $\frac{W}{m K}$

where A is the cross sectional area of the aluminum section

k is the thermal conductivity of the sample

dT is the temperature difference between the top and bottom surface of the sample

dx is the thickness of the samples.

Testing of through plane thermal conductivity of the prepared composites was performed to investigate if there is an enhancement in the thermal conductivity by adding waste CB. Farmer and Covert (1996), Han et al. (2008), Sweeting and Liu (2004) stated that the in-plane thermal conductivity of carbon fiber reinforced composite is high enough to allow the heat spreading along the surface of the laminate. However, carbon fiber reinforced composite reports low through plane

thermal conductivity. Figure 5-12 shows the difference between through-plane and in-plane directions.

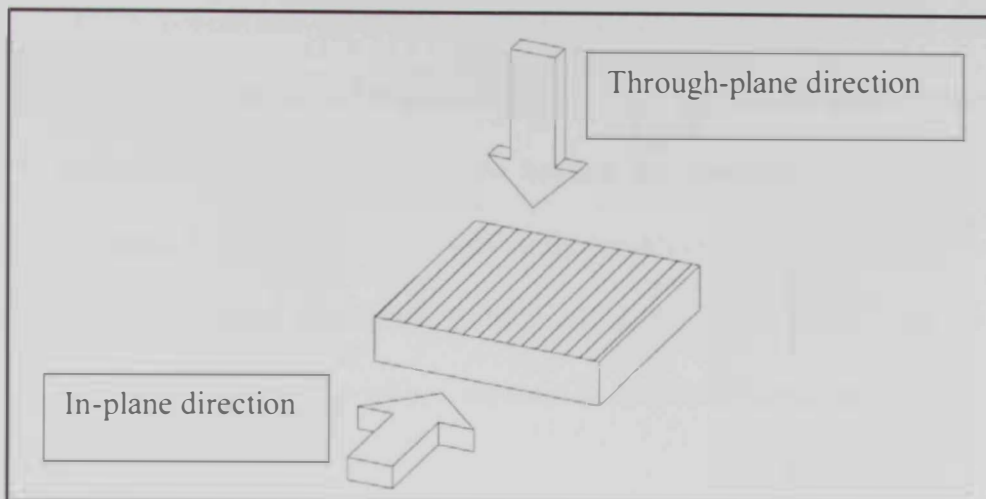


Figure 5-12: Schematic illustration of through-plane and in-plane directions

Both in-plane and through plane thermal conductivity of carbon fiber laminate are effective for heat dissipation. Han et al., (2008) demonstrated that the through plane thermal conductivity of carbon fiber laminates can be increased by interlaminar interface nanostructuring. The generated polymer rich region interface between the carbon fiber lamina is contributing an important role in increasing the thermal resistance of the carbon fiber laminate (Han et al., 2008).

5.5.1 Through plane thermal conductivity measuring technique

A heat conduction unit from Armfield (UK) shown in Figure 5-13 was used to determine the through-plane thermal conductivity of the CFRP composite samples.

The through plane thermal conductivity was investigated with different Wt. % of waste carbon black added to the CFRP. In a practical situation, the heat conduction occurs in three dimensions but requires a complex analysis to obtain. The adopted

apparatus is capable of investigating the one-dimensional heat through plane flow rate with respect to the temperature gradient and perpendicular area.

The heat conduction apparatus consists of two cylindrical metal bars arranged for one dimensional conduction experiments equipped with an array of temperature sensors. One of the cylindrical bars is the heating bar connected with an electrical heater. The heater is connected to a controllable electrical power source as shown in Figure 5-13. The second metal bar is the cooling element in which the water is supplied from a laboratory tap with a constant flow rate to maintain a steady state condition (equilibrium).

The conduction unit provides the capability of changing the power supplied to the heating element. Thermocouples connected to data acquisition to provide real time monitoring of the temperature gradient to allow the user to detect the steady state condition and hence record the temperature values across the bar. The apparatus is designed to clamp 48mm solid specimen between the heating and cooling elements. However, the in contact surface with working bars is 25.4mm (1 inch) in diameter.

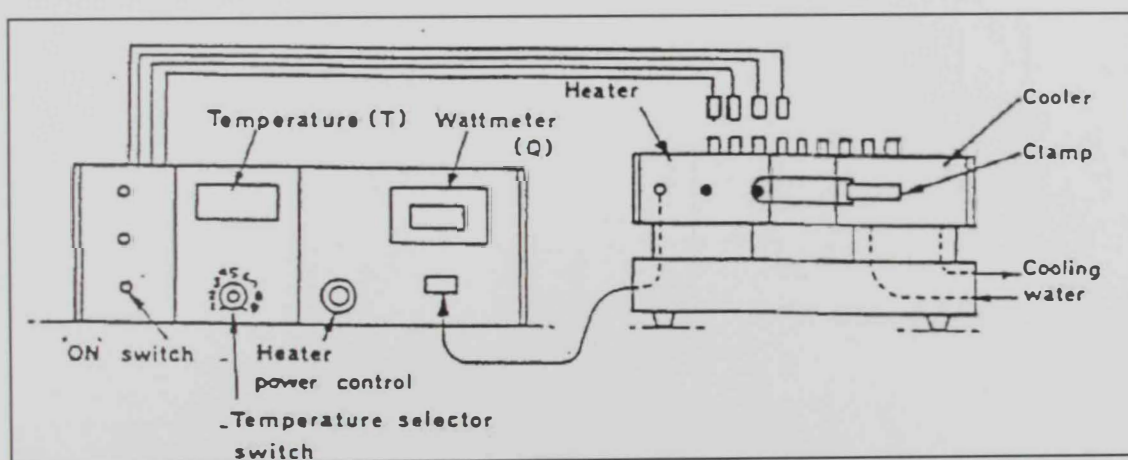


Figure 5-13: Thermal conductivity apparatus (Experimental operating and maintenance manual)

Thermal conductivity is obtained from the mentioned Fourier's law equation (5) stated above. The temperature thermocouples are placed with 10mm intervals along the linear apparatus bar. The heater power is displayed on a digital readout Wattmeter with an auto transformer power output varying from 0 to 100 Watts as shown in Figure 5-13.

Four thermocouples are installed with specific intervals along the working section to measure the temperature at four different locations namely (T_1, T_2, T_3 and T_4). The location of the thermocouples and the distance between them are described in Figure 5-14. Note that the contact thermal resistance was neglected, this is because the difference in thermal contact conductance of metallic bar is much higher than the total through plane thermal conductivity of the CFRP samples.

The temperatures at the four locations are taken after 30 minutes in order to allow the heat flow to reach to equilibrium state. Equilibrium state must satisfy the following equation:

$$T_1 - T_2 = T_3 - T_4 \quad (6)$$

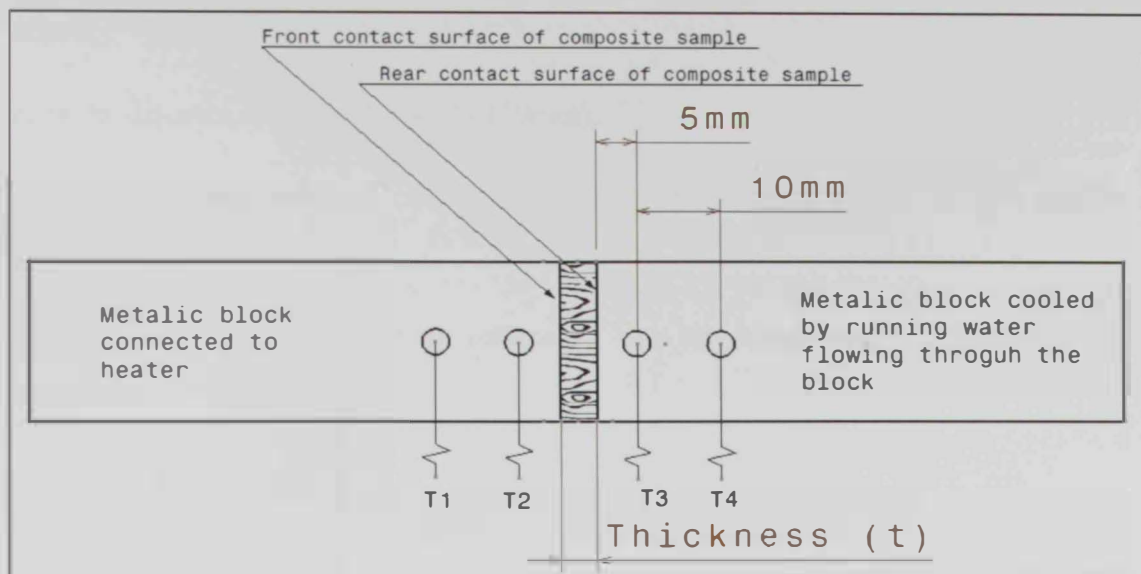


Figure 5-14: Setup and location of thermocouples

To measure the thermal conductivity using equation (5), the plot of the temperature profile at steady state must be determined along the thickness $\frac{\Delta T}{\Delta X}$.

where:

ΔT : is the temperature difference between the top and the bottom surfaces of the sample.

Δx : is the thickness of the sample.

However, the thermocouples T_2 and T_3 were placed 5mm from the surface of the sample. Hence, the temperatures of the top and bottom surfaces will be determined using a linear interpolation as described below in equations (7) and (8) below.

The temperature of the top of the sample T_A can be determined by the following equation:

$$T_A = T_2 - \frac{d_B}{d_A} (T_1 - T_2) \quad (7)$$

where:

d_A is the distance between T_1 and T_2 (10mm).

d_B is the distance between the location of T_2 and the top surface of the sample (5mm).

The temperature of the bottom surface T_D can be determined by the following equations:

$$T_D = T_3 + \frac{d_D}{d_C}(T_3 - T_4) \quad (8)$$

where:

d_A is the distance between T_3 and T_4 (10mm).

d_B is the distance between the top surface of the sample (5mm) and the location of T_3 .

Finally, the through plane thermal conductivity is given by:

$$k = \frac{A}{\Delta x * Q}(T_A - T_D) \quad (6)$$

5.5.2 Through plane thermal conductivity result

The temperature distribution along the working bar was recorded where the sample was in contact between them. The records are listed in Table 5-6.

Table 5-5: Temperature distribution along the working bar

CB Wt. %	Heating rate (W)	T1	T2	T3	T4	$\Delta 1$	$\Delta 2$
0%	19.35	153.9	149.5	29.8	25.6	4.4	4.2
2%	20.3	160.3	155.2	31	27	5.1	4
5%	20.3	158.5	155	29.9	26.9	3.5	3
8%	20.3	157.25	152.5	29.6	24.4	4.8	5.2
16%	19.3	161	157.8	30	27	3.2	3

It was noticed during the experimental work that the temperatures at the four locations did not change at a certain level after 30 minutes. This gives an indication that the equilibrium condition was reached. The difference between T_1 and T_2 is approximately equal to the difference between T_4 and T_3 . This is because the thermocouples are misaligned and not well placed vertically in the working bar. This will result in taking a temperature reading at a place different from the required place. Then, the top (T_A) and the bottom temperature (T_D) of the sample were determined from the four temperature readings using equations (7) and (8). The values are listed in Table 5-7. Moreover, the plot of temperature distribution along the working bar is shown in Figure 5-15.

Table 5-6: Determination of T_A and T_B

CB Wt. %	Heating rate (W)	T1	T2	T3	T4	T_A	T_D
0%	19.35	153.9	149.5	29.8	25.6	147.3	31.9
2%	20.3	160.3	155.2	31	27	152.65	33
5%	20.3	158.5	155	29.9	26.9	153.25	31.4
8%	20.3	157.3	152.5	29.6	24.4	150.1	32.1
16%	19.3	161	157.8	30	27	156.2	31.5

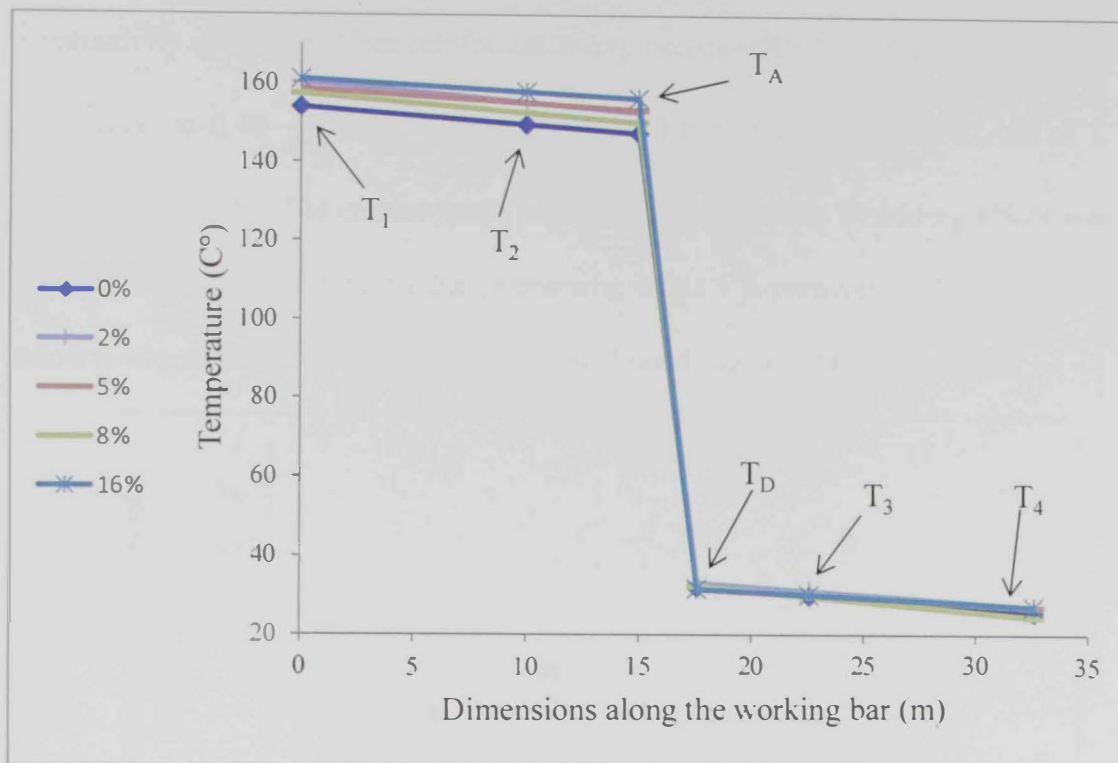


Figure 5-15: Temperature distribution along apparatus bar for all the prepared carbon fiber reinforced samples.

After determination of surface temperatures, the conductivity was calculated using equation (5) and the results are listed in Table 5-8.

Table 5-7: Result of thermal conductivity for different Wt. % of waste CB

CB (Wt. %)	Heating rate (W)	Δx (m)	T_A (C°)	T_D (C°)	Thermal Cond. (W/K.m)
0%	19.35	0.00137	147.3	31.9	0.47
2%	20.3	0.00147	152.65	33	0.51
5%	20.3	0.00145	153.25	31.4	0.49
8%	20.3	0.0016	150.095	32.13	0.56
16%	19.3	0.0026	156.2	31.5	0.82

Figure 5-16 shows the result of thermal conductivity for different Wt. % of waste CB. The result shows that the thermal conductivity increases as the wt. % of

the waste CB in the CFRP composite increases. The measured through plane thermal conductivity of carbon fiber reinforced epoxy composite without adding waste CB was equal to $0.46 \frac{W}{K.m}$. The thermal conductivity increased as the Wt. % of CB reached up to 16%. The enhancement on thermal conductivity by adding 8% of waste CB was 24%. It is anticipated that immersing waste CB particles in the carbon fiber reinforced composite will increase the thermal conductivity of the composite.

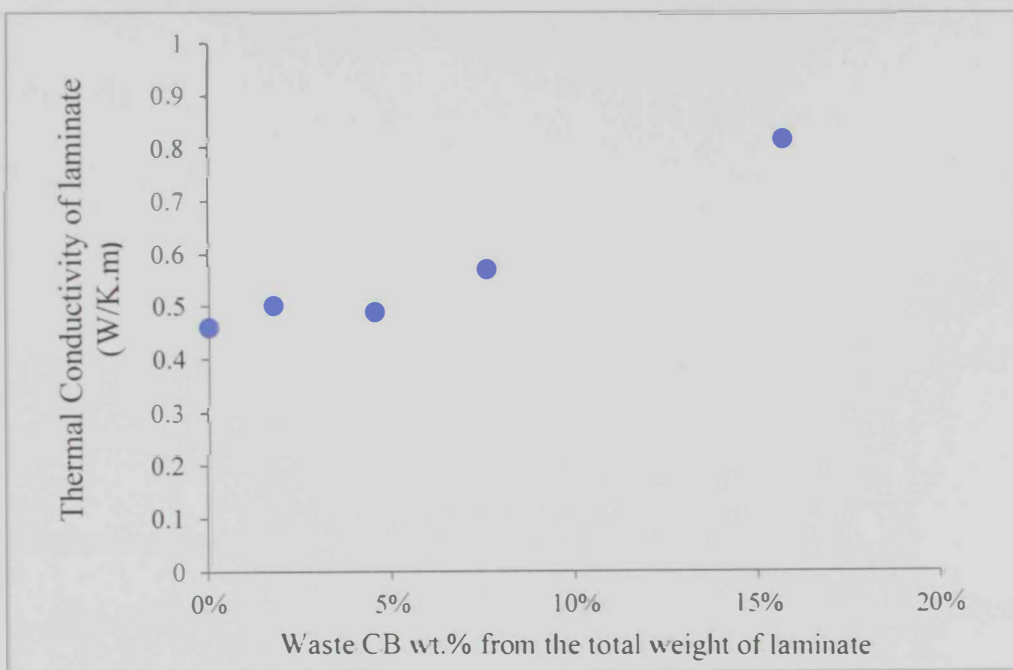


Figure 5-16: Thermal conductivity of the laminate vs. wt. % of waste CB

The buildup of extra rich layers of polymer between the carbon fiber plies did not affect the thermal conductivity performance. This is also confirmed by the equation of total thermal resistance connected in series.

Below is an example of the resistance of two materials connected in series:

$$R_{\text{Total}} = \frac{L_{\text{total}}}{k_{\text{eff}} \cdot A}$$

A: is the cross sectional area.

L: is the depth.

k: is the thermal conductivity of the material.

$$R_{\text{carbon fiber ply}} = \frac{L_1}{k_1 \cdot A_1}$$

$$R_{\text{rich polymer layer}} = \frac{L_2}{k_2 \cdot A_2}$$

$$R_{\text{Total}} = R_{\text{carbon fiber ply}} + R_{\text{rich polymer layer}}$$

$$\frac{L_{\text{total}}}{k_{\text{eff}} \cdot A} = \frac{L_1}{k_1 \cdot A_1} + \frac{L_2}{k_2 \cdot A_2}$$

$$A = A_1 = A_2$$

$$\frac{L_{\text{total}}}{k_{\text{eff}}} = \frac{L_1}{k_1} + \frac{L_2}{k_2}$$

Since $L_2 \ll L_1$

The effect of extra rich layer of polymer on the total thermal conductivity will be small compared to the effect of carbon fiber ply.

5.6 Mechanical properties

The mechanical performance of the material was investigated by studying its flexural strength. The mode of failure of this type of composite is a relatively complex process. Generally, the properties of the final composite laminate will depend on the following:

1. The properties of the fiber and the resin.
2. The orientation of the fiber and the stacking angles.
3. The nature of the interfacial bond between the fiber and the resin (Callister et al., 2008).

5.6.1 Flexural strength

In this study, the effect of loading waste CB into CFRP on the mechanical properties was investigated. The effect of adding different Wt. % of waste CB was examined by the studying the flexural strength. Flexural strength was tested by using three point bending test ,following the standard test method D790.

The test is performed using a simple beam supported at two points and loaded at the midpoint. The maximum flexural stress takes place in the middle of the outer surface of the tested beam. The stress is computed from the thickness of the sample, the bending moment and the moment of inertia of the cross section. While, the maximum tensile stress occurs at the bottom specimen surface below the loading point. The flexural stress can be determined by using the following equation:

$$\sigma_f = \frac{3PL}{2bd^2} \quad (9)$$

where :

σ_f = stress in the outer fibers at midpoint, MPa,

P= load at a given point on the load-deflection curve, N,

L= support span, mm,

b=width of beam tested, mm,

d=depth of beam tested, mm

The modulus of elasticity was determined and is defined as the ratio within the elastic limit, of stress to corresponding strain. It is calculated using the following equation:

$$E_B = \frac{L^3 m}{4bd^3} \quad (10)$$

where;

E_B - modulus of elasticity in bending (MPa),

L = support span (mm),

b = width of tested beam (mm),

d = depth of tested beam (mm),

m = slope of the tangent to the initial straight-line portion of the load-deflection curve, N/mm of deflection.

The three points bending test was performed using an MTS Universal test machine with testing speed 2 mm/min. The span length = 40 x sample thickness. This is required to induce tensile failure in the outer fiber of beam along its lower surface as it is recommended by the test standard D790 for a highly anisotropic composite laminate. The span to depth ratio must be high to ensure the failure will occur in the outer fibers of the sample and is due to the bending moment. (ASTM-2014)

5.6.2 Flexural Strength Result

The test was performed for CFRP composite samples consisting of 4 woven carbon layers mixed with epoxy resin at different percentage of waste carbon black. Each percentage was tested with 3 specimens. The stacking of all the carbon fiber plies are fixed with 0° ordination. In this study, the stiffness of the carbon fiber

laminate was the same for all the prepared samples. Thus, the only variable is the effect of different Wt. % of waste CB in each sample.

The result of flexural strength from three points bending test are listed in Table 5-8. The test was performed on 3 specimens for each Wt. % of CB. The load vs. deflections curves for all the samples are recorded in Appendix E.

Table 5-8: Flexural strength result obtained from three points bending test

Waste CB (Wt. %)	Flexural strength (MPa)			Average (MPa)	Standard Deviation
	Sample 1	Sample 2	Sample 3		
0%	654.1	631.6	691.8	659.2	30.4
2%	589.1	697	590.7	625.6	61.8
5%	555	632.5	632.5	606.7	44.7
8%	477.4	511.3	457	481.9	27.4
16%	252.5	266.7	263.1	260.8	7.4

As shown, the deviation range between the three samples is acceptable. The result obtained provides an indication on the effect of loading the waste CB into the carbon fiber composite laminate. Figure 5-17 describes the flexural strength trend as a function of waste CB Wt. %. The average flexural strength of laminate which consists of 4 layers of carbon fiber reinforced epoxy without adding waste CB was 659 MPa. Whereas, at 2% of loading waste CB into CFRP, the average flexural strength decreased to a value of 626 MPa. The reduction in flexural strength was approximately 5%. In the main, loading waste carbon black into CFRP was negatively affecting the flexural strength. The drop in flexural strength reached to 261 MPa at loading 16% of waste CB which means that the negative impact on flexural strength reached to 60% reduction.

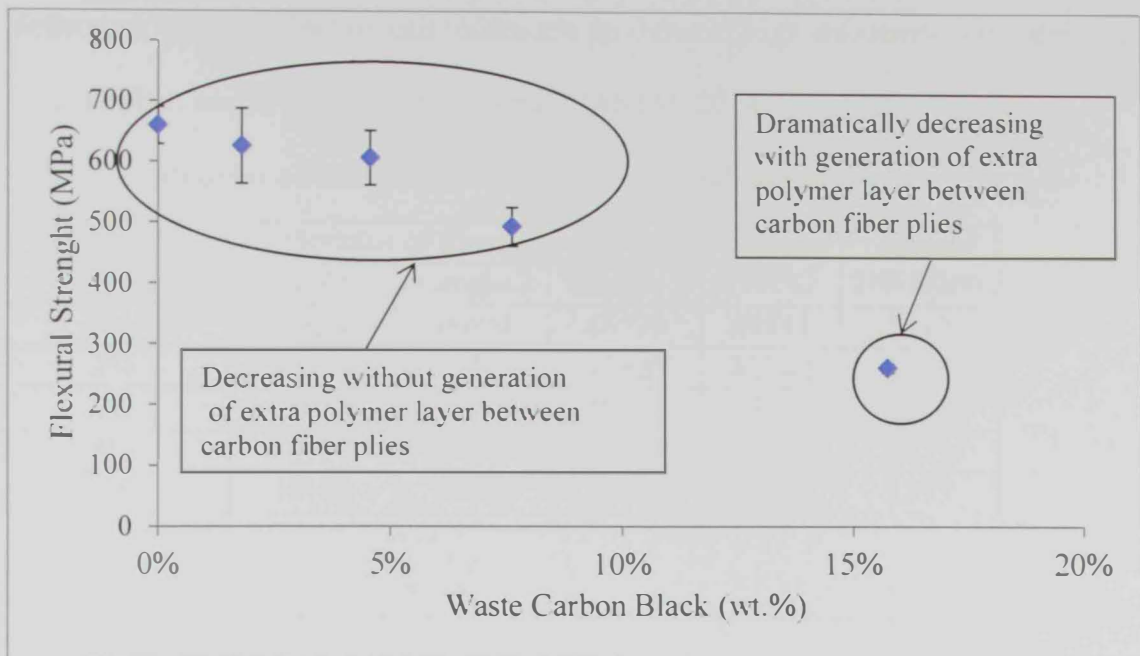


Figure 5-17: Flexural strength obtained from three points bending test

It was also noted that the flexural strength slightly decreased for waste CB loadings between 2% and 8% due to the reduction of adhesion between the carbon fiber plies. For the CFRP sample with 16 wt. % waste CB, the flexural strength was dramatically decreased. Note that at this loading percentage, extra rich layers of CB mixed with epoxy are generated between the fiber plies. These layers will be a bonding barrier between the carbon fiber plies that will reduce the interlaminar structure between the plies. Thus, the negative effect on the flexural strength for waste CB loading with 16 wt. % was due to the reduction of bonding adhesion along with the effect of extra polymer layers generation between the carbon fiber plies.

The modulus of elasticity was calculated based on equation(10). The result in Figure 5-17 shows that as the wt. % of waste CB increases, the modulus of elasticity decreases. The modulus of elasticity is sensitive to the ply stacking sequence. Even though, the span length to depth ratio was increased to reduce the effect of shear

deflection. Shear deflection can reduce the modulus of high anisotropic composite in case the span length to depth ratio is small. (ASTM, 2014)

Table 5-9: Modulus of elasticity from three points bending test

Waste CB (Wt. %)	Modulus of Elasticity (MPa)			Average (MPa)	Standard Deviation
	Sample 1	Sample 2	Sample 3		
0%	51021	49604	48599	49741	1217
2%	42257	42249	41800	42102	262
5%	46483	46429	48790	47234	1348
8%	41979	39451	42759	41397	1729
16%	30178	30844	32684	31235	1298

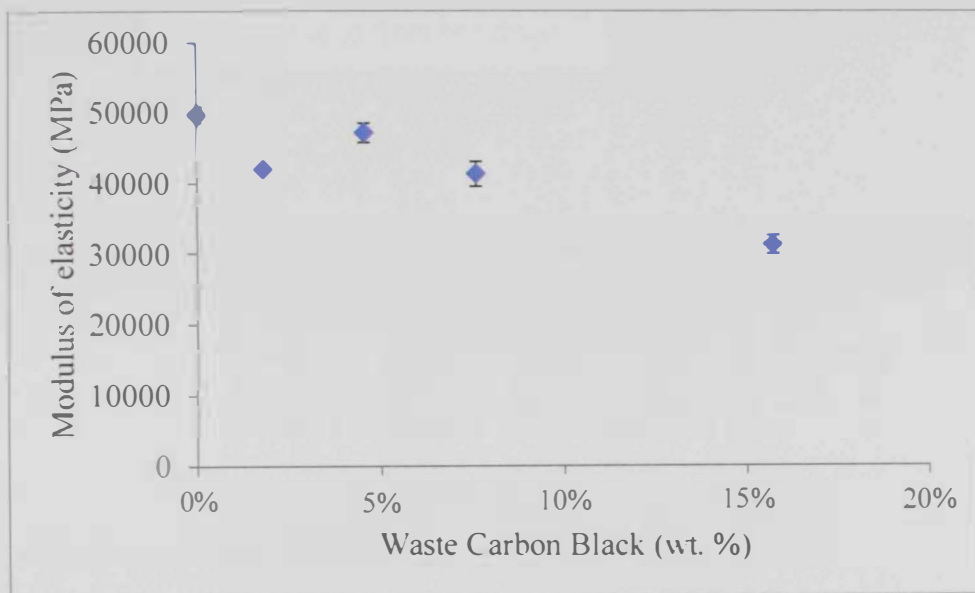


Figure 5-18: Modulus of elasticity obtained from three points bending test

It was noticed that the resin properties has a major contribution to the final properties of the composite material. However, the limitation of an epoxy resin is its brittleness. Also, the bonding with fiber and manufacturing defects are major reasons for the failure modes that generate cracks and propagate through the composite laminate, and this is called delamination. Delamination can be avoided by enhancing the interlaminar properties through enhancing the properties of the epoxy resin

(binder). Figure 5-18 shows that the fracture in the sample without waste CB occurred mainly due to the fiber breakage in the middle of the outer surface of the composite laminate. Above this wt. %, the fracture is initiated by fiber breakage along with the effect of delamination through the interlayer. Figure 5-19, 5-20, 5-21 show examples of the fracture due to fiber breakage and due to delamination. The increase of waste CB in the CFRP will result in reduction of interlaminar properties and decrease the flexural properties of the final composite laminate.

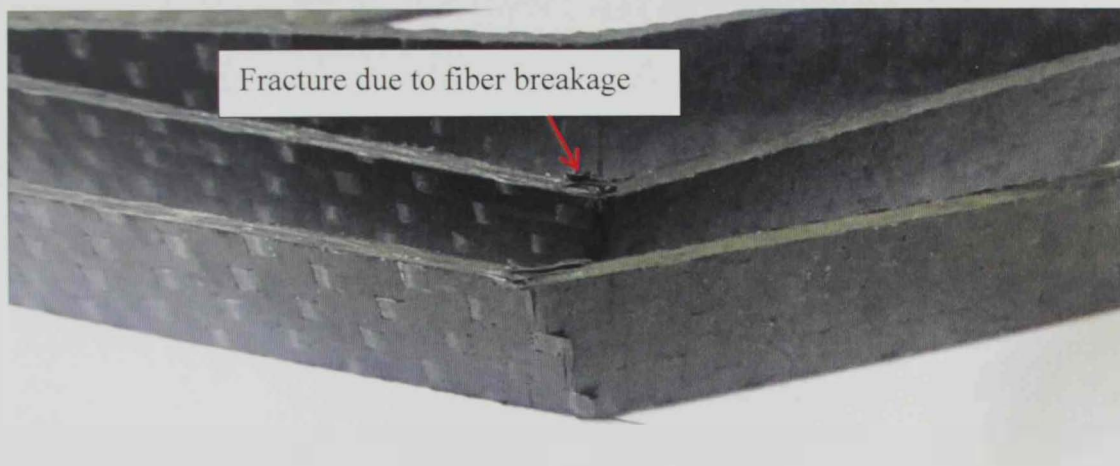


Figure 5-19: Fracture for sample with 0% of waste CB

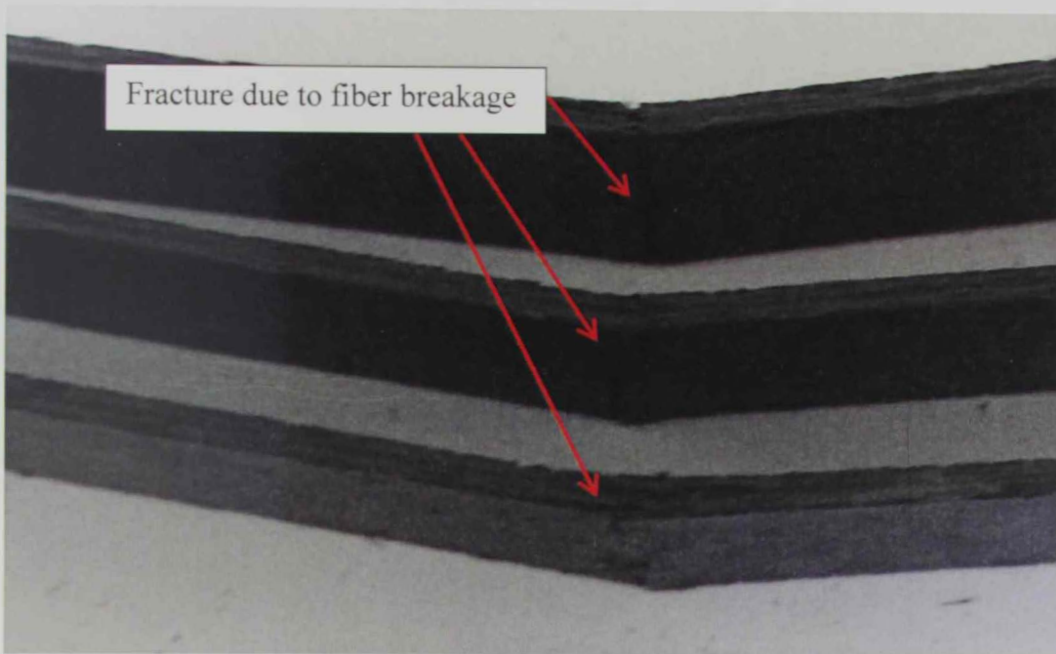


Figure 5-20: Fracture for sample with 2% of waste CB

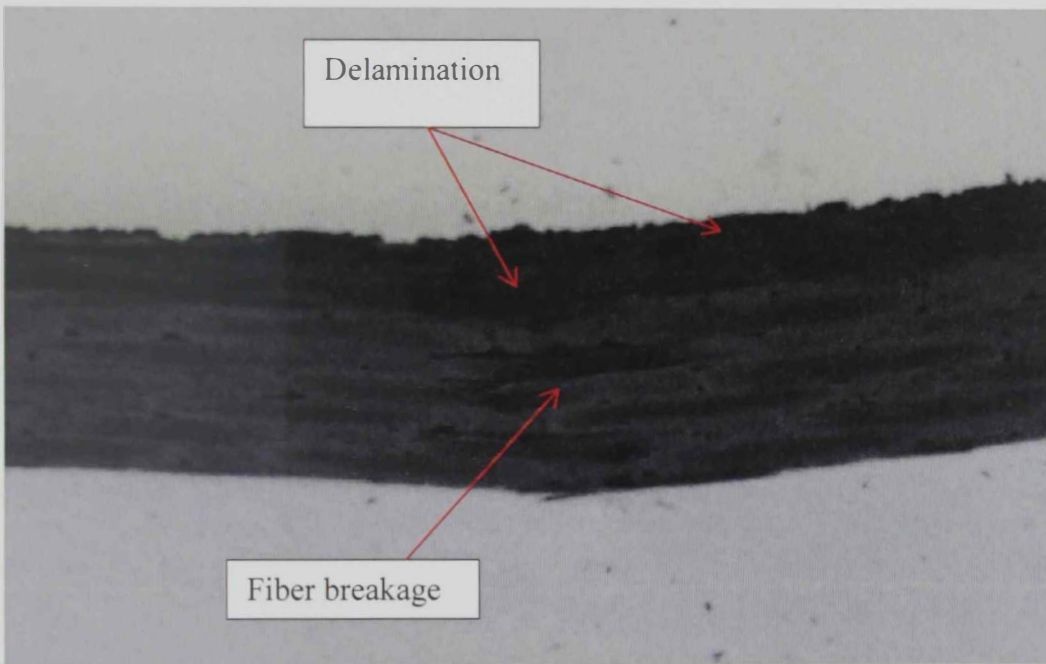


Figure 5-21: Fracture for sample with 8% of waste CB

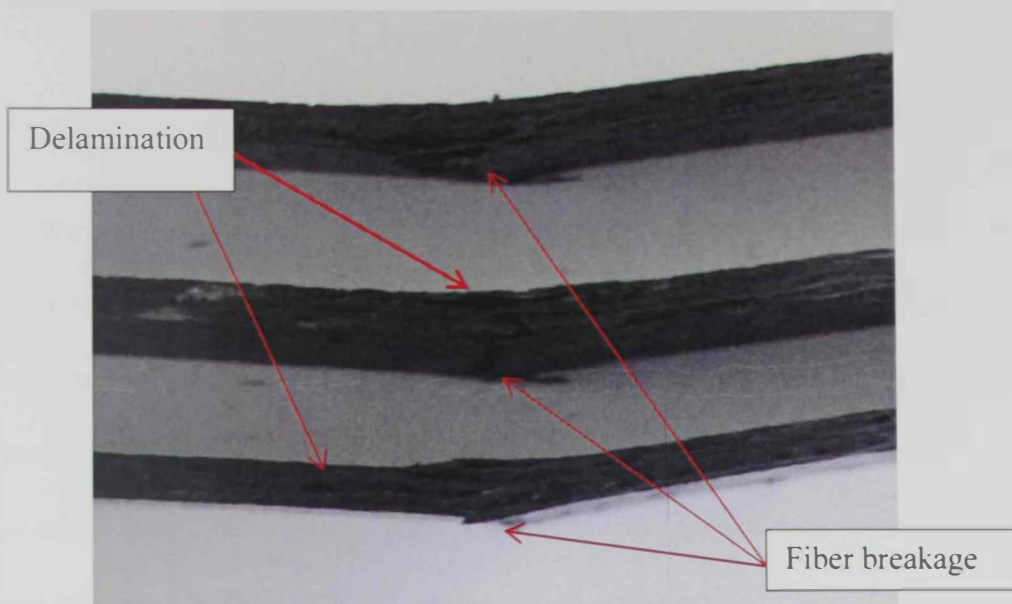


Figure 5-22: Fracture for sample with 16% of waste CB

CHAPTER SIX

SUMMARY AND CONCLUSION

We have found that the electrical conductivity of post heat treated carbon black increases as the temperature of heat treatment increases. XRD results demonstrated the existence of crystalline compositions of ZnO and ZnS in the waste CB powder. Also, as the annealing temperature increases up to 1000 °C, the characteristic peaks of ZnO decreases, however, ZnS characteristic peaks increases. For heat treatment at 1250 °C, both ZnO and ZnS characteristic peaks was not present with respect to the growth of new characteristic peaks related to amorphous carbon and initiation of graphite structures (100). Moreover, the intensity of peak at $2\theta=25^\circ$ increases with slight shifting backward. It was also noted from TGA analysis that the oxidation temperature increases and the residual weight percentage decreases as the annealing temperature increases. This contributes to the reduction of carbonaceous weight percentage as the temperature of annealing increases. Raman spectrum demonstrated the G peak for annealing temperature above 1000°C.

The results showed that the electrical conductivity for the annealed carbon black at 1250°C was improved to a value 40 σ/cm . Furthermore, impregnating a high amount of annealed carbon black (40 wt. %) in a polymeric matrix resulted in a low electrical conductivity of 0.0034 σ/cm . Adding CB resulted in decreasing the decomposition temperature slightly.

The electrical conductivity measurement of carbon fiber/epoxy laminates showed that as the wt. % of waste carbon black increases up to 2%, the in-plane

conductivity increases due to creation of carbon network in the extra polymer rich region generated on the surface of the composite. However, loading waste carbon black with more than 2% will not affect the surface conductivity significantly. Through plane electrical conductivity was increasing up to a specific point then the value started to drop down due to generation of extra layer between the carbon fiber laminas. Also, the result of thermal conductivity showed that the value of thermal conductivity was increasing as the wt. % of waste CB increased in the composite. However, the generation of an extra rich layer between the fiber laminas will not affect negatively on the thermal conductivity.

Nevertheless, adding waste CB to the carbon fiber laminate resulted in decreasing the flexural strength of the composite as it has been revealed from the three point bending test. Enhancing the electrical conductivity by utilizing waste tire was achieved. Thermal conductivity of the prepared sample increased as the loading of waste carbon black increased. Achieving high flexural strength with respect to increasing the electrical and thermal conductivities are conflicting scenarios. The filler loading was a main important factor to increase the electrical/thermal conductivity. Reduction of flexural strength can be mitigated by enhancing the dispersion of the loaded filler and the aggregate particle size.

It is recommended to blend 5 wt. % of waste carbon black annealed at 1250°C into CFRP to provide enhancement in the both through-plane and surface electrical conductivity. The surface conductivity was enhanced 80% by blending 5 wt. % of waste carbon black. The through plane resistivity reduced 51% by adding 5 wt. % of

waste carbon black. However, the flexural strength was negatively affected with reduction of 8% only by blending 5 wt. % of waste carbon black.

Further studies can be done by enhancing the heat treatment of waste carbon black. Higher heat treatment temperature that reaches to 3000°C is required to graphite the waste carbon black. Waste carbon has the potential to convert to graphite by graphitization process and hence the electrical conductivity will be enhanced. Also, more researches can be conducted to investigate the possibility of utilizing waste carbon black in modern manufacturing processes such as Selective Laser Sintering (SLS) to produce valuable conductive, made of carbon based polymer composite.

Bibliography

- Ahamad, T. & Alshehri, S. M. (2014). Thermal degradation and evolved gas analysis: A polymeric blend of urea formaldehyde (UF) and epoxy (DGEBA) resin. *Arabian Journal of Chemistry*, 7, 1140–1147.
- Alayavalli, K., & Bourell, D. (2010). Fabrication of modified graphite bipolar plates by indirect selective laser sintering (SLS) for direct methanol fuel cells. *Rapid Prototyping Journal*, 16(4), 268-274.
- Annala, M., & Löfgren, B. (2006). Compatibilization of conductive polyethylene/polyaniline blends. *Macromolecular Materials and Engineering*, 291(7), 848-857.
- Antunes, R.A., Oliveira, M.C.L., Ett, G. & Ett, V. (2011). Carbon materials in composite bipolar plates for polymer electrolyte membrane fuel cells: A review of the main challenges to improve electrical performance. *Journal of Power Sources*, 196(6), 2945-2961.
- Arai, Y. (1993). *Structure and Properties of Pitch-Based Carbon Fibers* (NIPPON STEEL TECHNICAL REPORT No.59). California: Nippon Steel Corporation.
- ASTM Standards. (2014). *Standard Test Methods for Flexural Properties of Unreinforced and Reinforced Plastics and Electrical Insulating Materials*. (ASTM D790-10). United States, ASTM International.

- Bandaru, P. R. (2007). Electrical Properties and Applications of Carbon Nanotube Structures. *Journal of Nanoscience and Nanotechnology*, 7, 1-29.
- Banerjee, P., & Mandal, B. M. (1995). Conducting polyaniline nanoparticle blends with extremely low percolation thresholds. *Macromolecules*, 28(11), 3940-3943.
- Besmann, T.M., Klett, J. W., Henry, J. J., & Lara, C.E. (2000). Carbon/Carbon Composite Bipolar Plate for PEM Fuel Cells. *Journal of the Electrochemical Society*, 147, 4083-4086.
- Betancur, M., Daniel Martínez, J. & Murillo, R. (2009). Production of activated carbon by waste tire thermochemical degradation with CO₂. *Journal of Hazardous Materials*, 168 (2009), 882–887.
- Callister, W. D., Rethwisch, J. & Rethwisch, D. (2008). *Fundamentals of Materials Science and Engineering*. 3rd Ed. New York, USA: John Wiley & Sons.
- Celzard, A., Maréchal, J., Payot F., Furdin, G. (2002). Electrical conductivity of carbonaceous powders. *Carbon*, 40, 2801-2815.
- Cho, M. S., Park, S. Y., Hwang, J. Y. & Choi, H. J. (2004). Synthesis and electrical properties of polymer composites with polyaniline nanoparticles. *Materials Science and Engineering*, 24(1), 15-18.
- Daniel Martínez, J., Puy, N. (...), & Murillo, R. (2013). Waste tyre pyrolysis – A review. *Renewable and Sustainable Energy Review*, 23, 179-213.

- Darmstadta, H., Roy, C. (...), & Kaliaguinea, S. (2000). Solid state C-NMR spectroscopy and XRD studies of commercial and pyrolytic carbon blacks. *Carbon*, 38, 1279-1287.
- Du, L. (2008). *Highly Conductive Epoxy/Graphite Polymer Composite Bipolar Plates in Proton Exchange Membrane (PEM) Fuel Cells*. (Doctoral Dissertation). University of Akron (Ohio USA), (2008). Retrieved from: https://etd.ohiolink.edu/ap/10?0::NO:10:P10_ACCESSION_NUM:akron1202345378.
- Dweiri, R. & Sahari, J. (2007). Electrical Properties Carbon-Based Polypropylene Composites for Bipolar Plates in Polymer Electrolyte Membrane Fuel Cell (PEMFC). *Journal of Power Source*, 171 (2007), 424-432.
- European Tyre and Rubber Manufacturers' Association. (2010). *End of life tyres*. Brussels: European Tyre and Rubber Manufacturers' association, 2010.
- Farmer, J. D. & Covert E. E. (1996). Thermal conductivity of a thermosetting advanced composite during its cure. *Journal of Thermophysics and Heat Transfer*, 10(3), 467-475.
- Gurunathan, K., Murugan, A. V., Marimuthu, R., Mulik, U. & Amalnerkar, D. (1999). Electrochemically synthesised conducting polymeric materials for applications towards technology in electronics, optoelectronics and energy storage devices. *Materials Chemistry and Physics*, 61(3), 173-191.

- Hahn, H.T., & Tsai, S.W. (1980). *Introduction to Composite Materials*. 2nd Ed. Boca Raton, Florida: CRC Press.
- Han, S., Lin, J. T., Yamada, Y. & Chung, D.D.L. (2008). Enhancing the thermal conductivity and compressive modulus of carbon fiber polymer–matrix composites in the through-thickness direction by nanostructuring. *CARBON*, 46, 1060-1071.
- Hoa, S. V. (2009). *Principles of Manufacturing of Composite Materials*. 1st Ed. Lancaster, Pennsylvania: DEStech Publications.
- Inaba, M., (2009). *Secondary Batteries- Lithium rechargeable systems- Lithium-Ion. Negative Electrodes: Graphite*. Doshisha University, Kyoto, Japan: Elsevier Publication.
- Inagaki, Mi. (2009). Advanced Carbon Materials. Shigeyuki Somiya. *Handbook of Advanced Ceramics*. 2nd Ed. Salt Lake City, Utah: American Academic Press.25-44.
- Kim, M., Lim, J. W., Kim, K. H. & Lee, D. G. (2013). Carbon fabric/phenolic composite bipolar plate reinforced with nano-size carbon black. *Composite Structures*, 96, 569-575.
- Kim, M., Yu, H. N., Lim, J.W. & Lee, D.G. (2012). Bipolar plates made of plain weave carbon/epoxy composite for proton exchange membrane fuel cell. *International Journal of Hydrogen Energy*, 37(5), 4300-4308.

- Kumar, A. & Reddy, R. G. (2003). Polymer Electrolyte Membrane Fuel Cell with Metal Foam in the Gas Flow-Field of Bipolar/End Plates. *Journal of New Materials for Electrochemical Systems*, 6 (2003), 231-236.
- Leu, N. G. and Ming, C. (2012). Effect of different graphite materials on the electrical conductivity and flexural strength of bipolar plates fabricated using selective laser sintering. *International Journal of Hydrogen Energy*, 37 (4), 3558-3566.
- Liao, S., Yen, C., Weng, C. C. (...), & Hsiao, Y. (2008). Preparation and properties of carbon nanotube/polypropylene nanocomposite bipolar plates for polymer electrolyte membrane fuel cells. *Journal of Power Sources*, 185, 1225-1232.
- Li, Q., Li, Y., Zhang, X., Satishkumar, B. (...), & Chikkannanavar. (2007) Structure-Dependent Electrical Properties of Carbon Nanotube Fibers. *ADVANCED MATERIALS*, 19, 3358–3363.
- Li, Z.Q., Lu, C.J., Xia, Z.P., Zhou, Y. & Luo, Z. (2007). X-ray diffraction patterns of graphite and turbostratic carbon. *Carbon*, 45, 1686-1695.
- Mallick, P.K. (2008). *Fiber-Reinforced Composites*. 2nd Ed, Boca Raton, Florida: CRC Press.
- Mangalgi, P. (2008). Composite materials for aerospace applications. *Journal of Composites*, 22(3), 657-664.
- Manoj, B. Kunjomana, A.G. (2012). Study of Stacking Structure of Amorphous Carbon by X-Ray Diffraction Technique. *International Journal of Electrochemical Science*, 7, 3127 – 3134

- Minto, C.D.G. & Vaughan, A.S. (1996). Partial phase mixing in solution-processed polyaniline-poly (methyl methacrylate) blends. *Synthetic Metals*, 81, 81-86.
- Mis-Fernandez, R., Azamar-Barríos, J.A. & Ríos-Soberanis, C.R. (2008). Characterization of the powder obtained from wasted tires reduced by pyrolysis and thermal shock process. *Journal of Applied Research and Technolog*, 6(2), 95-105.
- Mohanty, A., Srivastava, V.K., Sastry, P. U. (2013). "Investigation of Mechanical Properties of Alumina Nanoparticle-Loaded Hybrid Glass/Carbon-Fiber-Reinforced Epoxy Composites." *Journal of applied science*.
- Mohsin, M., Hossin, A., Haik, Y. (2011). Thermal and Mechanical Properties of Poly(vinyl alcohol) Plasticized with Glycerol. *Journal of Applied Polymer Science* . 122, 3102–3109.
- Nakamizo, M., Kammerech, M. & Walker, P.L. (1973). Laser Raman Studies on carbons. *Carbon*, 12 (1973), 259-267.
- Nikolic, G., Zlatkovic, S., Cakic, M., Cakic, S., & Lacnjevac, C. (2010). Fast Fourier Transform IR Characterization of Epoxy GY Systems Crosslinked with Aliphatic and Cycloaliphatic EH Polyamine Adducts. *Sensors*, 10(1), 684-696.
- P.A Hilton LTD, (1991). *Heat Conduction Unit. Experimental operating and maintenance manual*. King's Somborne, Hampshire, England Vol. H940M/E/5/076.

- Pantea, D., Darmstadt, H. & Kaliaguine, S. (2003). Heat-treatment of carbon blacks obtained by pyrolysis of used tires: Effect on the surface chemistry, porosity and electrical conductivity. *Journal of Analytical and Applied Pyrolysis*, 67, 55-76.
- Park, M. S. & Jin, S. (2009). Effect of Graphite Nanofibers on Poly(methyl methacrylate) Nanocomposites for Bipolar Plates. *Bull. Korean Chem. Soc.*, 30(3), 671-674.
- Popov, V. N. & Lambin, P. (2006). *Carbon Nanotubes*. 1st Ed. New York, USA: Springer Publications.
- Pozegic, T.R., Hamerton, I., Anguita, J.V. (...), & Silva, S. R. P. (2014). Low temperature growth of carbon nanotubes on carbon fibre to create a highly networked fuzzy fibre reinforced composite with superior electrical conductivity. *CARBON*, 74, 319-328.
- Pozio, A., Zaza, F., Masci, A. & Silva, R. F. (2008). Bipolar plate materials for PEMFCs: a conductivity and stability study. *Journal of Power Sources*, 179, 631-639.
- Rane, U.G., Sabnis, A. A., & Shertukde, V. V. (2014). Synthesis and Characterization of Imide Containing Hybrid Epoxy Resin with Improved Mechanical and Thermal Properties. *International Journal of Polymer Science*, 2014, 1-10.

- Saleha, T. A., Al-Saadi, A. A. & Gupta, V. K. (2014). Carbonaceous adsorbent prepared from waste tires: Experimental and computational evaluations of organic dye methyl orange. *Journal of Molecular Liquids*, 191, 85-91.
- Sweeting, R. D. & Liu, X. L. (2003). Measurement of thermal conductivity for fibre-reinforced composites. *Composites*, 35, 933-938.
- Taherian, R., Hadianfard, M. J. & Golikand, A. N. (2013). Manufacture of a Polymer-based Carbon Nanocomposite as Bipolar Plate of Proton Exchange Membrane Fuel Cells. *Materials and Design*, 49, 242-251.
- Undria, A., Sacchib, B., Cantisanib, E. (...), & Toccafondia, N. (2013). Carbon from microwave assisted pyrolysis of waste tires. *Analytical and Applied Pyrolysis*, 104, 396-404.
- Xu, Z., Liu, L., Huang, Y. (...), & Li, J. (2009). Graphitization of polyacrylonitrile carbon fibers and graphite irradiated by γ rays. *Materials Letters*, 63, 1814-1816.
- Yin, Q., Li, A., Wang, W., Xia, L. & Wang, Y. (2007). Study on the Electrical and Mechanical Properties of Phenol Formaldehyde Resin/Graphite Composite for Bipolar Plate. *Journal of Power Sources*, 165(2), 717-721.

Appendix A: TGA graphs for waste carbon black

Figure A-1: TGA for waste CB annealed at 500°C

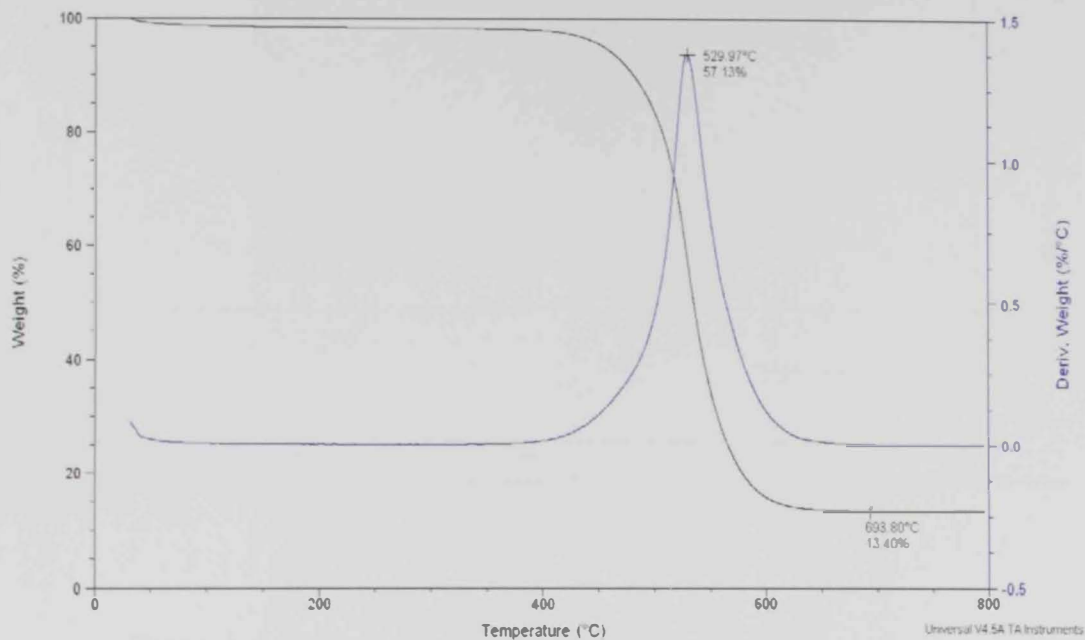


Figure A-2: TGA for waste CB annealed at 750°C

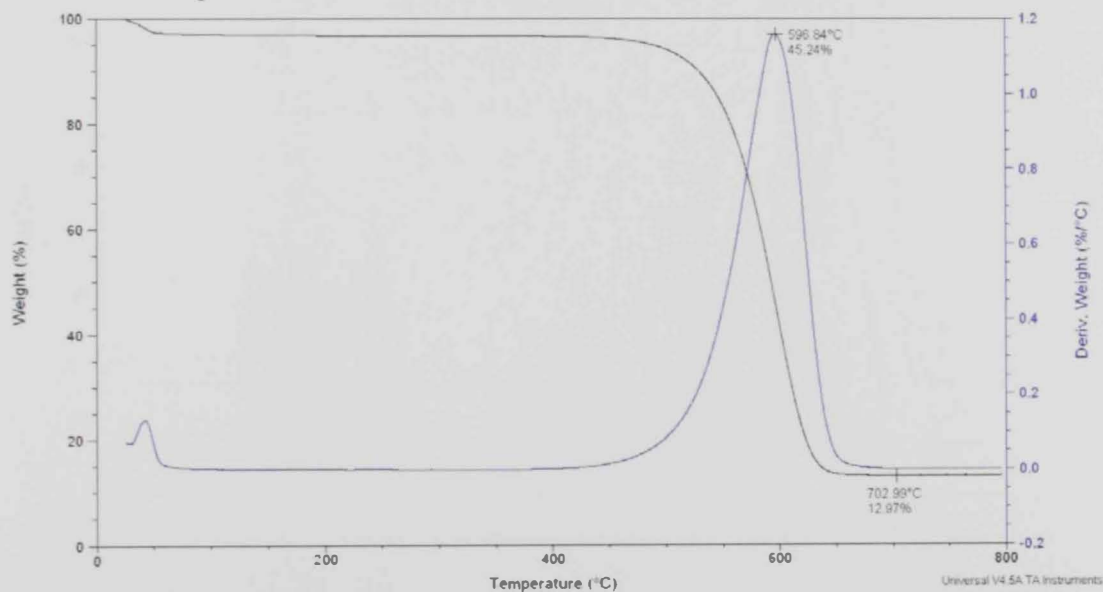


Figure A-3: TGA for waste CB annealed at 1000°C

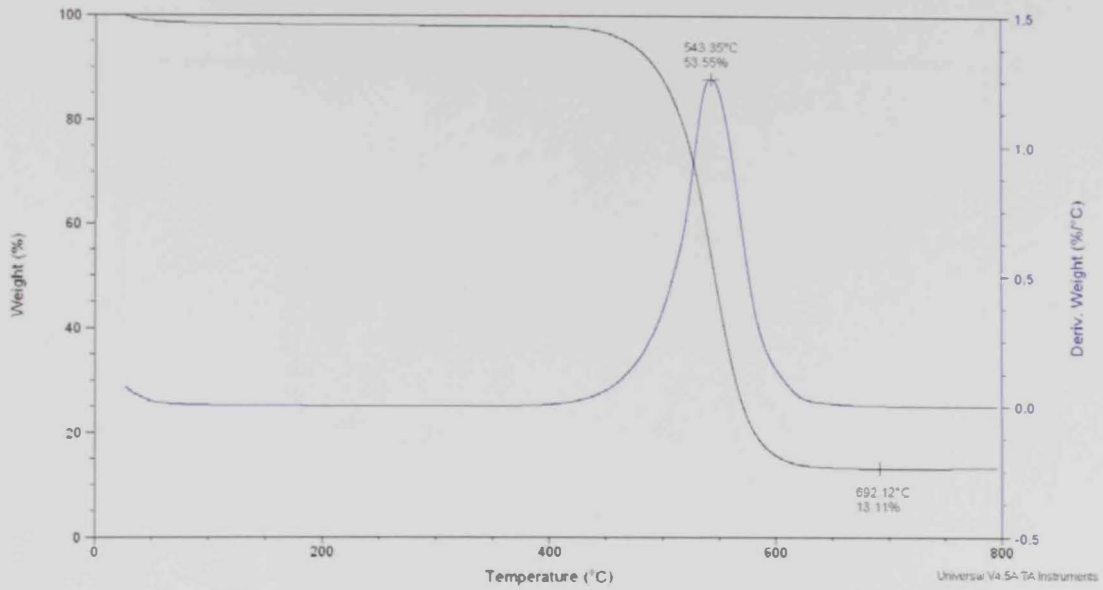


Figure A-4: TGA for waste CB annealed at 1250°C (sample 1)

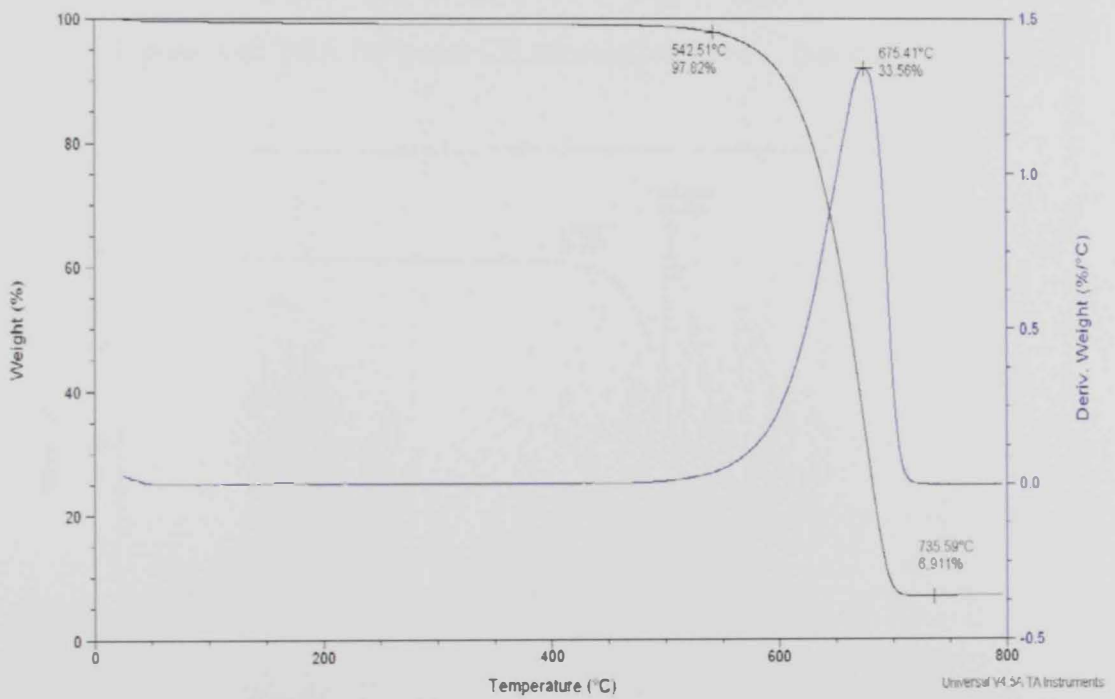


Figure A-5: TGA for waste CB annealed at 1250°C (sample 2)

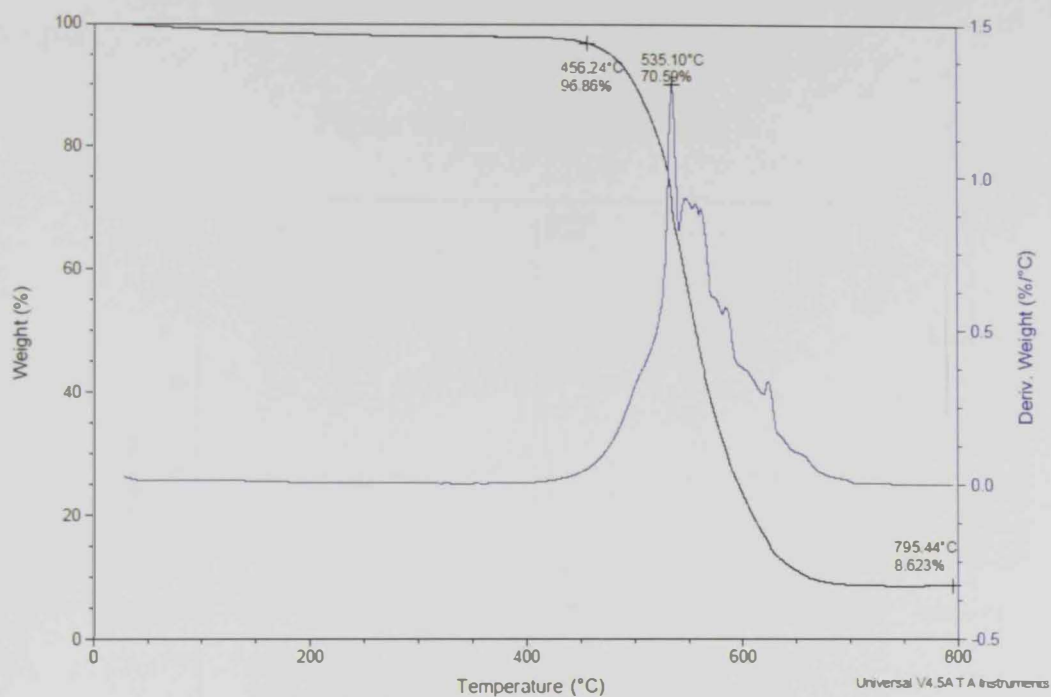
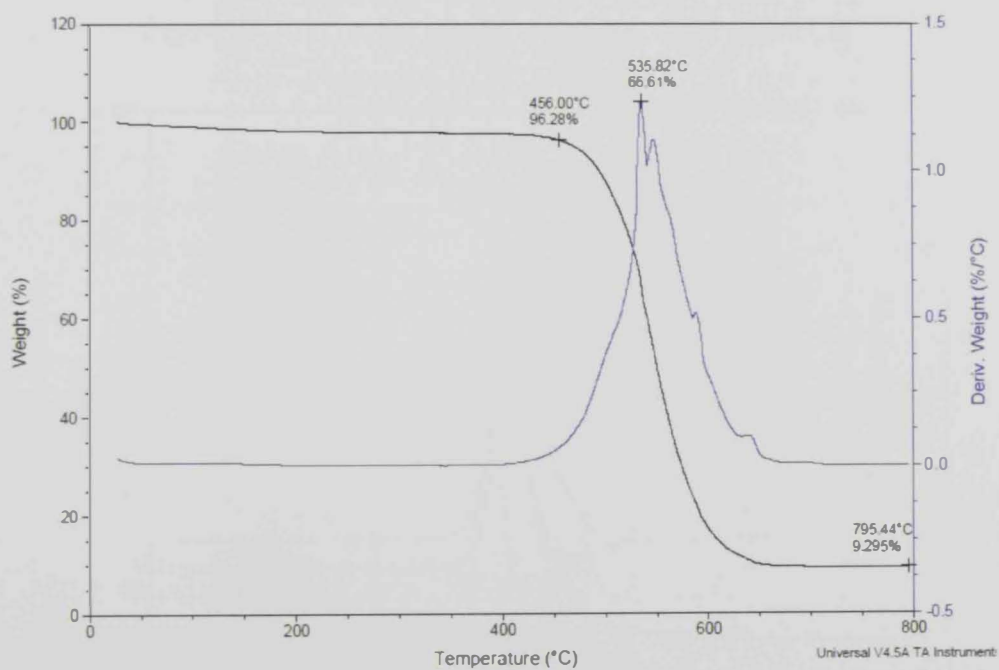


Figure A-6: TGA for waste CB annealed at 1250°C (sample 3)



Appendix B: TGA graphs for waste carbon black blended in epoxy

Figure B-1: TGA for Neat Epoxy

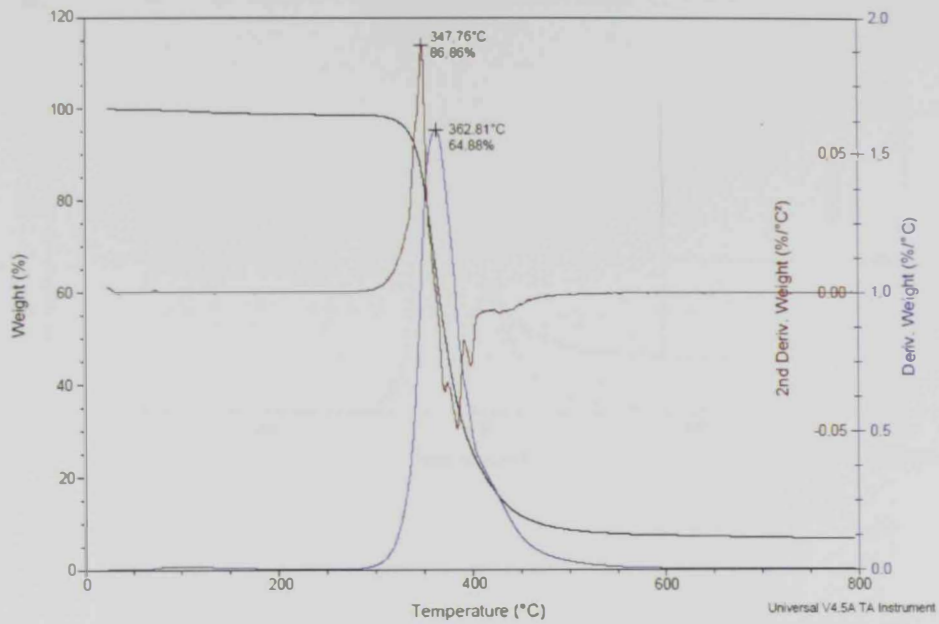


Figure B-2: TGA for Epoxy with 3 wt. % of waste CB

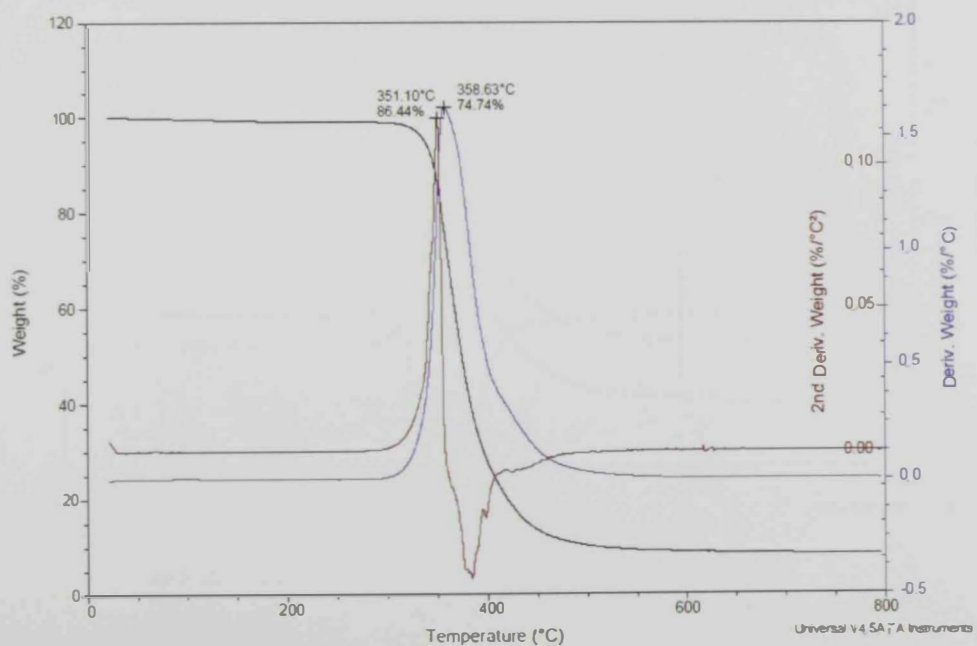


Figure B-3: TGA for Epoxy with 6 wt. % of waste CB

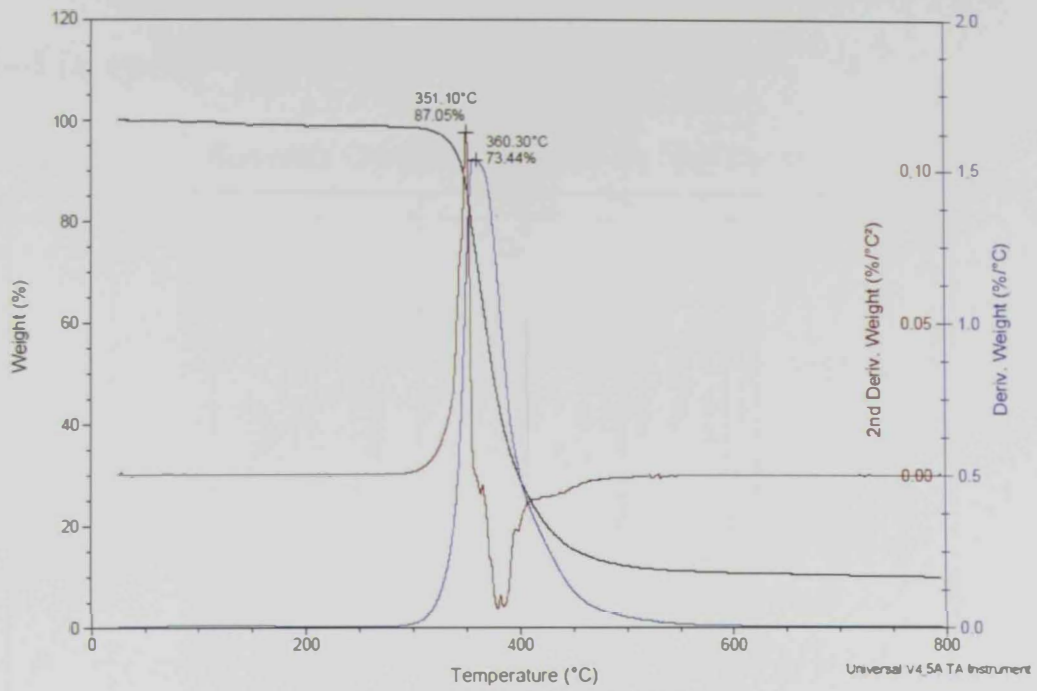
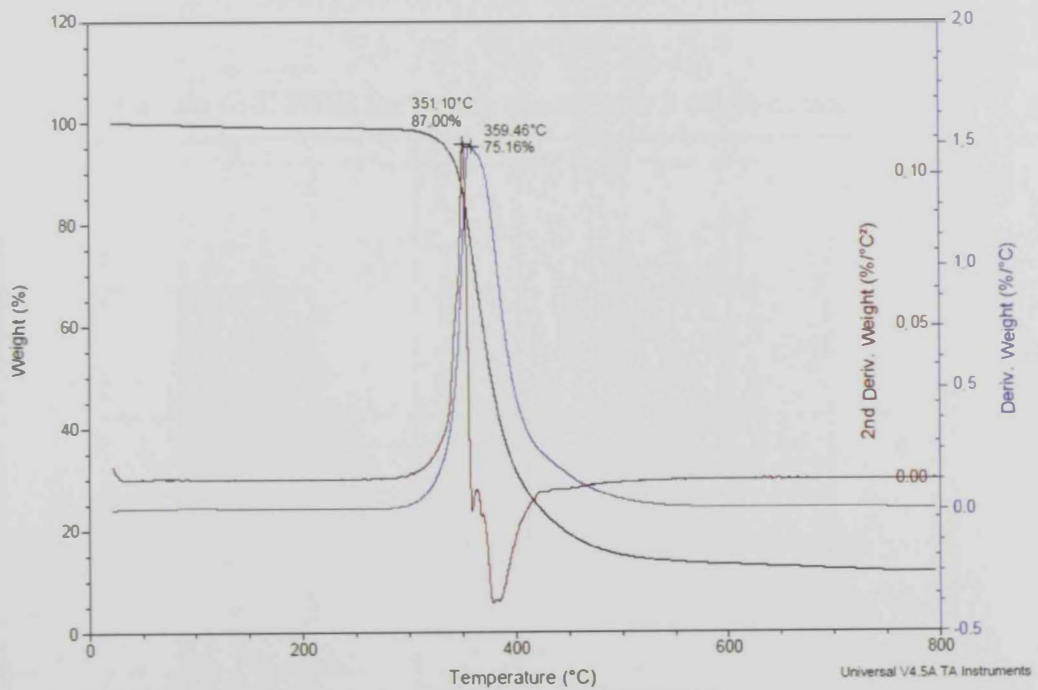
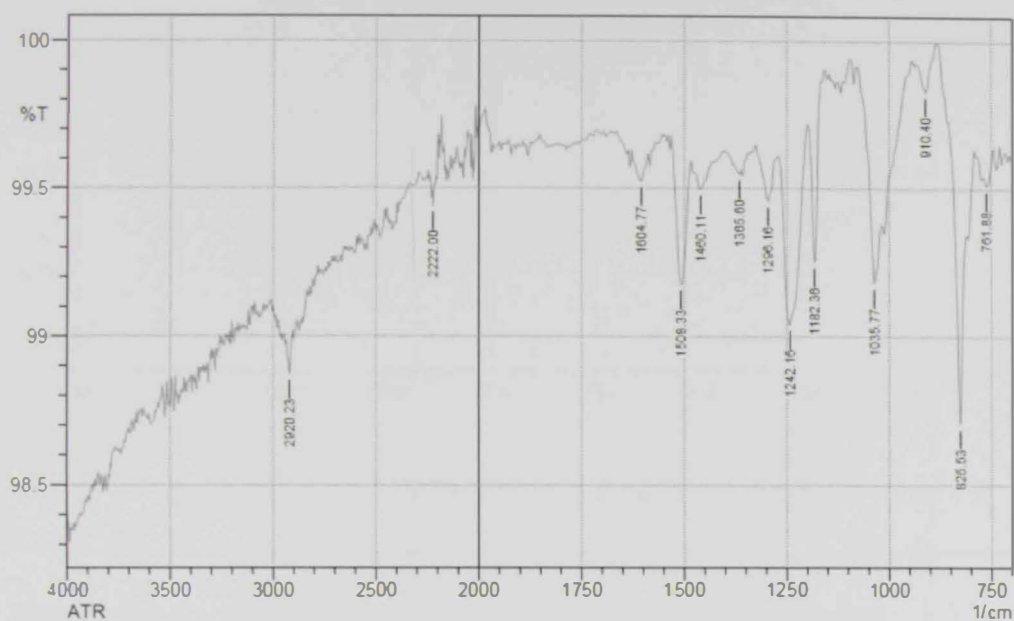


Figure B-4: TGA for Epoxy with 9 wt. % of waste CB

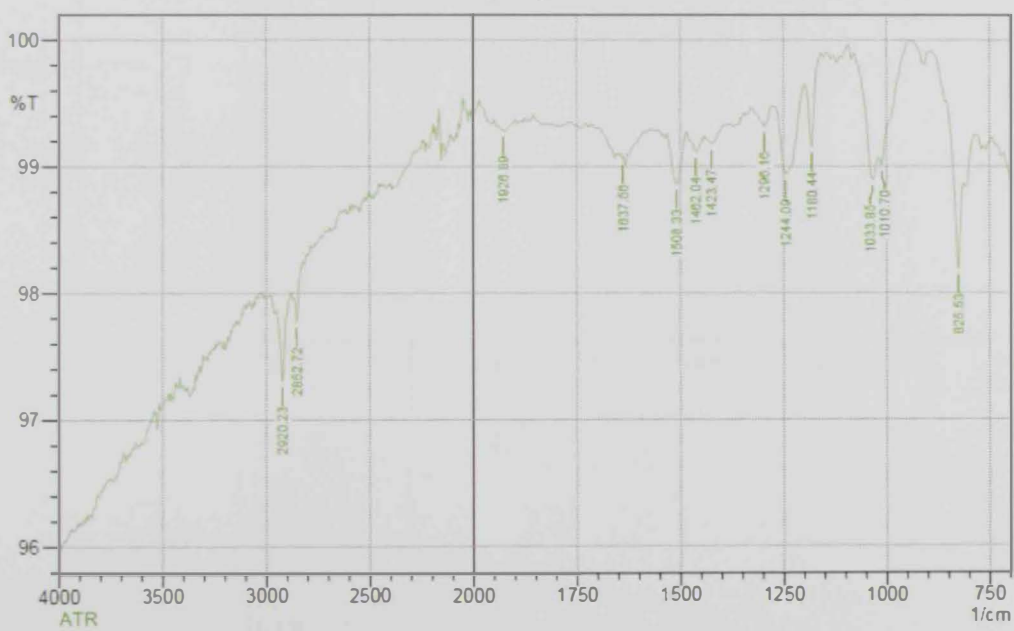


Appendix C: FTIR Spectrums for waste carbon black blended in epoxy

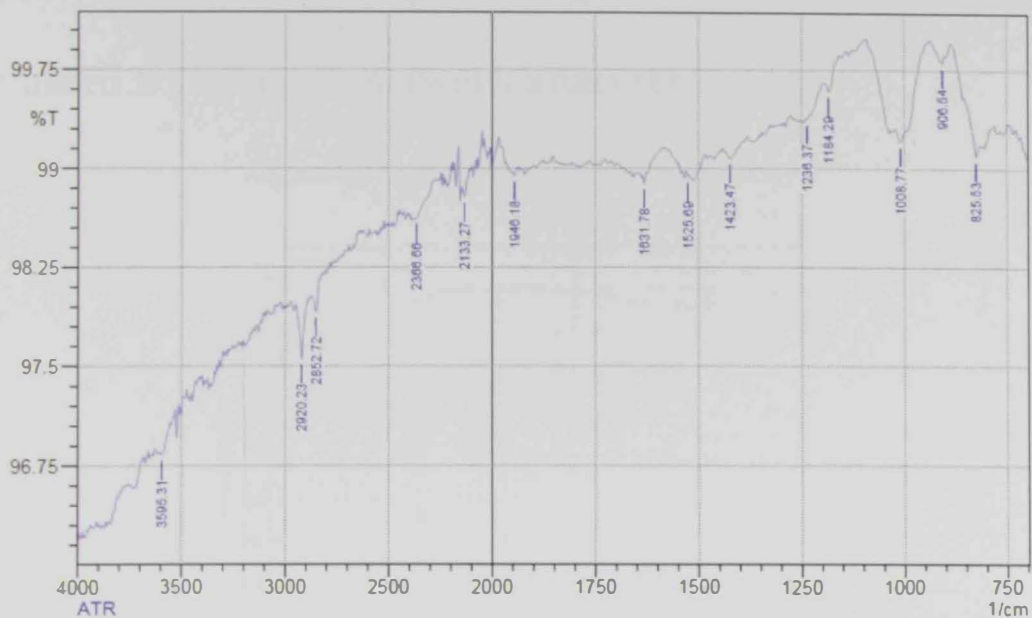
Appendix C-1: FTIR spectrum for Neat Epoxy



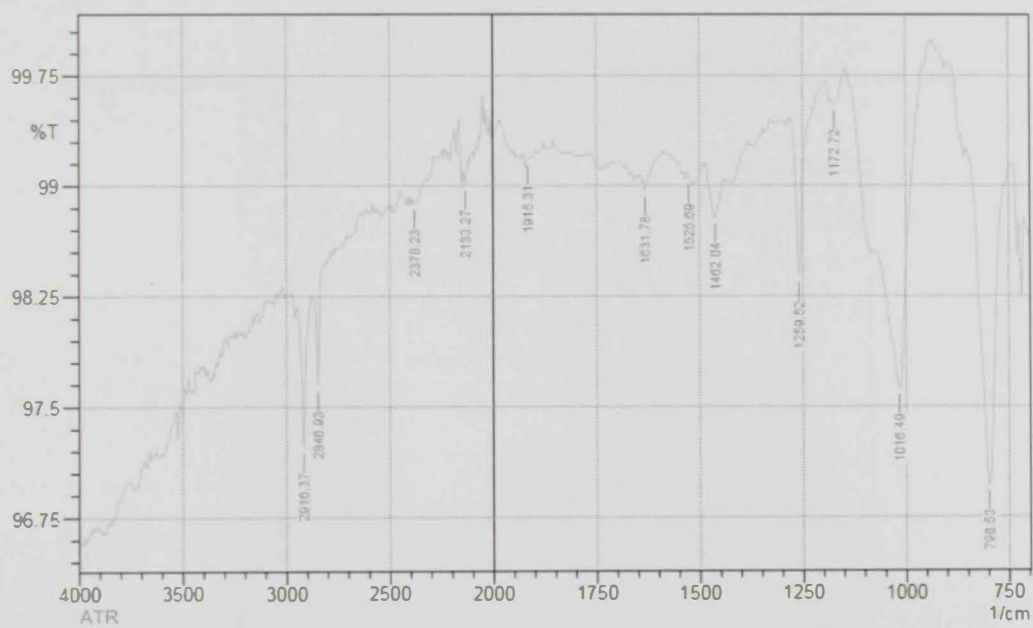
Appendix C-2: FTIR for Epoxy mixed with 3 wt. % of waste CB



Appendix C-3: FTIR for Epoxy mixed with 6 wt. % of waste CB

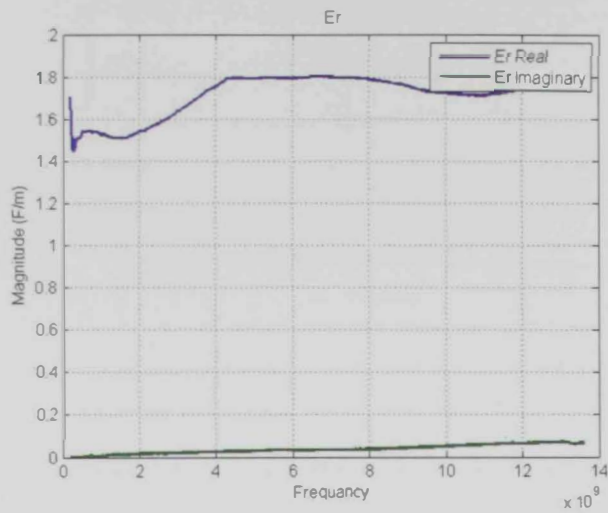


Appendix C-4: FTIR for Epoxy mixed with 9 wt. % of waste CB

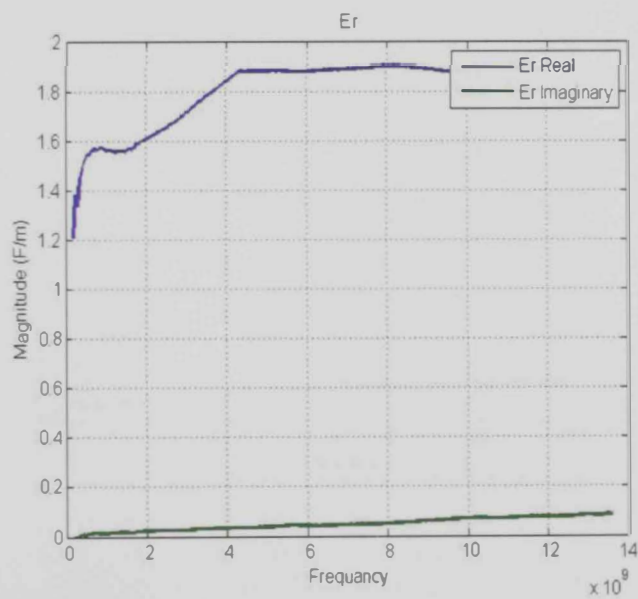


Appendix D: Permittivity and Reflection coefficient obtained from vector network analyzer

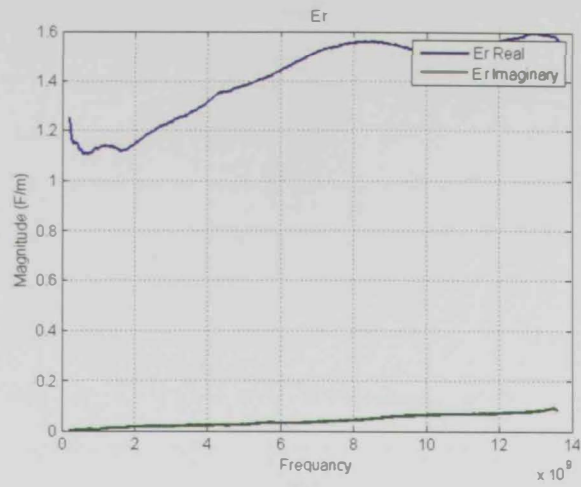
Appendix D-1: Permittivity of Neat Epoxy



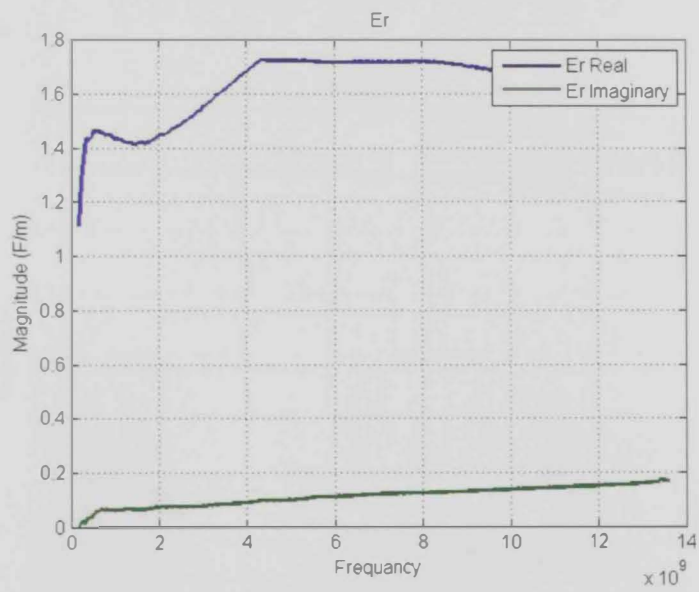
Appendix D-2: Permittivity of Epoxy with 2 wt.% of waste carbon black

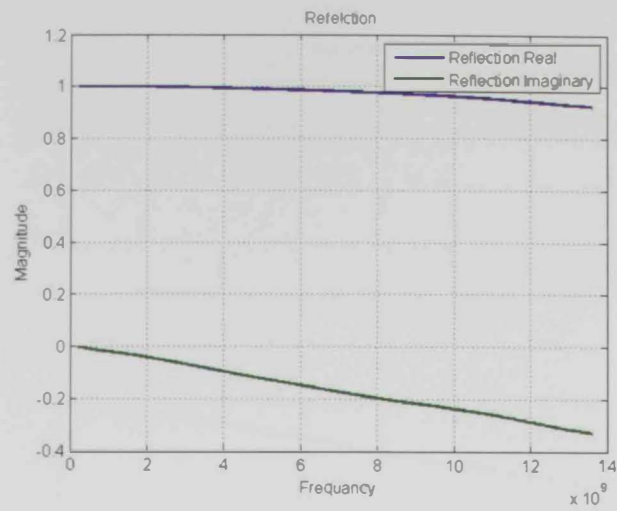
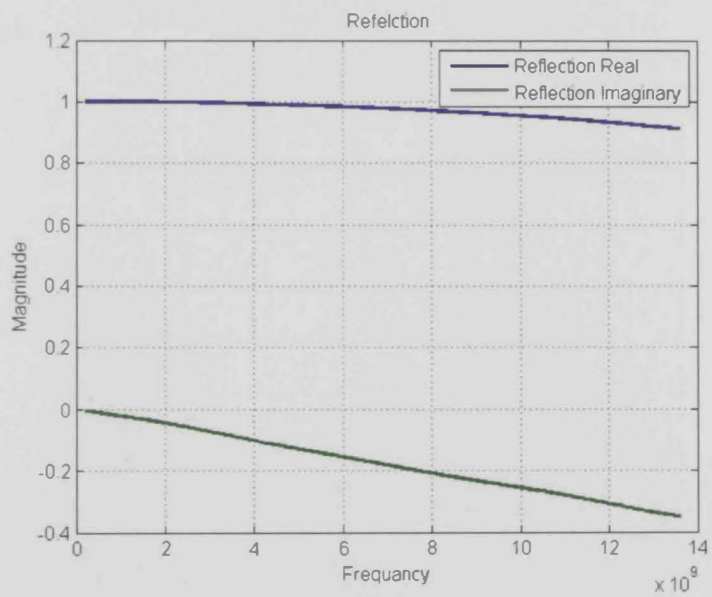


Appendix D-3: Permittivity of Epoxy with 5 wt. % of waste carbon black

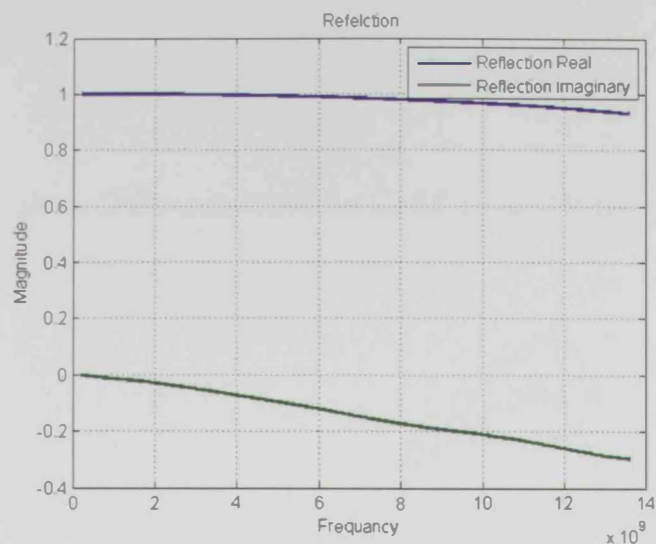


Appendix D-4: Permittivity of Epoxy with 10 wt. % of waste carbon black

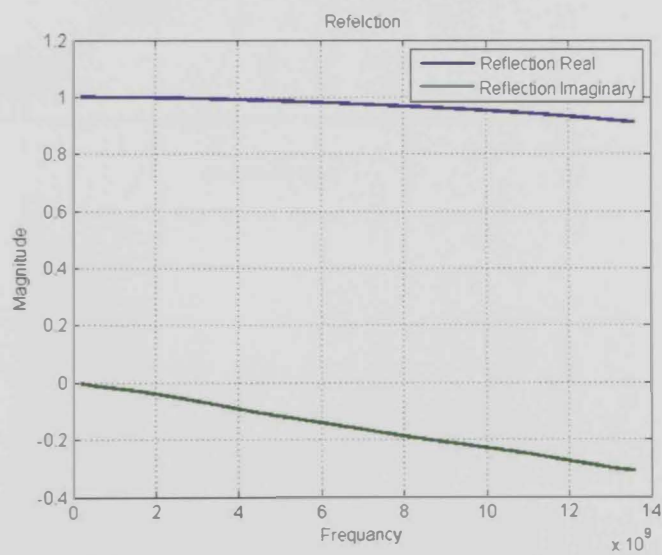


Appendix D-5: Reflection coefficient S_{11} of Neat EpoxyAppendix D-6: Reflection coefficient S_{11} of Epoxy with 2 wt. % of waste carbon black

Appendix D-6: Reflection coefficient S_{11} of Epoxy with 5 wt. % of waste carbon black

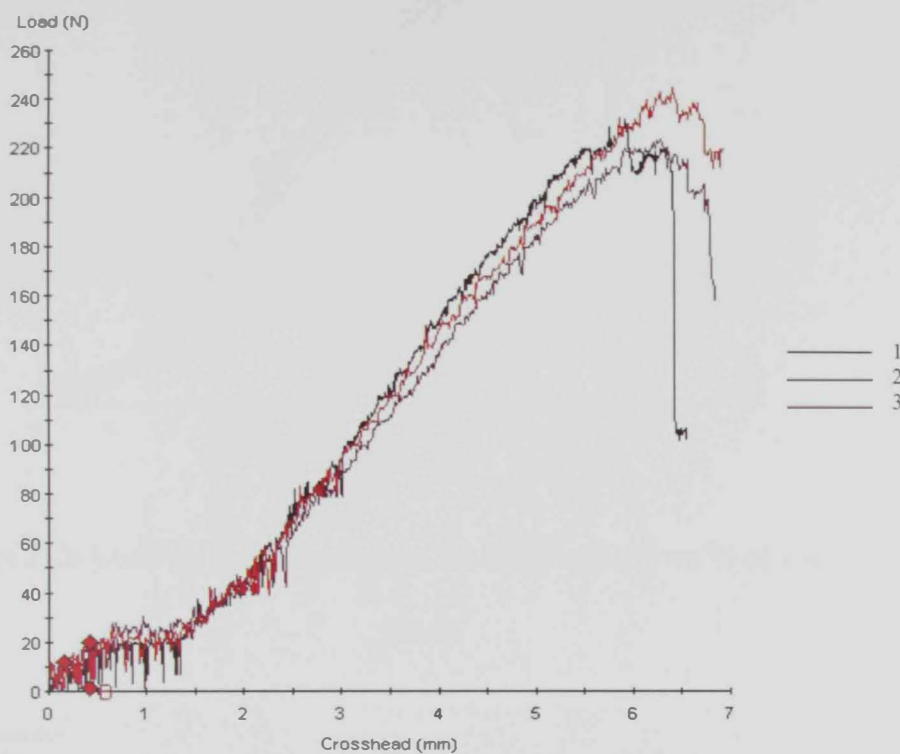


Appendix D-7: Reflection coefficient S_{11} of Epoxy with 10 wt. % of waste carbon black

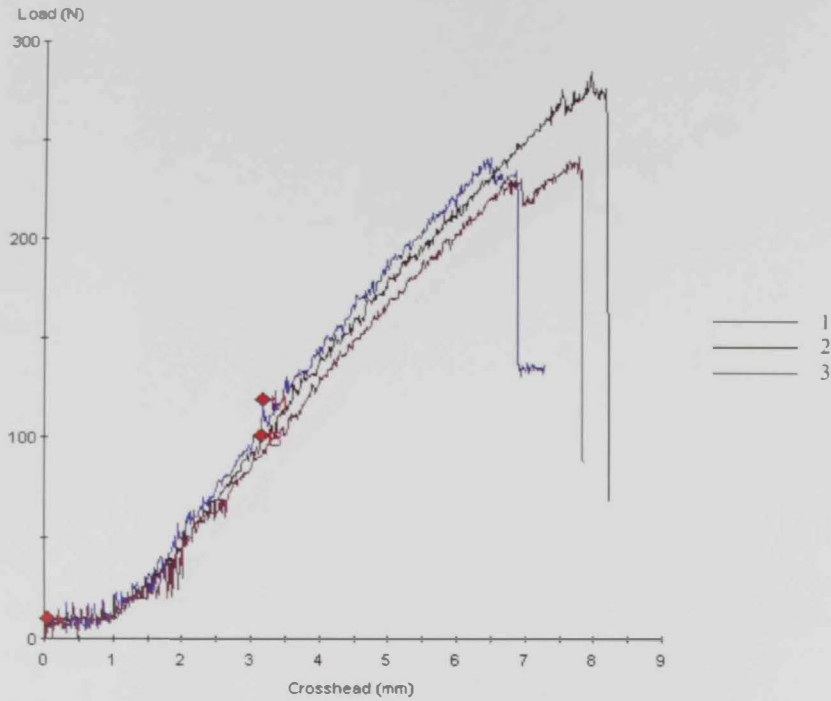


Appendix E: Load vs. deflection curves from three points bending test.

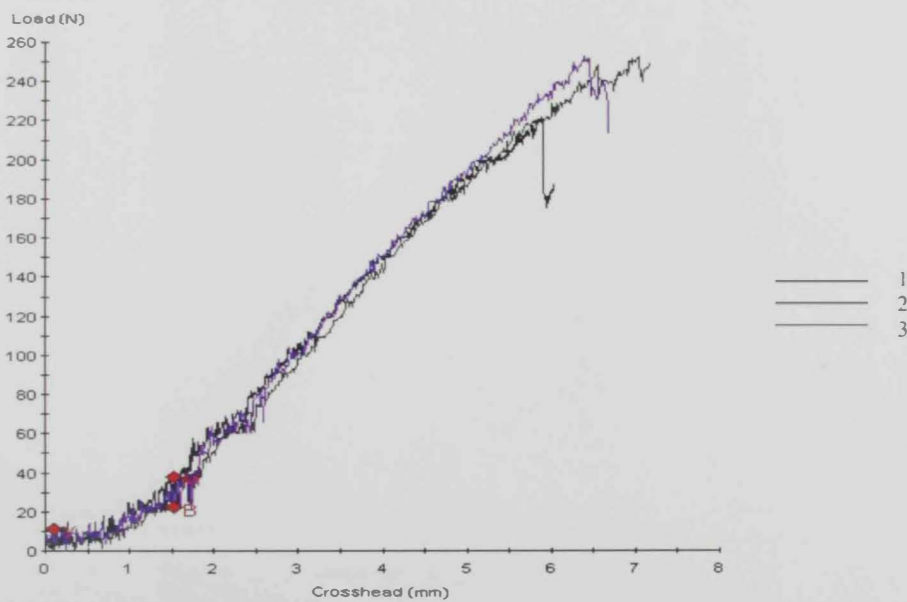
Appendix E-1: Load vs. Deflection curve for CFRP without waste carbon black



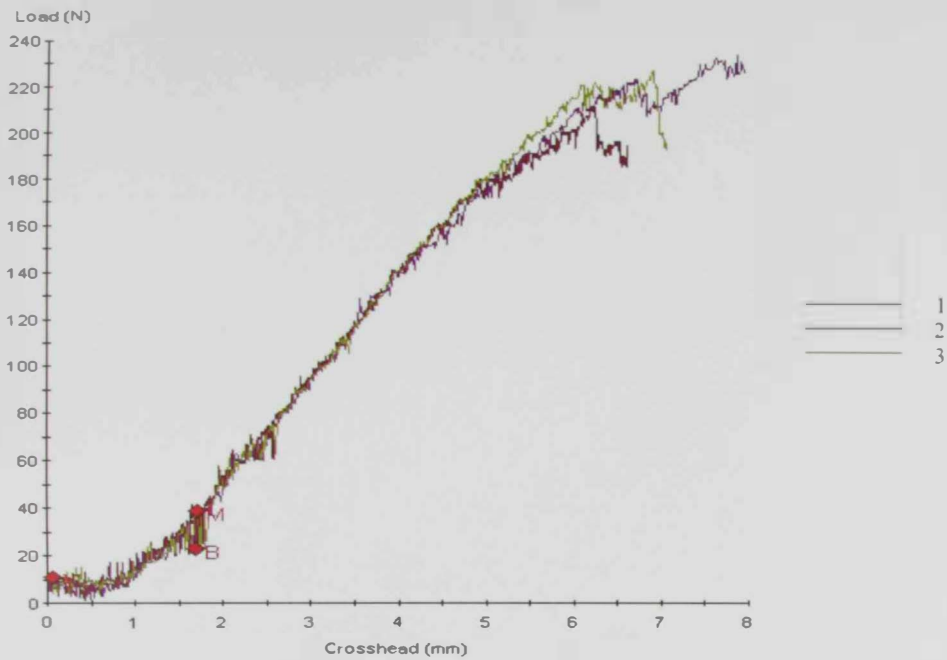
Appendix E-2: Load vs. Deflection curve for CFRP with 2 wt. % of waste carbon
black



Appendix E-3: Load vs. Deflection curve for CFRP with 5 wt. % of waste carbon
black



Appendix E-4: Load vs. Deflection curve for CFRP with 8 wt. % of waste carbon
black



Appendix E-5: Load vs. Deflection curve for CFRP with 16 wt. % of waste carbon
black

